IChF
Institute of Physical Chemistry PAS

PhD Dissertation

ITO Microelectrodes and Microelectrode Arrays for the Analysis of Cell Cultures and Biomedical Applications

Karthika Kappalakandy Valapil

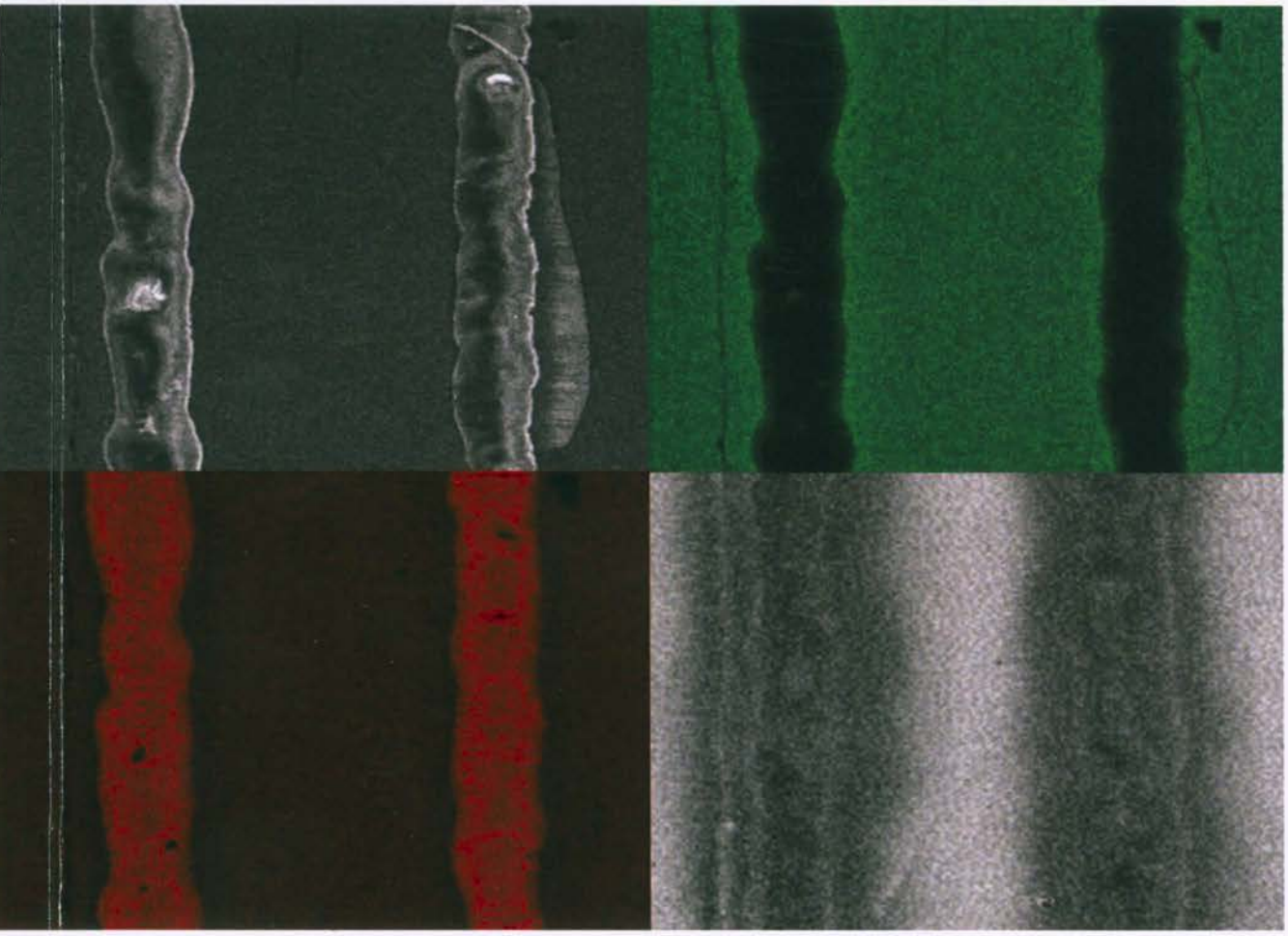

Ph.D. Dissertation

ITO microelectrodes and microelectrode arrays for the analysis of cell cultures and biomedical applications

Karthika Kappalakandy Valapil

Supervisor: Prof. Martin Jönsson-Niedziółka

Auxiliary supervisor: dr inż. Emilia Witkowska Nery

This dissertation was prepared within the international doctoral studies at the

Institute of Physical Chemistry of Polish Academy of Sciences

Marcina Kasprzaka 44/52, 01-224 Warsaw

Warsaw, March 2024

Acknowledgements

I am incredibly thankful to my supervisors for inspiring, guiding and supporting me through five years of my Ph.D.

- Prof. Martin Jönsson-Niedziółka for his dedicated time, for all the scientific insights and experience that helped me strengthen my academic skills and scientific temper.
- dr inż. Emilia Witkowska Nery for her resourceful scientific contribution, for standing by me throughout tough times and believing in my ability.

I am grateful to both of my supervisors for the scientific freedom, creating a positive working atmosphere and making me feel at home. It has been a pleasure working with you!

I thank my parents, Manoharan and Shylaja, my brother Kiran, and my sisters, Ninju and Paru, for being my constants and for never being conventional.

I thank my friends turned family Rasmi, Abhinsree, Aswathi, Nithula, Sanjana, Kiran, Aravind, Anusree, Visakh, Ajmal, Athira, Arshad, Seema, Sujeeth, and Revathi for their love, help, personal support, scientific discussions and criticisms that keeps me going. I am grateful for my friends, Mounika, Sangami, Sakthi, Sharat, Elavenil, Debjita, Ariba, Lucielly, João, Vishnu, Jeena, Praveen and Elżbieta in Warsaw who stood by me, supported me, fed me, and took care of me like family.

I do not have enough words to thank my colleagues from the Sensor Arrays group, Charge Transfer Processes in Hydrodynamic Systems group and other co-workers at the IPC, PAS for their scientific suggestions and collaborations. They have been warm and welcoming, and I am grateful for the time we spent together. I would like to specially mention Elżbieta Jarosińska, Martyna Durka, Wojciech Mazurkiewicz, Marcin Filipiak, Steven Linfield, Magdalena Wiloch, Wojciech Nogala, Ewelina Kuna and Marta Podrażka.

I thank the administration staff of IPC, PAS for their official support during my studies.

Finally, I am grateful for all the right people whom I met at the right time.

This work was partially financed by:

National Centre for Research and Development

within the grant LIDER/38/0138/L-9/17/NCBR/2018

List of Publications

1. Fabrication of ITO microelectrodes and electrode arrays using a low-cost CO_2 laser plotter (DOI: 10.1039/d3lc00266g).

Authors: **Karthika Kappalakandy Valapil**, Marcin Szymon Filipiak, Weronika Rekiel, Elżbieta Jarosińska, Wojciech Nogala, Martin Jönsson-Niedziółka and Emilia Witkowska Nery.

2. Guidelines on the development of sensors and application of data analysis tools for potentiometric electronic tongues (DOI: 10.1088/978-0-7503-3687-1ch3).

Authors: **Karthika Kappalakandy Valapil**, Elżbieta Jarosińska, Marcin Szymon Filipiak, Wojciech Mazurkiewicz and Emilia Witkowska Nery.

3. Paper-based electrochemical sensors and how to make them (Work) (doi.org/10.1002/celc.202000512).

Authors: Wojciech Mazurkiewicz, Marta Podrażka, Elżbieta Jarosińska, **Karthika Kappalakandy Valapil**, Dr. Magdalena Wiloch, Dr. Martin Jönsson-Niedziółka and Dr. Emilia Witkowska Nery

Abstract

This thesis explores the potential of electrochemistry as a non-intrusive, highly sensitive, and cost-effective analytical tool for investigating cellular processes. Emphasizing its broad applicability, the study underscores the ethical advantages of electrochemical biosensing based on cell cultures, presenting a viable alternative to animal testing in medicine, biotechnology, and environmental science.

The long-term objective of this research is to develop a multielectrode design that enables cell growth and electrochemical analysis at various points of 3D cell cultures. Such a setup will be used for drug screening through viability studies by analysing glucose and oxygen consumption in cell cultures of immortalised hepatocytes. In this thesis, I successfully developed low-cost indium tin oxide (ITO) microelectrodes and MEAs, demonstrating their versatility, availability and stable performance. The work also explores the synthesis of osmium polypyridyl complexes and Prussian blue analogues as mediators for glucose sensing.

The first chapter highlights the significance of cell culture-based biosensing, overviews the important factors in electrode fabrication, basic electroanalytical methods and glucose sensing. The second chapter explores different electrode fabrication techniques. The main focus of this chapter features the comprehensive procedures and characterisation of ITO electrodes prepared using a CO_2 laser plotter. In the third chapter, electrochemical impedance spectroscopy (EIS) is used as a tool to illustrate an application of these cost-effective, simple, easy-to-use electrodes. The ITO microelectrode arrays are employed to characterise HeLa, HepG2 and mouse hepatocyte cell cultures through the EIS technique. The measurements showed conductivity variations and surface modifications of the electrodes in response to the attachment and detachment of the cell cultures.

Chapter four discusses biosensing and my current interest in developing a glucose biosensor that can be adaptable for lactate and glutamate measurements. This chapter also describes the importance of mediators in glucose biosensors. Mediators are employed in glucose sensors to enhance the effective flow of electrons between the electrodes and the glucose oxidase enzyme. Therefore, they enhance the sensor's sensitivity and enable precise monitoring of glucose levels. In this work, simultaneously, two strategies are used for the synthesis of mediators. One of the approaches is using a mediating redox hydrogel that contains an osmium polymer complex with the general formula cis-[(Os(N-

$N)_2(PVI)_{n+1}Cl]^+$(n = 9). The synthesis of Prussian Blue analogues of the general formula $A_x[R(CN)_6]_{1-y}\cdot wH_2O$ using flash light sintering is the other approach.

In conclusion, the research underlines the potential of electrochemistry in advancing biosensing for cellular studies and biomedical applications. The successful development of low-cost ITO microelectrodes and MEAs marks an important milestone in this study. They can be employed as any normal working electrodes in the market. As an example of their application, electrochemical impedance spectroscopy was used to study cell culture dynamics. The promising results obtained from the ongoing efforts in synthesizing mediators also open exciting possibilities for glucose biosensing.

Streszczenie

W niniejszej pracy przedstawiono możliwość zastosowania metod elektrochemicznych jako nieinwazyjnego, bardzo czułego i opłacalnego narzędzia analitycznego do badania procesów komórkowych. Podkreślono szerokie zastosowania elektroanalizy, wskazując na etyczne aspekty wykorzystania biosensorów elektrochemicznych w hodowlach komórkowych, które mogą stanowić alternatywę dla eksperymentów z udziałem zwierząt w medycynie, biotechnologii i naukach o środowisku.

Długoterminowym celem badań przedstawionych w niniejszej pracy jest opracowanie układu wieloelektrodowego, który umożliwi wzrost komórek w trójwymiarze i analizę elektrochemiczną w różnych punktach hodowli komórkowej. Układ zostanie wykorzystany do badań przesiewowych leków poprzez ocenę żywotności komórek, w tym analizę zużycia glukozy i tlenu w hodowlach unieśmiertelnionych hepatocytów. W ramach tej pracy pomyślnie opracowano metodę wytwarzania stabilnych i wszechstronnych mikroelektrod i ich macierzy (MEA, ang. microelectrode arrays) z tlenku indu i cyny (ITO), za pomocą niedrogiej i szeroko dostępnej aparatury. W pracy zbadano także możliwość zastosowania kompleksów polipirydylowych osmu i analogów błękitu pruskiego jako mediatorów wykrywania glukozy.

W pierwszym rozdziale podkreślono znaczenie wykorzystania biosensorów w analizie hodowli komórkowych, ważne czynniki związane z wytwarzaniem elektrod, podstawowe metody elektroanalityczne i sposoby pomiaru glukozy. W rozdziale drugim omówiono różne techniki wytwarzania elektrod, zawierając kompleksowe procedury przygotowania elektrod przy użyciu plotera laserowego CO_2 oraz metody ich charakteryzacji. Trzeci rozdział obejmuje wykorzystanie elektrochemicznej spektroskopii impedancyjnej (EIS) jako narzędzia do analizy hodowli komórek HeLa, HepG2 oraz pierwotnych mysich hepatocytów, z wykorzystaniem wcześniej opracowanych macierzy czujników. Pomiary wykazały zmiany przewodności i modyfikacje powierzchni elektrod w odpowiedzi na adhezję komórek do podłoża oraz ich późniejsze podziały.

Rozdział czwarty omawia charakteryzację i wykorzystanie biosensorów z wyszczególnieniem moich obecnych zainteresowań, jakim jest opracowanie biosensora glukozy, który można przystosować do pomiarów mleczanu i glutaminianu. W tym rozdziale zwarto opis znaczenia mediatorów w biosensorach glukozy. Mediatory stosuje się w celu zwiększenia efektywnego przepływu elektronów pomiędzy elektrodą a enzymem - oksydazą glukozową. W efekcie, mediatory zwiększają czułość

czujnika i umożliwiają precyzyjne monitorowanie poziomu glukozy. W niniejszej pracy zbadano możliwość zastosowania dwóch typów mediatorów, polimeru na bazie osmu o wzorze ogólnym cis-$[(Os(N\text{-}N)_2(PVI)_{n+1}Cl]^+$(n = 9) i analogów błękitu pruskiego o wzorze ogólnym $A_x[R(CN)_6]_{1-y}\cdot wH_2O$. Do syntezy analogów błękitu pruskiego wykorzystano nową metodę, w której reakcja indukowana jest impulsami świetlnymi o wysokiej intensywności[ang. flash light sintering].

Podsumowując, niniejsza praca doktorska podkreśla udział metod elektrochemicznych w rozwoju technologii biosensorów do zastosowań biomedycznych, szczególnie w badaniach monitorowania hodowli komórkowych. Kamieniem milowym było opracowanie metody wytwarzania mikroelektrod i ich macierzy na bazie ITO za pomocą niedrogiej i szeroko dostępnej aparatury. Jako przykład zastosowania opracowanych elektrod, wykorzystano elektrochemiczną spektroskopię impedancyjną do badania dynamiki hodowli komórkowych. Obiecujące wyniki uzyskane w zakresie syntezy mediatorów otwierają również ekscytujące możliwości rozwoju biosensorów glukozy.

List of abbreviations

2D	Two-dimensional
3D	Three-dimensional
AC	Alternating current
ACPA	4,4'-azobis (4-cyanopentanoic acid)
AIBN	Azobisisobutyronitrile
ATP	Adenosine triphosphate
CAD	Computer-aided design
CE	Counter electrode
CV	Cyclic voltammetry
DMEM	Dulbecco's Modified Eagle's Medium
DPI	Dots per inch
EDX	Energy-dispersive X-ray spectroscopy
ECIS	Electrical cell-substrate impedance sensing
EIS	Electrochemical impedance spectroscopy
ELISA	Enzyme-linked immunosorbent assay
FcDM	Ferrocenedimethanol
FLS	Flash Light Sintering
GCE	Glassy carbon electrode
GDH	Glucose dehydrogenase
GOx	Glucose oxidase
HCFs	Hexacyanoferrates

HPLC	High-performance liquid chromatography
ITO	Indium tin oxide
LIG	Laser-induced graphene
MEAs	Microelectrode arrays
OCP	Open circuit potential
PB	Prussian Blue
PDMS	Polydimethylsiloxane
PPI	Pulses per inch
PVI	Poly (vinyl imidazole)
RE	Reference electrode
ROS	Reactive oxygen species
SECM	Scanning electrochemical microscopy
SEM	Scanning Electron Microscope
TBACl	Tetrabutylammonium chloride
TEAP	Triethylammonium phosphate
WE	Working electrode

Table of Contents

1 Introduction

Biosensing measurements in cell cultures represent a pivotal frontier in scientific studies, offering a powerful means to unravel the complexities of cellular behaviour. In biosensing, these measurements involve applying advanced techniques to monitor and analyse the physiological responses of cells within a controlled culture environment. The significance of biosensing in cell culture lies in its ability to provide real-time, highly sensitive, and specific information about cellular activities. This approach utilizes various sensors and devices to detect and quantify biomolecules, signalling pathways, and metabolic processes occurring within cultured cells. Such measurements contribute to our understanding of cell functions, including responses to stimuli, viability changes, and cellular metabolism alterations.

This thesis titled " ITO microelectrodes and microelectrode arrays for the analysis of cell cultures and biomedical applications" investigates electrochemistry's potential as a low-cost, highly sensitive, and non-intrusive analytical technique for studying biological processes. Chapter 1 is a general introduction to the thesis. This chapter briefly overviews cell cultures, their scientific relevance, and how measurements can be conducted in cell cultures. An outline of biosensors, fundamental electroanalytical methods employed for biosensing and two electrochemical mediators for glucose sensing are provided here. Additionally, it includes descriptions of microelectrodes and microelectrode arrays (MEAs).

1.1 Cell cultures as a robust scientific tool

Cell cultures are one of the most important and versatile research models. In practice, cell culturing refers to isolating cells from eukaryotes or prokaryotes and enabling their growth under favourable physiological conditions[1]. Cell cultures offer vast possibilities for studies in numerous scientific domains, from biology, biochemistry, medicine, physiology, metabolism, etc. Ross G. Harrison was the first to employ this method to investigate the origin and development of nerve fibres *in vitro*. In 1907 he isolated small parts of frog embryonic tissue known to yield nerve fibres, and the end of a growing nerve was brought under direct observation while alive[2]. Subsequently, the process has been continuously improved and modified so that cell-related experiments can be carried out easily with the help of cell banking facilities[3]. The main advantages of using cell cultures, compared to whole organisms or tissues, are the cost and ethical considerations. Cell cultures offer a more cost-effective

and controlled experimental platform, reducing reliance on animal models while eliminating ethical concerns and providing insights into cellular processes with human relevance. Cell cultures are simple to work with, homogenous, and provide more flexibility in choosing the sensing techniques than experiments with whole organisms. Besides, due to their vast array of biomolecular mechanisms, living cells make interesting choices as a model system[4]. In such a model we can manipulate biomolecular pathways directly or through genes to answer questions related to how the cell operates. Additionally, the uniformity of cell populations and well-defined culture systems eliminate interfering genetic and environmental variables. This allows data generation with a high degree of reproducibility and consistency that is not possible when studying whole organ systems[1].

The cells used in laboratories can generally be divided into two categories: primary cells and established cell lines[5,6]. Primary cells are the cells that are directly prepared from an organism's tissues. Regarding the bulk production of primary cultures for experimental works, it is typical to disaggregate tissue samples to create a cell suspension that can form a cell monolayer under suitable culture circumstances. The source of the original tissue sample plays an essential role in the success and reproducibility of these cultures. Important factors to consider include species, age, sex, tissue type, and disease state. Furthermore, it's critical to demonstrate that the *in vitro* model shares the intended desired traits with the species of origin. If grown under the right microenvironment and physiological conditions, primary cells can grow and proliferate, but they are only able to do so a finite number of times[7]. This is because each time the cells divides, part of its DNA's telomere is lost and after a certain number of cell divisions, they reach senescence and proliferation stops[8]. During the senescence state, the primary cells reach a maximum passage limit called the 'Hayflick limit'. The culture remains remarkably stable and retain characteristics of original tissue cells only until the 'Hayflick limit' is reached[9,10]. On the other hand, established cell lines are able to escape the normal constrains of the cell cycles and grow indefinitely. This make them extremely useful for long-term research. These immortal cell lines were primarily isolated by disaggregation and culture of tissue from clinical tumours and embryos. **Figure 1** illustrates the sequence of steps involved in the culture of primary cells and established cell lines. During the generation of novel cell lines, studies have employed a range of methods like transforming primary cells with viral oncogenes, irradiation, chemical treatments, or recombinant vectors encoding oncogenes. The first human cell line that could divide and grow endlessly in a laboratory is the HeLa cell line. They are from cervical carcinoma tissue of Henrietta Lacks, isolated (without her knowledge and consent) by George Otto Gey and colleagues[7]. HeLa cells are also one of the oldest and most

used human cell lines. 3T3, HEK-293T cells, HepG2, A549 cells are some of the other popular immortalized cell lines.

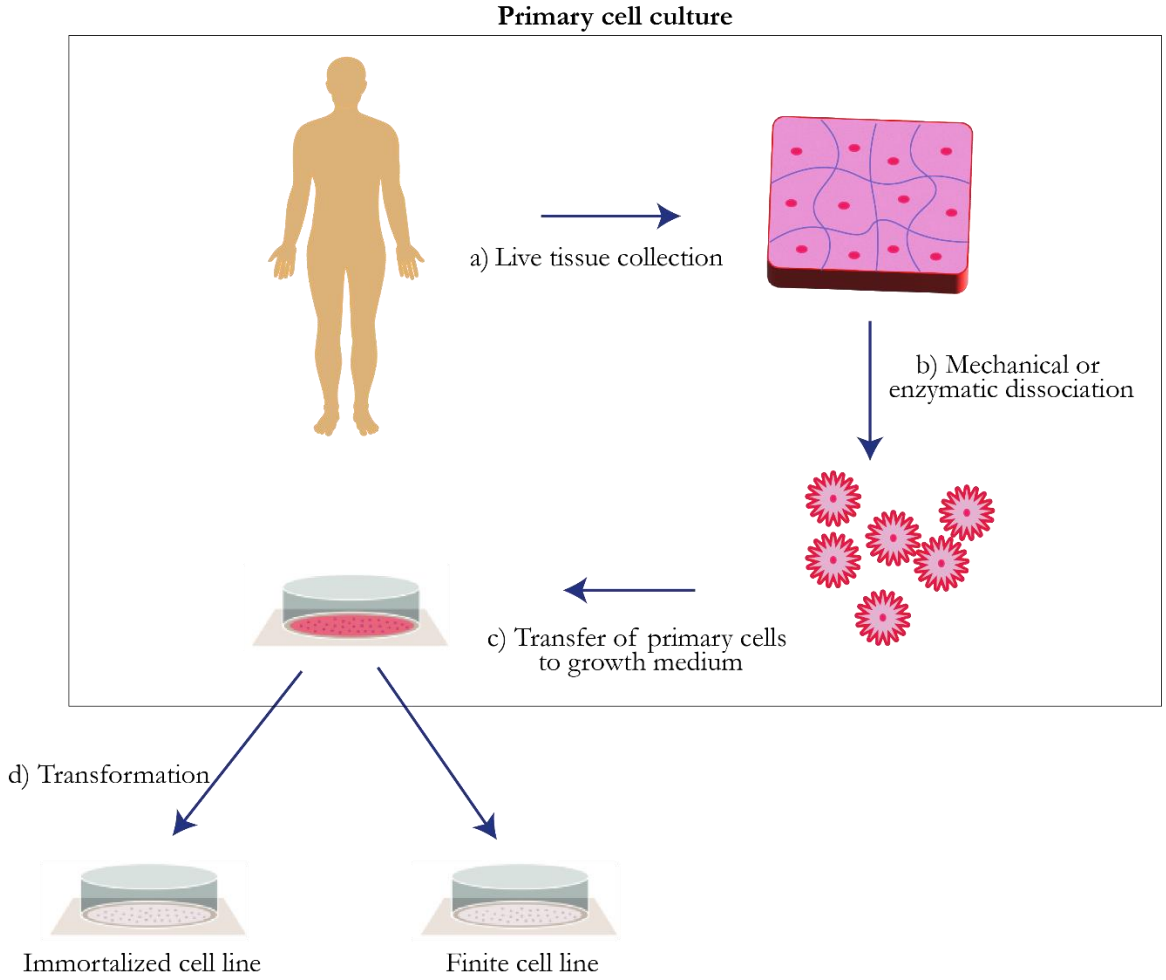

Fig. 1 The sequence of steps involved in the culture of primary cells and established (immortalized) cell lines. First, tissue is collected from a living organism (a), then tissue samples are disaggregated (b) to create a cell suspension that can form a cell monolayer under suitable growth media (c). Under proper microenvironment and physiological conditions, primary cells can grow and proliferate a finite number of times. After genetic transformation, the primary cells give rise to an immortalized cell line (d) and has the potential to divide indefinitely.

Although cell cultures on petri dishes and well plates through in vitro experiments have contributed amply to our present understanding, there is much more to be known in this domain. Primary cells and immortalized cell lines usually adopt one of the two growing forms; they either grow as monolayers or are free-floating in culture media. Cells grown as monolayers are referred to as 2-dimensional cultures and are adherent in nature. On the other hand, free-floating cells are the result of a suspension culture, where cell proliferation occurs in a 3-dimensional manner[11–15].

In 2-dimensional cell culture, cells are grown on a flat and rigid surface, and their cell proliferation is at a rapid pace. All the cells receive equal amounts of nutrients and are exposed to the same growth conditions; hence, they are highly replicable, and their behaviours can be easily interpreted. The monolayer cell culture is very well suited for long-term cultures, and most cell-based assays consider this technique very valuable. However, 2-dimensional cell cultures do not sufficiently reflect *in-vivo*-like cell structure or function. Most of the cells in an *in vivo* environment are encircled by extracellular matrix and other cells in a three-dimensional manner. The 3D cultures allow cells to grow in a more native-like microenvironment. In such systems, cells form aggregates or spheroids, and the cell structure is preserved by mimicking cell-cell interactions, cell differentiation, cell-extracellular matrix regulatory mechanisms and signalling networks[11,12]. Therefore, the nutrient distribution in not expected to be equal among all cells in the culture. Similarly, the cells experience varying availability of oxygen, metabolites and signalling molecules. Based on the method by which cells are grown, 3D cell culture models can be categorized into: i) suspension cultures on non-adherent plates; ii) cultures in concentrated medium or in gel-like substances; and iii) cultures on a scaffold[14,15].

The 3-dimensional cell cultures find applications in different fields of research by acting as a bridge between conventional 2-dimensional monolayer systems and animal models[15]. **Figure 2** provides a schematic model of 2D and 3D cell cultures. There is no denying that 3-dimensional cell cultures are better than the 2-D in terms of resemblance to the living organism. They are widely studied and are still improving. In some cases, the internal environment resembles the core cells in tumour cells, enabling them to recreate the characteristics and structure of tumour cells *in vivo*. Therefore, these models provide a more precise representation of the impacts of drugs or other experiments[11–13]. Nevertheless, the complete transition of the research activities to the 3-dimensional cultures is restricted by their higher cost and lack of proper analytical techniques.

1.2 Analysis of cell cultures

Cell cultures provide an opportunity to study the behaviour of individual cells in a controlled environment. They have evolved as one of the crucial components in cellular and molecular biology laboratories by acting as a good model system for studying specific physiological and biochemical processes. Some of the main research interests include understanding cell metabolism[16–18], cell viability[19–21], proliferation[21–23], migration[24–26], differentiation[27–29], oxidative stress[30–32], signaling[11,33], neurotransmission[34–38], electrophysiology[37], cell morphology[39], gene expression[11] and more. Apart from basic research they are also suitable for high-throughput screening (HTS) in areas of

biopharmaceutical production, medical studies, the life sciences, and related fields. Their main applications include cancer research, stem cell research, drug discovery, tumour models and immunotherapy, tissue engineering[11], vaccine production, disease modeling[40], and more.

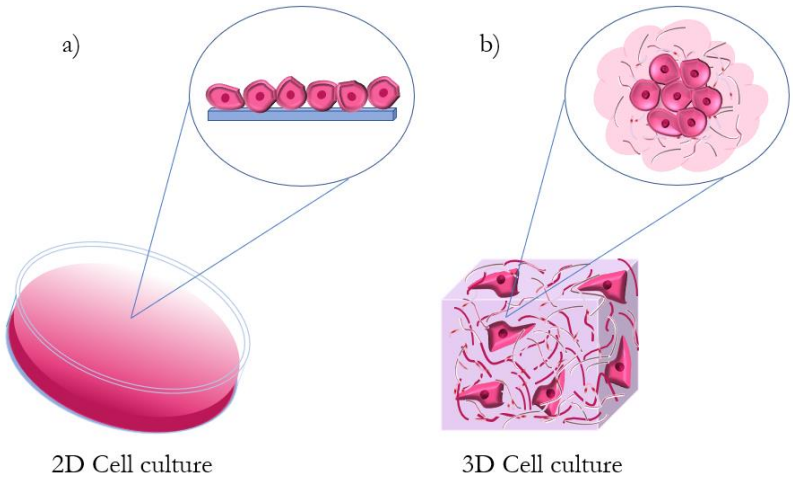

Fig. 2 Schematic models of a) 2-dimensional (2D) and b) 3-dimensional (3D) cell cultures.

Cell culture metabolism refers to the biochemical processes that occur within cells when they are grown in a laboratory environment. These processes are similar to that occur in cells *in vivo* (in living organisms), but they can be influenced by a variety of factors, including the composition of the culture medium, the growth conditions, and the cell type. Cell culture metabolism involves a variety of processes; a) energy production to carry out their functions; cells produce energy through processes such as glycolysis, the citric acid cycle, and oxidative phosphorylation. b) Biosynthesis; the energy produced is used to synthesize molecules such as proteins, lipids, and nucleic acids. c) Waste elimination; cells produce waste products because of their metabolic processes. These waste products can accumulate and affect cell growth and function. In cell cultures, waste products can be removed from the culture medium through processes such as medium change and dialysis. d)Regulation; cell metabolism is regulated by a variety of factors, including hormones, growth factors, and signalling pathways. These factors can affect the way cells use energy and synthesize molecules[17,41–43].

A viable cell is one that is alive, functioning normally, and able to carry out its regular activities[19,21]. Cell viability is the ability of cells to maintain their metabolic and physiological functions. It is a vital indicator of the well-being of cells through function of certain genes, proteins, and pathways that affect cell survival or death after exposure to toxic agents. It is also a critical aspect of many cellular processes, including tissue development, wound healing, and immune response. There are many

factors that can affect cell viability, including environmental factors such as temperature, pH, glucose, and oxygen levels, as well as genetic and epigenetic factors that regulate cellular processes. In addition, external factors such as drugs, toxins, and environmental stressors can also affect cell viability by altering cellular processes and causing damage to cellular components. These reasons make cell viability assessment an extremely helpful means to study cellular and higher-level behaviour of organisms. It is an important parameter in drug discovery, toxicology, and tissue engineering, as it can be used to evaluate the effectiveness of drugs, assess the toxicity of chemicals, monitor the growth and differentiation of cells in tissue engineering applications[44,45].

In addition to primary cell cultures and immortalized cell lines, three-dimensional (3D) cultures and organoids are emerging as important tools for studying cell viability in a more complex and physiologically relevant environment[46]. Researchers can use a variety of assays to evaluate the number of viable cells, including assays for measuring metabolic activity, proliferation, apoptosis, and cell membrane integrity. These tests rely on a number of cellular processes, including enzyme activity, cell membrane permeability, cell adhesion, adenosine triphosphate (ATP) synthesis, coenzyme creation, and nucleotide absorption activity. Such tests can also be based on dyes or stains that selectively penetrate living cells or dead cells. They can be broadly classified as; (i)dye exclusion assays, (ii)colorimetric assays, (iii)fluorometric assays, (iv)luminometric assays, and (v)flowcytometric assays.[19]

Another important reason to study cell culture is that they can contribute to our understanding of the role of oxidative stress in various diseases, and conditions. Oxidative stress is a condition that arises when there is an imbalance between the production of reactive oxygen species (ROS) and the cell's ability to detoxify them[30–32]. ROS are highly reactive molecules that can damage cellular components such as DNA, proteins, and lipids, leading to cell dysfunction and death. Cell cultures can be exposed to various oxidative stressors, such as hydrogen peroxide, paraquat, and tert-butyl hydroperoxide, to induce oxidative stress[47]. Researchers can measure the levels of ROS, antioxidant enzymes, and markers of oxidative damage in the cells to evaluate the effects of the stressors. For example, one common approach is to measure the levels of intracellular ROS using fluorescent probes that are sensitive to oxidation. The level of oxidative damage to cellular components can also be assessed by measuring markers such as lipid peroxidation products or protein carbonyls. In addition, cell cultures can be used to study the protective effects of antioxidant compounds, such as vitamins C and E, or natural compounds found in plants, such as flavonoids and phenolic acids[47]. Researchers can examine

the effects of these compounds on the levels of ROS and oxidative damage in the cells and identify potential mechanisms of action.

Studying signaling[11] and neurotransmission[34,36–38] of the organisms are possible with the analysis of neural cell cultures. One of the ways cell cultures are used to study signalling and neurotransmission is by measuring the levels of neurotransmitters and their metabolites in the culture medium. This can be done using techniques such as high-performance liquid chromatography (HPLC)[48], enzyme-linked immunosorbent assay (ELISA)[49], NMR[50] and electrochemistry[36–38]. By measuring the release of neurotransmitters from cells in response to different stimuli, researchers can identify the signalling pathways involved in neurotransmission. This makes it possible to evaluate the effects of drugs or other compounds on these pathways. Cell cultures can also be used to investigate the expression and function of neurotransmitter receptors, which play a critical role in transmitting signals between neurons. By growing cells expressing specific receptors and studying their responses to different stimuli, researchers can identify the functional properties of these receptors and their role in neurotransmission. In addition, cell cultures can be used to study the downstream signalling pathways activated by neurotransmitter receptors[35]. By examining the effects of specific drugs or signalling molecules on these pathways, researchers can identify potential therapeutic targets for treating disorders of the nervous system, such as depression, anxiety, Parkinson's disease or schizophrenia.

1.3 The prospects of using electrochemistry to understand biological processes in cell cultures

Electrochemistry is the study of how electricity and chemicals interact with each other[51–55]. In the field of electrochemistry, cell cultures are used to study the effects of electrical and chemical stimuli on live cells. Living cells, which exist at the interface of biology and electronics, have been a very effective aid to electrochemists for exploring biological mechanisms through their perspective. By measuring the electrochemical properties of biological molecules, cells, and tissues, electrochemical techniques have revolutionized our understanding of fundamental biological processes. In this context, we will explore the applications of electrochemistry in biology, highlighting the main classification, key techniques, and their contributions to our understanding of biological systems. Electrochemistry in biology can be very specific, as it allows for the measurement of various electrochemical parameters with high sensitivity and selectivity.

Cell cultures has been recognized as a valuable technique for investigations centred on cells[12]. Therefore, many cell culture models are used to analyse the performance of electrochemical biosensors[56]. The measurements in cell culture can be easily adapted to accommodate different investigational needs, or to extend the experiments to *in-vivo* systems. Cells can be grown in large quantities, making them readily available for sensing applications. This allows for a high degree of flexibility in experimental design and enables researchers to investigate electrochemical phenomena in cells and tissues with high precision and accuracy. Once cell culture-based experimental conditions are optimized, results statistically analysed and all the necessary test hypotheses are completed, and scientifically proven, the studies can be extended to more complex animal studies. This way provides a cost-effective, reproducible, and ethical approach for examining molecular mechanisms of living beings and identifying potential therapeutic targets.

1.3.1 Electrochemical biosensors

According to the IUPAC definition, a biosensor is a device that uses specific biochemical reactions mediated by isolated enzymes, immunosystems, tissues, organelles or whole cells to detect chemical compounds by electrical, thermal or optical signals[57]. As per a more commonly used definition, biosensors are analytical devices designed for the detection of biomolecules. A biosensor measures biological or chemical reactions by producing signals corresponding to the concentration of an analyte involved in the reaction[58,59]. The first description of biosensors by Leland Clark and Champ Lyons in 1962 was about electrode systems for continuous monitoring in cardiovascular surgeries[60]. Since then, researchers have paid close attention to the development of electrochemical biosensors; as a result, the number of studies on electrochemical biosensors has expanded, and they have been a hot topic in scientific research for several decades. The field has been investigated through theoretical and experimental works, including other types of biosensors, such as optical, thermometric, piezoelectric, magnetic, and combinations of more than one type[61].

The use of cell cultures for biosensing applications can be mainly divided into two parts, electrochemical and optical sensing techniques. Cell analysis has traditionally been carried out optically and the frequently used techniques include fluorescence microscopy, surface plasmon resonance, and Raman spectroscopy[62]. Technologies like optical coherence tomography and multiphoton microscopy are used for 3D analysis. The price of the aforementioned imaging equipment, and light scattering found in 3D cultures, as well as their limited penetration, points to the necessity for novel analytical techniques. In addition to miniature optical sensors and optical fibre-based systems, electrochemical

methods have also proven to be excellent choices for cell-based studies[62–64]. Although optical biosensing approaches are highly sensitive and provide rapid detection times, electrochemical analysis offers a complementing strategy. Both optical and electrochemical biosensing have different uses, and therefore different results are obtained from each.

The main interests of this work lie in electrochemical biosensors. An electrochemical biosensor combines biological recognition elements with electrochemical sensing techniques to detect and quantify specific target molecules. A biosensor typically consists of three main components: a biological recognition element, a transducer, and a signal processor (**Fig.3**)[61,65,66]. The biological recognition element (e.g. enzyme, antibody, nucleic acid) of the biosensor is designed to detect the specific biological analyte of interest. It typically interacts with the analyte and may lead to a signal change that can be detected by the transducer. The transducer is responsible for converting the signal generated by the biological recognition element into an electrochemical or optical signal that can be measured. The processed signal can then be displayed on a display device such as a digital readout or computer screen. Within the biosensor, each of these elements has a specific purpose. Once the choice of biological recognition element and the type of measurements to be performed are confirmed, the crucial step is designing of the transducer. The critical component of the transducer is the electrode, which serves as the interface between the biorecognition element and the electronic readout. One of the main benefits is that electrochemical techniques can provide real-time measurements of cell behaviour, such as changes in metabolism or the release of signalling molecules. This is because electrochemical sensors can detect chemical and electrical changes in the extracellular environment, which are directly related to cellular activity. Electrochemical sensors are also very versatile, as they can measure a wide range of analytes, including neurotransmitters, metabolites, and proteins. Besides, electrochemical biosensors can be successfully miniaturized as demonstrated by their incorporation into the tips of scanning-probe microscopes, microelectrodes, or electrode arrays, which enable highly localized analyte detection[67]. As the field continues to advance, new applications and discoveries emerged leading to breakthroughs in medicine, biotechnology, and environmental science.

Given the crucial roles biomolecules play in regulating physiological functions, measuring them is of great interest. Fluctuations in the amounts of biomolecules can be the root cause of development of a malfunction or disease. Therefore, any method that can determine the concentration, evaluate the mechanism, or detect the presence of biomolecules can be employed as a crucial preventative, diagnostic, or therapeutic tool. Biomolecules are released quickly in small amounts from specific places

within a complex microenvironment, making it difficult to measure them. Electrochemical biosensors are commonly employed to meet intricate measurement requirements. Electrochemical biosensors allow the analysis of small sample volumes because in general they are not heavily reliant on reaction volume. In biochemical tests like immunoassays that requires minimal sample preparation, electrochemical detection can achieve low detection limits. Compared to the spectrophotometric detections, electrochemical analysis remains least affected by chromophores, fluorophores, and other sample components. Hence, electrochemical experiments can be employed to analyse whole blood or similarly complex samples and the measurements can be designed to eliminate interference from fat globules, red blood cells, haemoglobin, or bilirubin. Numerous electrochemical sensors have been fashioned for biomolecular detection based on various measurement conditions[58,59,68,69]. The study of cell membranes and the transport of ions across them,[70,71] and the investigation of redox reactions in living organisms (such as respiration and photosynthesis)[72,73] are important applications of electrochemical biosensors. Analysis of neurotransmitters and their interactions with receptors[34–38,74–76], understanding the mechanisms of electrochemical signalling in the nervous system[37,77–79], detection of DNA damage and mutations[80,81], development of biosensors for medical diagnosis and treatment[68,69,82,83], evaluation of drug efficacy and toxicity[84,85], development of implantable devices for drug delivery and monitoring[86,87], characterization of proteins and their binding interactions[88–91], monitoring of glucose and other metabolites in blood for diabetes management[92–94], are other significant domains of electrochemical studies.

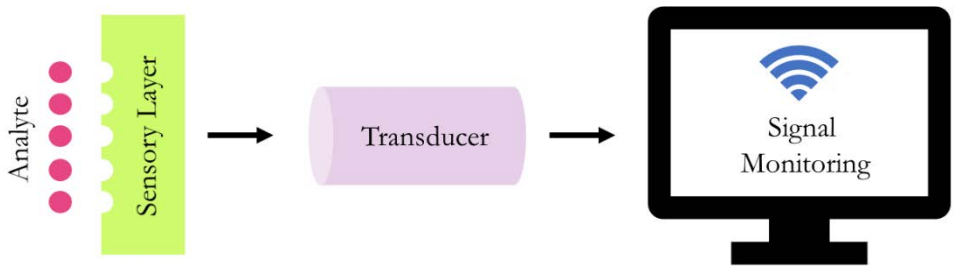

Fig.3 General components of a biosensor.

1.3.2 Miniaturization of electrochemical biosensors

Miniaturized electrochemical biosensors offer several advantages over conventional sensors. Miniaturized sensors are widely investigated due to their ease of portability and integration into compact devices. They are suitable for cheap and mass production, enabling point-of-care applications, reducing sample volumes, reducing analysis time, and enabling multiplexed measurement

options.[95–97] They can also be integrated into wearable technology, continuously monitoring biomarkers and other properties. The area and size of all the components, especially the electrodes, play an important role in the performances and activities of miniaturized sensors. Generally, miniaturized systems have micro to nanoscale dimensions electrodes and a higher sensitivity than a larger macro electrode. Macro electrodes have dimensions in the cm to mm range and have a large surface area, which can accommodate more biomolecules. However, macro electrodes are often made of materials that are not biocompatible, which can lead to cytotoxicity and tissue damage in biological applications. In the case of noble metals, larger electrodes can notably increase the cost of the final device. The large size of macro electrodes can make them difficult to integrate into miniaturized biosensors, limiting their potential use in portable and wearable devices.

This work shines a light on the importance of microelectrodes. Microelectrodes (MEs) are electrodes with at least one critical parameter on the micron scale. William Hyde Wollaston presented them for the first time in 1801, and they were used for the first measurements in biological tissues to measure the concentration of oxygen in the 1940s[96,98]. Microelectrodes are being used in a wide range of research fields, including biology, corrosion, energy, kinetics, instrument development, and surface modification[96,98]. They are typically made of a conductive material like carbon or metal. Microelectrodes can be used to detect a wide range of biomolecules, the common targets are glucose, neurotransmitters, pH, and oxygen. The use of microelectrode systems for electrochemical biosensors is appealing due to their smaller, less invasive footprint. As a result of reduced electrode size, electrochemical detection of molecules in and across limited areas like isolated bio-membranes and cells has opened up interesting new study directions. Smaller electrodes enable localized recordings of both analytes of interest and concentration profiles. Microelectrodes offer additional benefits, such as minimized ohmic resistance (iR) stemming from low faradaic currents ($\leq$ nA), increased current densities, and enhanced signal-to-noise (S/N) ratios[98].

Often a set of microelectrodes closely spaced or positioned on a single substrate, allowing real-time simultaneous measurements at multiple sites are effectively employed. They are collectively called a microelectrode arrays (MEAs). The main difference between a microelectrode and a microelectrode array is that the arrays allow for spatially resolved measurement, whereas microelectrodes are limited to single-point measurements. Additionally, MEAs are useful for studying complex systems, such as neural networks, where multiple measurements are required to understand the system's behavior[98]. MEAs that monitor multiple single neuron activities are becoming an indispensable part of

electrophysiological studies. Although there are strong incentives for the development of miniature electrochemical systems for biosensors that can identify a variety of biological molecules and stimuli, and while there are some examples of *in vitro* and/or *in vivo* microelectrode use in biosensing in the literature, a rapid, easy to fabricate, low-cost system is still needed.

1.3.3 The choice of electrode materials

This section discusses the significance of the nature of a biosensing electrode. An appropriate electrode material should be stable, have low electrochemical impedance and generate a minimal foreign body response. Microelectrodes for biosensing have been made from a wide range of materials, mostly noble metals like platinum or gold are used. Carbon materials, certain metal oxides (e.g. ITO), semiconductors, or conducting polymers are also employed frequently[99]. Based on established scientific literature[95,100–103] and credible experiments in basic biomolecule sensing, platinum and ITO have been selected as our preferred electrode materials.

Platinum

Platinum is a well-known material suitable for a wide range of purposes, from sensors to catalysts. Due to its superior chemical and electrical properties, platinum is widely used as an electrode material in electrochemistry. Some of the domains that use platinum electrodes include fuel cells[104,105], metal-air batteries[105,106], electrochemical sensors[105,107], neural stimulation[105,108] and mechanical actuators[105,109]. Biomedical researchers and engineers prefer platinum as an electrode material because of its high electrical conductivity, inertness to oxidation, stability, and low toxicity[99,101]. The inert nature of platinum enables the electrodes to maintain their performance and longevity as biosensors throughout the measurement process. Pt-based biosensors are employed in the medical, agricultural, and food sectors[101]. Gluconic acid, glutamic acid, lactic acid, uric acid, and several carcinogens may all be quickly and effectively detected in human fluids using platinum-based biosensors[101].

Platinum metal can be processed using various fabrication techniques to form electrodes of different shapes, sizes and textures. Electrochemical deposition (ED), magnetron sputtering, chemical vapor deposition (CVD), thermal evaporation, atomic layer deposition (ALD), photo-deposition (PD) and plasma assisted deposition are well known methods for the synthesis of platinum or platinum-based electrodes[110].

Efforts were made to fabricate Pt electrodes using a combination of sputtering and photolithography. Sputter deposition of platinum is a thin-film coating process where platinum atoms are dislodged from

a solid platinum target through bombardment with high-energy ions. The free atoms travel through a vacuum environment and then adhere to a substrate, eventually forming a thin film. Sputter-deposition is the preferred method for achieving a controlled and uniform distribution of Pt on a substrate, especially when aiming for low Pt loading and a narrow particle size distribution. Substrates function as a foundation onto which the electrode material is deposited. The substrate can either be removed afterwards, resulting in a freestanding electrode material, or it can be retained to offer both mechanical support and a site for attaching wires, where applicable[110–113].

Photolithography requires an ultra-clean environment free of even smaller particles that can affect the precision of microfabrication. Photolithography facilities often require specialized setups, such as vibration isolation and controlled temperature and humidity, beyond the standard conditions provided by a typical clean room that was accessible during this work. The whole fabrication procedure was difficult and time consuming for the preparation of microelectrodes as required for my research work. Therefore, using commercially available insulated platinum wires were preferred over preparing them through photolithography due to cost-effectiveness, time efficiency, and accessibility. Additionally, the quality of commercial wires is consistent offering a ready-made solution.

Indium tin oxide

Indium Tin oxide (ITO) is clear and transparent when it is a thin film, and it is yellowish to grey when it is a bulk material. It is a combination of indium oxide (In_2O_3) and tin oxide (SnO_2) in a typical weight ratio of 90:10[114]. Due to its excellent electric and optical characteristics (transmittance: >83%), such as low electrochemical background response, wide working potential window[115], low resistivity (R_s = ~5 Ω/sq.), high visible transmittance, high infrared reflectivity, and ultraviolet absorption[114,116], it is commonly used as an electrode substrate. It is attractive for scientific applications because of properties including excellent chemical stability, good surface area activity, ease of use, and commercial availability. ITO is often employed in electrochemistry for electroanalytic devices[117], sensing[102] and biosensing[103], as well as in optoelectronics[118], primarily in light-emitting diodes[119], liquid crystal displays[120], solar cells[121], transistors[122], and gas sensors[123].

With commercially accessible high grade ITO and established direct deposition techniques[124,125], the definition of patterns remains a potential bottleneck. Despite its popularity and widespread use, ITO electrode manufacturing currently lacks a quick, adaptable, economical, and accurate fabrication

approach that might replace the expensive and time-consuming lithography that is frequently employed to define patterns.

The manufacturing of ITO electrodes with the use of lasers marked a significant advancement in the direction of extremely reproducible, flexible, quick, and easy patterning. According to their function, laser sources may be broadly categorized into continuous wave lasers and pulsed lasers[126–128]. Additionally, depending on their gain medium, they can be classified into subcategories: gas lasers (for example, helium-neon lasers, argon ion lasers, and carbon dioxide lasers), solid-state lasers (such as ruby and Nd:YAG lasers), semiconductor lasers (such as diode lasers), and fibre lasers. Furthermore, gas-based lasers are classified into neutral atom lasers, ion lasers, molecular lasers, and excimer lasers. Out of the commercially available lasers, the Nd:YAG laser, semiconductor lasers (AlGaAs, GaAsSb, and GaAlSb), CO_2 laser, and excimer lasers (XeCl, KrF) are the ones that are most employed for surface engineering. The efficiency of the laser contact with the substrate is determined by the laser beam's intensity and the time of interaction. Another crucial element that influences the absorption of laser radiation is the wavelength of the incident laser beams[128].

ITO electrodes can be made using procedures like Laser Digital Patterning (LDP)[129] and Pulsed Laser Deposition (PLD)[130]. The use of a nanosecond Nd:YAG infrared laser to design ITO on its glass substrate by indirect laser ablation was reported[131]. Another interesting example uses the self-organization phenomena known as laser-induced periodic surface structures (LIPSS) to create patterns on ITO films deposited on borosilicate glass by scanning a linearly polarized nanosecond pulsed laser beam[132]. In addition to these instances, there are more publications on the laser patterning of ITO utilizing various lasers, such as a UV-excimer laser and a femtosecond-pulsed laser[133], but none of them has the benefit of being a widely accessible and ideally economical method of fabricating microelectrodes.

Despite their lower resolution and edge-quality limitations, CO_2 lasers are among the most widely used and well-established industrial and laboratory laser sources. First of all, CO_2 lasers are renowned for their high power and adaptability, making them appropriate for a diverse range of applications. CO_2 lasers are the highest power continuous wave lasers available on the market right now. They emit infrared light with a wavelength of 10.6 μm and are often employed in laser cutting, welding, drilling, and surface treatment owing to their great efficiency[134]. Due to their reduced capital and maintenance costs, CO_2 lasers are more economical than other high-power lasers, which makes them a popular

option for small enterprises like copy shops. They are far less expensive compared to the premium equipment models (**Table A1**). They are simple to maintain, require minimal assistance, and are easy to operate. Compared to many other laser types, they also have a longer lifespan. Even though CO_2 lasers may not provide the finest resolution or sharpest edges, their performance can be enhanced with the right settings, such as focus, speed, and power setting optimization. Moreover, the flaws may not have a significant impact depending on the application. In our circumstances, the advantages of CO_2 lasers surpass the shortcomings since their usage enables the performance of the described techniques in a limited resource environment. To further support this argument, I conducted tests using electrodes prepared at a nearby printing shop using the developed method.

CO_2 lasers are also utilized in processes for preparing components of microfluidic systems. In order to prepare a rapid prototype of polydimethylsiloxane (PDMS) microfluidic structures without a replication template, a novel laser through-cutting and pattern transfer process was developed. Use of a CO_2 laser significantly reduced the time and quantity of equipment required for microchannel processing[135]. Xurography, the method of using laser cutting to quickly transfer a pattern drawn in a computer-aided design (CAD) software to a plastic film or PDMS slab for microfluidics, has grown in popularity as CO_2 lasers have gotten cheaper and simpler to operate[136]. A microfluidic sensor that was recently introduced[137] is based on this technology. The sensor evaluates the biomass of MRC-5 fibroblast cells cultured in the microfluidic bioreactor. Apart from conventional PDMS channels, CO_2 lasers have also been used to pattern paper-based microfluidic devices and modify the surface properties of the paper[138,139]. CO_2 lasers are also used to directly make electrodes by carbonizing polymers to create laser-induced graphene (LIG) materials, either freestanding or on a backing material, such as ITO[140,141]. A possible step forward in lowering the high cost of utilizing laser technology for sensing applications is provided by the use of CO_2 laser processing.

In this study, I employed a CO_2-laser to directly imprint a desired electrode pattern on ITO coated glass surfaces using computer-aided design in AutoCAD, to obtain electrodes with widths as small as 25 μm. The resulting electrodes were characterized using electrochemical techniques, and the geometric characteristics of the electrodes were identified using optical and scanning electron microscopes. A supplementary technique was employed to make electrodes of larger area for which direct laser cutting's high resolution was not mandatory. In this method, a stencil was prepared using the laser, and the undesired ITO (outside the electrodes) was removed using wet etching. Although the resolution is reduced, this process is far more efficient than utilizing a laser to directly cut large

regions. The combination of the two techniques creates a comprehensive toolkit that enables the quick and inexpensive production of ITO electrodes for a wide range of applications (detailed description is provided in chapter 2). A low-budget innovation with limited resources is demonstrated here. Using a basic CO_2 laser plotter that is commonly available at a local copy shops, it is possible to fabricate micro electrodes and microelectrode arrays. These MEAs can be easily employed for *in vitro* studies. As an application, impedance spectroscopy is used to analyse cell cultures using the fabricated electrodes. The detailed description of these measurements is provided in chapter 3.

1.3.4 Electroanalytical Methods

Identifying any possible charge transfer processes in the electrochemical systems are the main source of information for the scientists. Potentials and/or currents generated by this charge-transfer mechanism can be measured and connected, theoretically or through calibration, to the chemical concentration of analyte in the solution in an electrochemical cell. An electrochemical cell is a system comprising a minimum of two electron conductors (electrodes) in contact with ionic conductors (electrolytes) and redox reactions take place in the set-up[142,143]. According to the specifics of the experimental design, these methods can be broadly classified into two groups: measurements at zero current conditions, generally referred to as potentiometric, and ones that involve current flow at an electrode under potential control, generally referred to as voltammetric[144].

In electrochemical biosensing, whole cells or cellular fragments can be used along with a transducer interface to generate a response to particular biological substrates or inhibitors[145]. This interaction can be converted to a measurable electronic output signal, which can be transformed into a quantitative measure of the analyte concentration. Depending on the constituents and analytes of interest, there are several types of biosensors like enzyme-based electrochemical sensors, electrochemical immuno- and aptasensors, pH sensors, and multiparametric microphysiometers. Examples of electrochemical techniques that are used for biosensing in cell cultures include potentiometry, voltammetry, amperometry, conductometry, and impedance spectroscopy.

1.3.4.1 Voltammetry/Amperometry

The voltammetry technique scans a potential across a predetermined range and uses controlled, time-dependent applied voltage to detect current. The current is measured by introducing a potential difference between a working electrode and a counter electrode. The ensuing plot of

current versus applied potential is a voltammogram. It is referred to as the electrochemical equivalent of a spectrum in spectroscopy, providing quantitative and qualitative data on the species involved in the oxidation or reduction. Several voltammetry techniques are employed for the study of redox activity of enzymes, proteins, and other biological molecules. Of these methods, cyclic voltammetry and amperometry are the most interesting for this study. As the name suggests, in cyclic voltammetry the potential is swept from an initial to final potential and back to the starting potential, often at the same sweep rate[144]. The resulting voltammogram is a current versus potential (I-E) curve. It is one of the fastest voltammetry techniques available, however not the most sensitive one. Amperometry is a specific case of voltammetry, in which a constant potential is maintained at the working electrode and current is measured as a function of time. Since there is no change in the potential, amperometry does not produce a voltammogram. Amperometric biosensors is commonly used to detect neurotransmitters, metabolites, and other small molecules that are important in cellular signalling[143].

1.3.4.2 Potentiometry

Potentiometry measures the potential difference between the two electrodes in a sample solution of an electrochemical cell under static conditions. This measurement is carried out in situations where there is minimal or negligible current flow between the electrodes[143,146]. It is based on the principle that the potential difference between the electrodes is proportional to the activity of ions of the analyte in the solution. This technique is best performed using ion-selective membrane electrodes. The glass pH electrode and ion-selective electrodes for ions like K^+, Ca^{2+}, Na^+, and Cl^- are very common examples of these kind. The sensors in these systems facilitates the selective detection of targeted ions. This recognition establishes a potential difference that is measured using a high impedance electrometer. Potentiometry is commonly used in various fields such as clinical diagnostics, environmental monitoring, and pharmaceutical analysis due to its simplicity, accuracy, and speed of measurement[143].

1.3.4.3 Conductometry

It is an electrochemical technique that measures the ability of a sample to conduct an electrical current. It is based on the principle that the ability of a solution to conduct electricity is influenced by the concentration and nature of ions present. In conductometry, a conductometer or conductivity meter is used, which consists of an electrode pair (usually made of platinum) that are immersed in the solution being analysed. An electric voltage is passed through the electrodes, the resulting current is

measured, and the corresponding conductivity is computed. By measuring changes in conductivity over time or in response to different stimuli, conductometry can provide valuable information about the chemical and physical properties of the solution, such as the presence of ions, the pH, or the temperature. Enzymes that generate charged products and, as a result ionic strength changes and enhanced conductivity, are frequently found in conductometric biosensors. Such systems are favourable as they do not require the use of a reference electrode; they work at low-amplitude alternating voltage, which prevents Faraday processes on electrodes; they are light-insensitive; and they can be readily shrunk and integrated using a low-cost thin-film standard technique[147]. Conductometry based detecting approaches has also been employed in biosensors for clinical analysis and environmental monitoring[96].

1.3.4.4 Impedance spectroscopy

According to Lorenz and Schulze's definition from 1975, electrochemical impedance spectroscopy (EIS) is a powerful analytical tool to interrogate how a material or electrochemical system responds when perturbed by a low-amplitude sinusoidal current or voltage excitation signal (approximately 2–10 mV)[148]. EIS measurement can be achieved by either applying a current perturbation and measuring the potential response in the galvanostatic mode or by applying a potential perturbation and measuring the current response in the potentiostatic mode[149,150]. The characteristics of impedance measurement are regulated by various parameters, encompassing the choice between potentiostatic or galvanostatic modulation, the perturbation amplitude, the frequency range, and the number of cycles employed to complete the measurement at each frequency[150]. Originally being employed for determining double-layer capacitance and used in AC polarography, EIS techniques have advanced as a highly important electroanalytical method[150–152]. EIS can be considered as a complementary technique for cyclic voltammetry[150]. The significance of EIS lies in its ability to discriminate between various processes in a real electrochemical system. Electrochemical impedance spectroscopy offers numerous advantages which include the employment of small signal analysis, and its capacity to investigate signal relaxations across an exceptionally broad frequency spectrum, spanning from frequencies below 1 mHz to greater than 1 MHz, all achievable through commercially available potentiostats[149,153].

Background

Impedance (denoted as Z and measured in ohms, Ω, using SI units) signifies the degree of resistance encountered by current (I) flow when subjected to an applied voltage within an electrical circuit. In the context of faradaic heterogeneous reactions, wherein charge transfer transpires at the electrode's surface, variations in impedance arise from a complex interplay of phenomena, including the adsorption of reacting species, ion diffusion, and charge transfer facilitated by redox species. These impedance alterations are intricately influenced by factors such as the nature of the electrode-solution interface, the properties of the electrolyte, the morphology, and the composition of the electrode materials[154,155].

Electrochemical impedance spectroscopy is a sensitive technique for characterizing the electrode-electrolyte interface. In the context of simple redox reactions, this interface is typically represented using the Randles equivalent circuit (**Fig. 4**). Four primary elements constitute the circuit: the solution resistance (R_s) is connected with a combination of electrical double-layer capacitance (C_{dl}) parallelly connected to a Warburg impedance (W) and charge transfer resistance (R_{ct})[149,154–156].

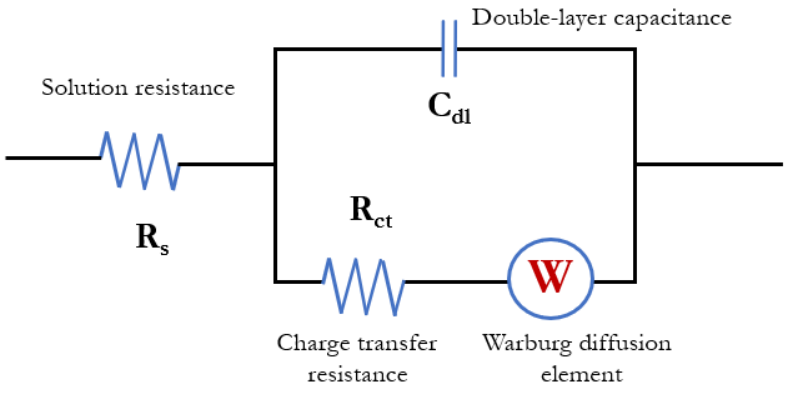

Fig. 4 A simple Randles circuit

In contrast to other electrochemical techniques, EIS measurements effectively distinguish between resistance (R) and capacitance (C). This distinction facilitates the separation of diffusion processes from other physiochemical processes in an electrochemical circuit. A clear differentiation between resistance and capacitance can be achieved because the resistance of the system remains independent of the frequency of alternating current, while capacitance shows an inverse dependence on it[154]. When subjected to an excitation signal, the electrochemical cell exhibits a pseudo-linear response, characterized by a phase shift. Considering a potentiostatic process in such a system, the current

response to a sinusoidal potential is a sinusoid at the applied frequency. The excitation signal is expressed as a function of time, as shown in the **equation (1)**[153,154]. Measuring the system's response to this perturbation signal allows the calculation of a transfer function. This transfer function represents the electrochemical impedance of the system within an electrochemical cell[150,153].

$$E_t = E_0 \sin(\omega t) \quad \textbf{(1)}$$

E_t is the potential at time t, corresponding to the radial frequency, ω, and E_0 is the amplitude of the signal. The radial frequency (ω) and the applied frequency (f) are related by **equation (2).**

$$\omega = 2\pi f \quad \textbf{(2)}$$

The response for the periodic potential perturbation follows the **equation (3)**. The current response corresponds to the same applied frequency, but it encounters a phase shift. The magnitude of the shift defines the phase angle Φ.

$$I_t = I_0 \sin(\omega t + \Phi) \quad \textbf{(3)}$$

Impedance is defined as the ratio of the applied voltage to the resulting current in an AC system. Impedance, denoted as Z (measured in ohms) is represented in a general form as provided in the **equation (4)**.

$$Z(\omega) = \frac{E_t}{I_t} \quad \textbf{(4)}$$

Time-dependent wave functions are represented as complex-valued functions in elementary quantum mechanics. Complex numbers are employed to address the inherent phase difference between the current flowing through circuit elements and the voltage across them[157]. Therefore, voltage and current vectors can be expressed as complex numbers comprising a real and an imaginary part. A periodic potential perturbation (ΔE) applied to a circuit, can typically be represented as a complex analogue of the corresponding simple periodic perturbation (**equation (5)**)[158].

$$\Delta E = E_0 \exp(j\omega t) \quad \textbf{(5)}$$

Equation 5 can also be written in a more general form (**equation 6**) considering an initial phase shift Φ_1, at t = 0. The vector corresponding to the response current can be described by **equation 7.**

$$\Delta E = E_0 \exp[j(\omega t + \Phi_1)] = E_0 \exp(j\Phi_1)\exp(j\omega t) = \widetilde{E} \exp(j\omega t) \quad \textbf{(6)}$$

$$\Delta I = I_0 \exp[j(\omega t + \Phi_2)] = I_0 \exp(j\Phi_2)\exp(j\omega t) = \widetilde{I} \exp(j\omega t) \quad \textbf{(7)}$$

Thus, the electrochemical impedance, as expressed in **equation (8)**, is a complex number that varies with frequency. The total impedance, is expressed as a combination of real (Z') and imaginary (Z'') impedance components. The resistance constitutes the real part and reactance the imaginary part of total impedance. The resistor in the circuit allows the passage of ac signals without any delay, thus the current and voltage signals are in phase. The resistance is therefore independent of the signal frequency and remains a constant real value. Reactance represents the opposition to the flow of alternating current in a circuit, arising from the effects of capacitance or inductance. In the case of capacitive and inductive reactance the input voltage and the resultant current is not in phase and they are frequency dependent. All the impedance measurements in this thesis are conducted in an inductor free electrical circuit, as a result the imaginary component is defined only by capacitive reactance.

$$Z(j\omega) = \frac{\Delta E}{\Delta I} = \frac{E'}{I'} = \frac{E_0 \exp(j\Phi_1)}{I_0 \exp(j\Phi_2)}$$

$$= Z_0 \exp j(\Phi_1 - \Phi_2) = Z_0 \exp(j\Phi) \qquad \textbf{(8)}$$

$$= Z_0(\cos\Phi + j\sin\Phi)$$

$$= \mathrm{Z}' + \mathrm{jZ}''$$

The real and imaginary components of impedance along with the phase angle shift (Φ) are the key attributes that characterize the impedance of a system. After receiving and validating the impedimetric data, it is typically analysed using the Nyquist and Bode plots, providing valuable insights into the electrochemical behaviour of the system[149,150,153,159]. When the real part of impedance (Z') is plotted on the X-axis and the imaginary part (Z'') on the Y-axis, it results a Nyquist Plot (**Fig. 5a**). A Bode plot consists of two distinct logarithmic plots: one depicting magnitude versus frequency and the other illustrating phase angle versus frequency (**Fig. 5b**). They are in general employed to assess capacitive systems, whereas Nyquist plots are more commonly utilized for the analysis of resistive processes.

Impedance and biosensing

By capturing real-time impedance variations at the bio-interface, impedimetric biosensors enable rapid and label-free detection, making them increasingly significant in advancing healthcare and scientific research. In the early 20th century, Hoeber and Fricke made the first significant contributions to the field of impedance measurements of biological samples. Following their methodology, Curtis and Cole conducted single-cell impedance measurements on Nitella cells in 1937[67].

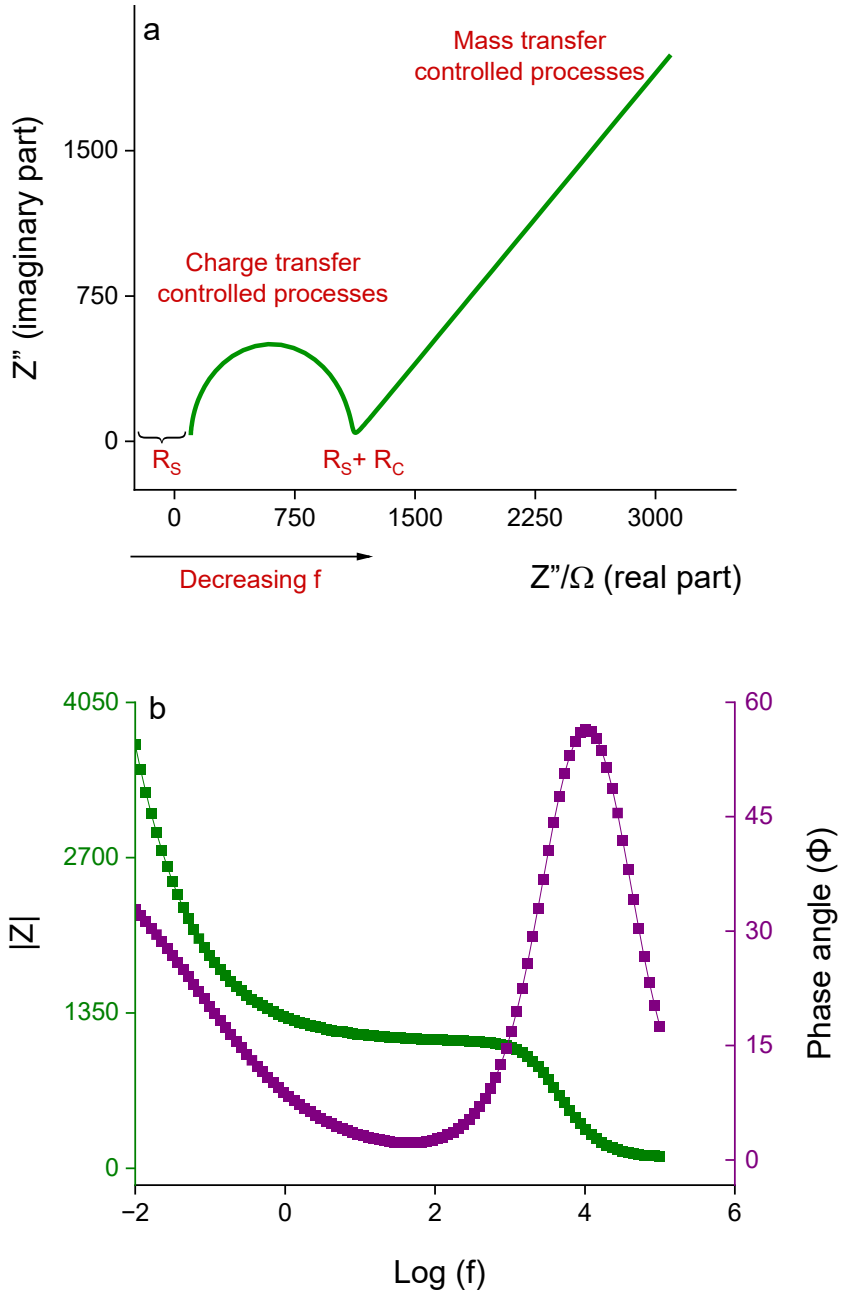

Fig. 5 Sample curve responses for a) Nyquist plot, b) Bode magnitude and phase angle plot.

Electrical cell-substrate impedance sensing (ECIS) is a method for keeping track of the viability and proliferation of cell cultures. On a collection of interconnected electrodes, cells are sown and grown. Information on cell attachment and spreading across the sensor region can be obtained by detecting fluctuations in the impedance spectra, recorded through the interdigitated electrodes. This technique is applicable to the study of diverse cell types, whether they are part of adherent cultures (fixed to a substrate) or suspended cultures. Moreover, ECIS has demonstrated its efficacy in assessing cell

behaviour within both 2D and 3D cell culture systems, irrespective of cell adhesion status. Importantly, the non-destructive nature of ECIS permits subsequent investigations, such as staining assays, cellular communication, and evaluating time dependent concentration changes to further explore cellular characteristics[96,142,160,161]. Impedance detection also finds applications in areas including cytotoxicity assays, and cardiac hypertrophy assays[67].

To measure individual cells in flow-through mode, impedance cytometers are created by integrating a set of electrodes into a microfluidic channel. With impedance cytometers, cell counting as well as the identification and characterization of various cell types in solution are both possible. Different cell characteristics can be extracted by probing cells at various AC frequencies: Higher frequencies (> 1 MHz) are utilized to examine the permeability and thickness of cell membranes, cytoplasm conductivity, and cell organelles. Lower frequency (<1 MHz) impedance measurements provide information on cell size and volume[67]. Microfluidic devices with built-in ECIS sensors are also used to analyse cell migration and proliferation inside 3D matrices like hydrogels. Automated real-time monitoring of cytotoxicity drug treatments, including drug-diffusion effects, has a lot of potential when impedance-based detection and cell/tissue encapsulation within 3D artificial matrices are combined. The use of 3D multicellular systems as *in vitro* test models has led to the development of novel systems for the EIS characterization of microtissues. EIS measurements can also be used to analyse and manipulate multicellular organisms, such as trapping, sorting, and counting of *C.elegans*, combined with subsequent electrophysiology, or fish embryos, which can be measured in response to cryoprotective chemicals, such as methanol and dimethyl sulfoxide (DMSO). Additionally, by observing parasite motilities, EIS measurements were used to test anthelmintic medications and to detect parasites in drinking water[67].

In this thesis, impedance spectroscopy was used to analyse cell cultures with the fabricated ITO microelectrode arrays. Cell-based impedance experiments evaluate the changes in electrical impedance relative to a current or voltage applied to the electrodes shielded with cell layer. It makes use of the electrochemical impedance spectroscopy (EIS) principles and provides a platform for the identification of a number of cell culture properties, including metabolism, adhesion, viability, motility, and proliferation[161]. A cylindrical set-up featuring a planar array consisting of eight circular ITO electrodes was employed to monitor the dynamics of HepG2, HeLa and mouse hepatocyte cell cultures (**Fig.24,** Chapter 3). This monitoring encompassed critical stages, including cell seeding, attachment to the electrode surface, and trypsin-induced detachment from the substrate.

1.4 Glucose sensing and electrochemical mediators

Biosensor-based technologies have highly evolved and play a great role in providing strong analytical tools with different applications, especially in medicine. Glucose biosensors dominate today's biosensor market[162].

Due to their excellent specificity and sensitivity, enzymatic amperometric glucose sensors are commercially successful glucose sensors in the market[163]. They are commonly based on the two enzyme families, oxidases and dehydrogenases. The commercially available enzymatic glucose sensors primarily utilize two enzymes, glucose oxidase (GOx) and glucose dehydrogenase (GDH)[162,163]. Both of these enzymes have differences in redox potentials, cofactors, turnover rate, and selectivity for glucose. The use of GDH for glucose sensing can be considered as a complementary approach of GOx-based sensing[162–164]. GDH catalyses the direct electro-oxidation of glucose. However, GDH may require specific cofactors and have a higher initial cost. GOx is readily accessible, cheep, exhibits superior resilience to varying pH levels, ionic strengths, and temperatures compared to many other enzymes, hence allowing fewer rigid conditions during the manufacturing process and relatively relaxed storage norms for use by lay biosensor users[162]. Hence GOx is employed as the recognition molecule for glucose sensing in this work. GOx catalyses the oxidation of beta-D-glucose by molecular oxygen, resulting in gluconic acid and the by-product hydrogen peroxide[165]. The hydrogen peroxide formed in this process is proportional to the amount of glucose reacted (**Scheme 1**). As hydrogen peroxide can be easily detected on a working electrode, electrochemistry can be used to indirectly assess the concentration of glucose.

So far, three generations of enzymatic biosensors have been suggested. The first generation relies on oxygen as a physiological mediator to measure peroxide formation; the second generation uses an integrated electron acceptor as a mediator that transports electrons from the enzyme active site to the electrode; and the third generation relies solely on the direct transfer of electrons between the enzyme and the electrode(without requiring any mediators)[165].

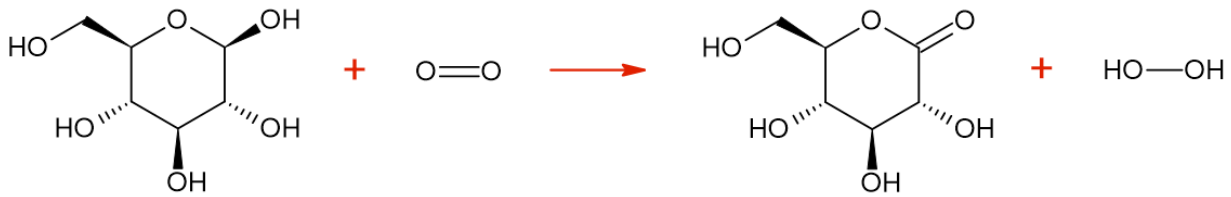

Scheme 1. Oxidation of D-glucose by molecular oxygen, producing gluconic acid and hydrogen peroxide.

Having higher selectivity for glucose, GOx is typically the standard enzyme found in popular first-generation biosensors. In the first-generation glucose sensors, measurements of peroxide formation offer simplicity, particularly for miniature devices[162]. While this approach provides a feasible option for a secure, implantable continuous glucose monitoring system, the requirement for a higher potential increases the likelihood of oxidizing more interference, leading to a loss of signal output[166]. Additionally, there is limited oxygen solubility in biological fluids, leading to fluctuations in oxygen tension[162]. In contrast, second-generation glucose sensing methods are not reliant on oxygen and solves the problems encountered with oxygen deficiency and interferents[162,166,167]. Given the increasing demand for point-of-care testing tools for self-monitoring of blood glucose, second-generation electrochemical sensor strips have emerged as the popular platform. To avoid the oxygen dependence, most of the commercial glucose biosensors have explored the use of various glucose dehydrogenases[167]. Nonetheless, glucose sensors employing glucose dehydrogenases (GDH) and pyrroloquinoline quinone (PQQ) dehydrogenases for the direct electro-oxidation of glucose can suffer from a lack of specificity and are vulnerable to interference from other sugars present in the body, including lactose, galactose, maltose, cellulose, and xylose[164]. Thus, there is still room for improvement for the second-generation sensors.

In case of the second-generation glucose sensors, mediators act as a bridge between the glucose molecules and the sensing system, facilitating the detection and analysis of glucose concentration. A good mediator can enhance the accessibility of the target analyte to the recognition site. They help in improving the response time, facilitate prompt and real-time measurements, allowing the system to make timely adjustments to blood glucose levels. A simple depiction of the second-generation glucose biosensor sensing mechanism can be viewed in **fig.6**. An important aspect of glucose biosensor fabrication is the development of mediators for wiring the biorecognition element onto the electrode surface. The use of a mediator is helpful to improve output from a simple modified or any bare working electrode. It is usually efficient compared to the direct electron transfer approach[168].

Both simplicity and reproducibility are the factors considered during the design and preparation of biosensors. In this chapter, simultaneously two strategies are applied for glucose sensing. Using redox hydrogels based on poly (vinyl imidazole) (PVI) polymer that contains cis-$Os(N\text{-}N)_2Cl_2$ redox centres as electron mediator is one of the strategies. In another method, Prussian Blue (PB) modified electrodes are used for the selective detection of hydrogen peroxide by its electroreduction in the presence of oxygen.

The interest in using polymer-bound osmium complexes as mediators have increased over the past decades. The hydrogel characteristics of enzymatic electrodes based on redox-polymer films allow rapid mass and charge transport, generating substantial current signals. These metallopolymer structures have osmium coordinatively bonded to poly (vinyl imidazole), poly (4-vinyl pyridine), poly (methacrylate), or similar polymers. Due to the ability to manipulate the mediator redox potential of the central metal via coordinating ligands, the relative stability of the resulting complexes in the reduced/oxidized states (Os^{II}/Os^{III}), and low redox potential, the osmium-based complexes outperform the iron and ruthenium analogues[169].

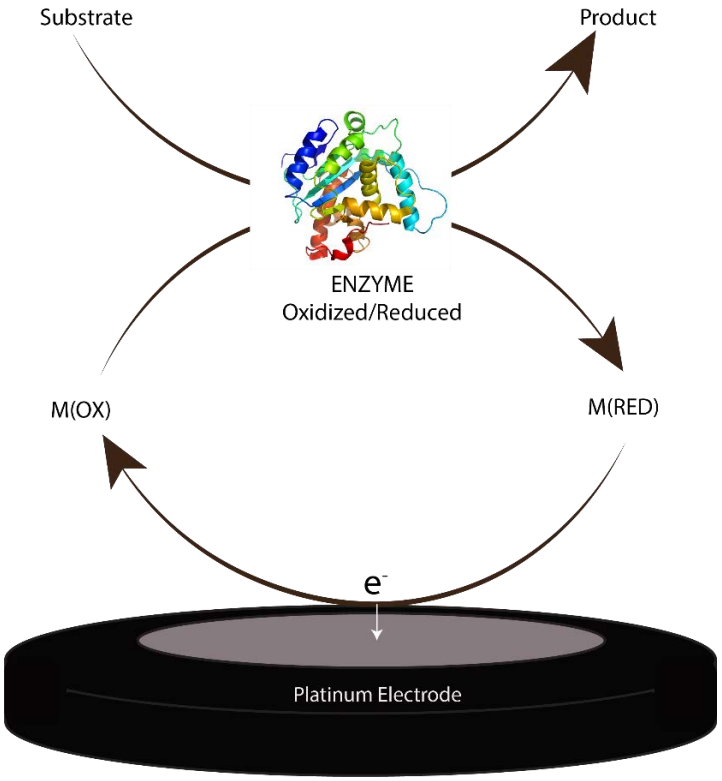

Fig.6 Functioning concept of second-generation biosensors.

This section mainly focuses on the mediating redox hydrogel that consist of osmium polymer complexes of general formula cis-$[(Os(N\text{-}N)_2(pol)_{n+1}Cl]^+$ (n = 9) (**Scheme 6,** Chapter 4). It is one of the most popular mediators quoted in the literature as well as present in the commercially available glucose prick tests. Modulation of the redox potential for the Os^{II}/Os^{III} transition of the central metal atom can be readily achieved by substitution of the polypyridyl ligands of electron-donating and withdrawing groups. The electron transfer events within this class of complex modified electrodes involve the transformation between stable oxidation states. Therefore, the transport of ions within the

deposited films must be realized to maintain electroneutrality. Electrons are transported in redox polymers by hopping through conjugated backbones and through collisions between immobile redox centres. Redox hydrogels are electron conducting matrices that allow the infusion of water-soluble biological substrates and products along with facilitating rapid electron transport. They electrically "wire" the reaction centres of co-immobilized enzymes to electrodes. The long and flexible tethers of the osmium metallopolymer enable the redox centres to effectively shuttle electrons between the enzyme and the electrode, enhancing the rate of the reaction[169–171]. **Figure 7** depicts electron conduction mechanism in redox hydrogels.

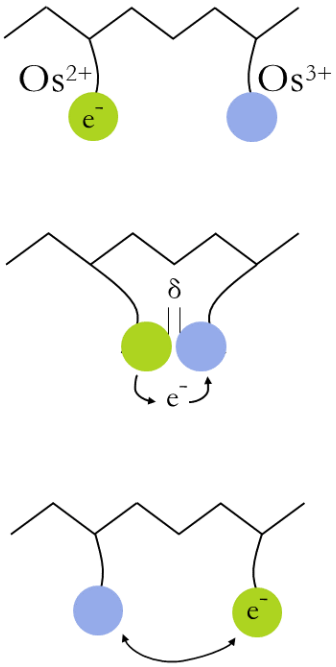

Fig 7. Schematic illustration of electron conduction in osmium-based redox hydrogels. In this mechanism electrons are transferred between reduced and oxidized redox centres tethered to the backbone of polymers.

The futuristic goal of this work is to develop a multielectrode platform which enables cell growth and electrochemical analysis at various points of the 3D cell culture. The system will be applied for drug screening through viability studies by measurements of oxygen and glucose consumption in cultures of immortalized hepatocytes. Since hepatocytes are not electrically active, the detection potential does not affect such cells. It was observed that when a simple glucose biosensor (with GOx immobilized on a working electrode) maintained at a single potential was used for system monitoring (as in chronoamperometry), any electron transfer reactions would encounter interferent molecules such as uric acid and ascorbic acid and ions like Cu^{2+} and Co^{2+}. Despite the enzyme being highly selective,

lowering the potential is advantageous to minimize the occurrence of such interfering reactions. Therefore the mediator should facilitate the detection of hydrogen peroxide at lower oxidation potentials than +700mV(vs. Ag/AgCl) observed for platinum[97,172] or -500mV used for reduction for example on gold nanoparticles[173,174].

Since 1994, Prussian Blue modified electrodes demonstrated selective hydrogen peroxide detection in the presence of oxygen. This drew significant attention towards transition metal hexacyanoferrates (HCFs), especially for their applications in oxidase-based biosensors. The scheme of biosensor operation included glucose oxidation by molecular oxygen producing hydrogen peroxide as a by-product. Prussian Blue is credited with having the greatest electrocatalytic activity for H_2O_2 reduction and therefore is the most suitable H_2O_2 transducer for its low potential detection[175]. Prussian Blue is ferric ferrocyanide ($Fe_4^{III}[Fe^{II}(CN)_6]_3$) with the iron(III) atom coordinated to nitrogen and the iron(II) atom coordinated to carbon existing as a face-centred-cubic structure with the space group Fm3m[176]. Prussian Blue's three dimensional open framework structure, high catalytic activity and selectivity comparable to the enzymes contributes to its significance to be used in a glucose biosensor[177]. The structural framework of PB exhibits high flexibility, which is capable of accommodating defects of up to 25% of a $[Fe^{II}(CN)6]^{4-}$ unit[178]. However, the structure can be disordered due to the presence of significant amounts of interstitial K^+ ions or uncoordinated occluded water[178]. This can cause variations in performance of PB.

Generally, electrocatalysts based on Prussian Blue is deposited on an inert electrode material like platinum, gold or carbon before use. The enzyme oxidase is immobilized onto the top surface of the modified electrode. Oxygen (O_2) is reduced to H_2O_2 in the presence of both oxygen and the other enzyme substrate, the produced H_2O_2 is electrochemically reduced on the surface of Prussian Blue modified electrode[177]. The working mechanism of a Prussian Blue-based glucose biosensor is provided in **figure 8**.

Chemical and electrochemical methods are very useful for preparation of Prussian Blue films. However, these traditional techniques often yield unstable complexes, limiting their electrochemical capabilities. Silva *et al.,* reported a novel, quick, flexible method for the synthesis of Prussian Blue and it analogues by oxidative print light synthesis (PLS)[179]. The process involved inkjet printing and flash light sintering (FLS). The product obtained from this photo assisted method critically simplifies the process of modification of electrodes because no further post-processing is required (for example cycling in KCl or KCl/HCl does not enhance the current as in the case of other procedures). The

compound may simply be dissolved, coated, and then covered with a layer of Nafion, thus making experiments much easier. Unfortunately, except when cycled in H_2O_2, the Prussian Blue prepared through FLS has similar stability as observed with other methods. The compound demonstrates increased stability during cycling in H_2O_2.

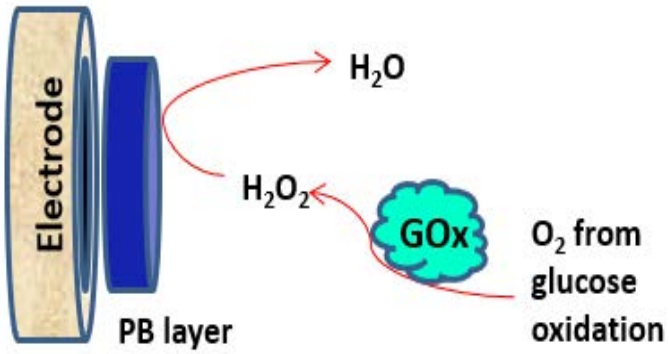

Fig.8 The working mechanism of a Prussian Blue-based glucose biosensor.

Established stabilization methods like covering the PB surface with organic polymers for example deposition of Nafion and electro-polymerization of non-conductive polymers on Prussian Blue, entrapment in sol-gel or conductive polymer matrixes[180] and use of non-iron hexacyanoferrates in combination with Prussian Blue are known[175,180–182]. Among these approaches, the use of mixed hexacyanoferrates are reported to be the most effective. An electrocatalyst, which is a bilayer of Prussian Blue and nickel hexacyanoferrate synthesized by N.A. Sitnikova and co-workers is even identified as 'super-stable' Prussian Blue[180]. In this work, the synthesis of Prussian Blue analogues through the flash light sintering technique is presented.

Flash Light Sintering (FLS), also known as Photonic Curing, is a rapid and efficient process used in the field of printed electronics and flexible electronics manufacturing[179,183,184]. This technique uses an intense pulsed white light from a xenon flashlamp encompassing the entire visible light spectrum with small regions of ultra-violet and a near infrared light (380 and 950 nm). The intense pulsed light is produced by an arc plasma phenomenon within the xenon flash lamp. On application of a potential difference between two tungsten electrodes, current flows through inert xenon gas between them and a glowing plasma arc is formed. Xenon gas is commonly employed in this process due to its high efficiency in converting applied electrical energy into white light, achieving approximately 50% conversion efficiency[185,186]. The flash intensity can be modified to control the energy density within a

range of 1–30 Jcm^{-2} for individual lamps. The systems equipped with multiple lamps can achieve energy densities of up to 150 Jcm^{-2}. The parameters of the pulses (such as pulse duration, number of pulses and the pulse frequency) can also be tuned according to the requirements[187].

FLS works by the selective light absorption by a film of precursor materials and generation of heat necessary to drive the reaction (in general by reduction) to the desirable product. The starting materials are drop coated or printed on a support substrate and exposed to the xenon lamp radiation. The absorbed light energy elevates the thin film's temperature to several hundred degrees Celsius, leading to evaporation of the solvents and thermal transformation of the materials (for example; sintering) without substrate damage. This instantaneous temperature rise lasts only few milliseconds[179,185,188]. Compared to the thin films used, the substrate carrier has a significantly larger thermal mass. Therefore, the time to establish a thermal equilibrium between the film and the substrate surpass the flash duration, causing a nonthermal equilibrium effect. As a result, the introduced heat energy dissipates rapidly and the high temperatures are not transmitted into the substrates[179,187,188].

FLS offers several advantages over traditional sintering methods, including shorter processing times, and lower energy consumption. The flash light sintering operates at ambient temperature and process is independent of substrates[185,188]. The synthesis of Prussian Blue analogues extends the applications of the technique. These set of complexes have the general formula $A_xP[R(CN)_6]_{1-y}\cdot wH_2O$, where A is an alkali metal cation, often potassium or sodium, P (coordinated to nitrogen of the cyanide group), and R (coordinated to carbon of the cyanide group) are transition metal cations, y represents the number of $[R(CN)_6]$ vacancies[175]. Thanks to being widely reported, nickel and cobalt were chosen as the metals for the synthesis. They belong to the iron triad family which makes them very likely to be the right choice. Although the electrocatalytic activity of Prussian Blue towards H_2O_2 is at least twice as high as that of nickel and cobalt hexacyanoferrates, it has been demonstrated that associating Prussian Blue with its Ni and Co analogues significantly enhances its stability. Moreover, the combination of Prussian Blue with nickel hexacyanoferrate analogue was identified as the most effective for indirect glucose sensing(up to 100mM) among the three metal complexes[175,189].

1.5 Summary

Electrochemistry is a powerful analytical technique for studying cellular processes. It can be performed in a non-invasive manner, which is important for studying live cells without damaging them. This allows to monitor cell behaviour over time, which can provide valuable insights into the

microenvironments and cellular operations. Electrochemical measurements are highly sensitive and can detect changes in cellular behaviour that may not be observable with other techniques. High-throughput electrochemical measurements for studying large populations of cells can be carried out. Such experiments are helpful to obtain statistically significant results and to study cellular functions under a variety of conditions. Besides, the approaches are relatively inexpensive, and require minimal equipment, thus electrochemical tests can be carried out without the usage of specialized tools or services. This makes them accessible to a wide range of applications including variety of biological procedures and complex interactions that occur within cell cultures during cell signalling, metabolism, and electrophysiology[68,69,190].

Cell cultures are being employed in different areas of electrochemistry. Electrochemical biosensing in cell cultures have gained wide acceptance. They can be used to monitor metabolic activity in various biological systems, including cells, tissues, and whole organisms. In addition, biosensors are employed for clinical diagnosis,[191] and monitor drug responses[192]. Cell cultures provide a stable and controllable source of biological material for biosensor development, and by carefully selecting and optimizing the cell culture conditions, researchers can ensure that the biosensor is highly specific and sensitive to the target analyte. With the continued advancements in biosensing technologies, it is likely that cell culture-based biosensing techniques will become more prevalent in many research and clinical applications. Besides, animal testing has been a controversial issue over the years, and cell culture-based biosensing offers the promise of reducing the dependence on animal testing for evaluating new pharmaceuticals.

Even though bio-sensing is very well known, electrochemical biosensing in cell cultures still has the potential to transform the fields of medicine, biotechnology, and environmental science by providing a rapid, accurate, and non-invasive tool for monitoring biological systems. While glucose biosensors are being widely investigated, developing low-cost systems for drugs screening in integrated systems is still a challenge[193–195].The focus of this thesis is the fabrication of ITO microelectrodes and microelectrode arrays for the analysis of cell cultures and biomedical applications. So far, laser-cut ITO microelectrodes and microelectrode arrays have been successfully developed as a low-cost platform for biosensing[196]. Immortalized cell lines like HeLa, Hep-G2 and mouse primary hepatocytes are used in this study to optimize the performance of the electrodes. These electrodes and electrode arrays can be used as any functional electrodes available in the market.

In the future, the developed sensors will be employed in an integrated multielectrode system that will enable the analysis of the cell viability and can be used for drug screening. The viability tests will be

conducted through simultaneous monitoring of glucose and oxygen in hepatocytes at various points of 3D cell cultures.

2 Fabrication and Characterization of Electrodes for Bio-sensing

The electrode is a fundamental component of any biosensor, and its properties can greatly influence the performance of the device. The choice of electrode material depends on the intended application, with factors such as conductivity, biocompatibility, and stability being critical considerations. Additionally, the surface chemistry and morphology of the electrode can also impact the sensitivity and selectivity of the biosensor. A critical aspect of electrode fabrication is the development of methods for patterning and miniaturization. In addition to the technical considerations of electrode fabrication, there are also practical considerations such as cost and scalability. The development of low-cost and scalable electrode fabrication methods is critical for the widespread adoption of biosensors in clinical and environmental monitoring applications. The continued development of electrode fabrication methods will enable the creation of biosensors with improved sensitivity, selectivity, and portability, potentially transforming healthcare and environmental monitoring.

This chapter presents different, easy, low-cost approaches for the preparation of platinum and ITO microelectrodes. The fabrication techniques and the characterization of electrodes are discussed herein. Platinum microelectrodes were fabricated using commercially available platinum wires with 25 and 15 micrometres diameters. In the case of ITO, microelectrodes and electrode arrays are successfully fabricated using techniques based on CO_2 laser irradiation.

2.1 Chemicals and materials

The chemicals 1,1'-ferrocenedimethanol (98%, Acros Organics), ferrocenemethanol (99% ABCR GmbH), KNO3 (99%, POCh), KCl (99.5 %, Chempur), KOH (≥85%, Sigma Aldrich), Ethanol (absolute 99,8%, POCh), sulfuric acid (96% Stanlab) were used as received. Argon (N5.0) and acetylene (technical grade) were from Multax. Borosilicate capillaries with I.D. 0.2-0.8 mm, O.D. 1.0-1.2 mm and quartz capillaries I.D 0.7, O.D 1.0 were from Sutter Instruments. Pt wire (5N, Ø 0.1 mm) and Ag wire (5N, Ø 0.5 mm) were from the Mint of Poland. Water was filtered and deionized from a Sartorius Arium Comfort I system and a Rephile NuZar U24 water system.

2.2 Methods

2.2.1 Glass capillary-sealed platinum microelectrodes

Platinum microelectrodes were prepared using commercially available Pt wires of 25 and 15-micrometre diameters. The wires were insulated with polyimide. Pt wires were cut using micro scissors under the microscope. To secure the wires, they were enclosed in glass capillary tubes, and sealed using hot glue. Once sealed properly without leaks, the capillary was filled with 1M KCl and a copper wire of desired length was inserted in the capillary to make electrical connection. The capillary offered stability, allowing for the secure handling of a more substantial entity than a 25 or 15 μm (diameter) wire, and simplified the connection with the copper wires.

2.2.2 Laser-cut platinum microelectrodes

This method focuses on fabricating MEAs using commercially insulated platinum wires of 15μm and 25μm diameters. The wires were cut with laser ablation using the GCC laser pro C180II model CO_2 (New Taipei City, Taiwan) laser plotter to ensure their even dissection to obtain disk-shaped microelectrodes. At first, the Pt wires were well secured and sealed on glass slides using scotch tapes to avoid random positioning and bending of thin wires when the laser is passed through them. Optimization of the laser ablation technique was a trial-and-error process that involved several combinations of speed, power, and other laser parameters. The electrodes were fabricated by attaching the laser-cut platinum wires to a copper wire using silver glue.

2.2.3 ITO Electrodes

2.2.3.1 Direct laser ablation of ITO patterns

A desktop CO_2 laser engraving machine - C180II purchased from GCC (New Taipei City, Taiwan) was used to directly pattern (ablate) a clean 25 x 50 x 1.1 mm ITO covered (~130 nm, Rs = 5 - 15 Ω/sq) glass plates obtained from Delta Technologies (Loveland, CO, USA) using a CAD design with the following parameters: speed 2.0, power 1%, and PPI (pulses per inch) 1500 (**Fig. 9**). The laser locally heats the ITO layer on the glass to the point where it cracks and separates off the glass plate. The ITO plates were then subjected to 15-minute sonication processes, first in acetone, then isopropanol, and finally in distilled water. Eight electrodes were present on each test plate. The dimensions of the contact pads (6 x 22.5 mm^2) define the spacing between electrodes. Copper tape was used to improve the electrical connections to the potentiostat, and Kapton tape was used to

conceal the connections so that only the electrodes were available to come in contact with the test solution.

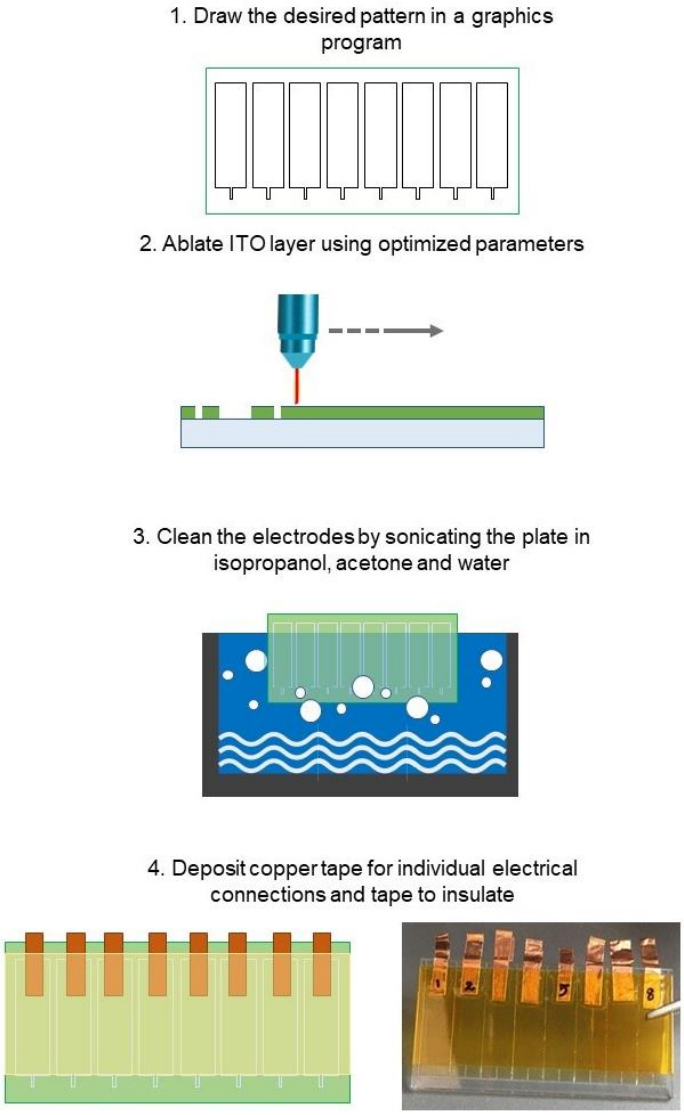

Fig.9 Step-by-step fabrication procedure of the directly ablated patterns[196].

2.2.3.2 Laser cutting of scotch tape stencils and chemical etching of the ITO patterns

Clean 25 x 25 x 1.1 mm ITO coated (~260 nm, R_s = 4–5 Ω /sq) glass plates supplied from Biotain Crystal (Fujian, China) were sealed with Scotch Magic Tape® from 3M (Saint Paul, MN, USA). The tape was cut using the same laser engraver and a CAD design with the following settings: speed 3.0, power 1%, and PPI 1500. Following patterning, the plates were immersed in an etching solution

(50 g $FeCl_3$ x $6H_2O$ + 80 mL distilled water + 20 mL of concentrated 36% HCl) for 2.5 minutes at 60°C. The plates were next subjected to 15 minutes of sonication in acetone, isopropanol, and distilled water to obtain 8 clean electrodes on each ITO plate (**Fig. 10**).

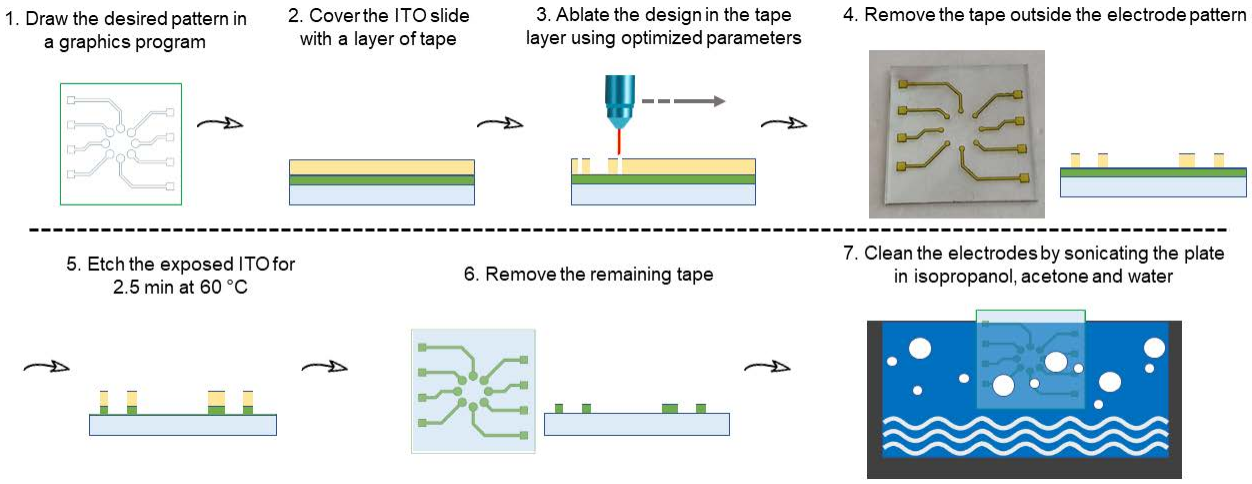

Fig. 10 Step-by-step procedure of the electrode fabrication using laser-ablated stencils[196].

2.2.4 Electrochemical Measurements

All the electrochemical measurements, unless stated otherwise, were performed with PalmSens4 potentiostat galvanostat, with an electrochemical impedance spectroscopy (EIS) module, which is controlled with PSTrace software. The three-electrode electrochemical cell consisted of a platinum wire counter electrode, and an Ag/AgCl (1M KCl) reference electrode. Platinum microwires and ITO microelectrodes were appropriately employed as the working electrodes. The performances of the fabricated ITO electrodes were first studied using the cyclic voltammetry (CV) technique with 1,1'-ferrocenedimethanol (FcDM) as the redox probe in potassium nitrate. In the case of Pt electrodes, the supporting electrolyte used is KCl along with the redox probe. The ITO electrodes were cleaned first with ethanol, then water, and dried before the measurements. Before use, Pt microelectrodes were electrochemically cleaned by cycling in 0.5M H_2SO_4.

2.2.5 Scanning electrochemical microscopy (SECM) analysis

Carbon nanoelectrode tips were prepared using a modified method[197] for all SECM tests. Due to increased C/H stoichiometry, acetylene gas under 1 bar of manometric pressure was employed instead of a propane-butane combination (Warning: Acetylene thermal pyrolysis at pressures more

than 1 bar can result in an uncontrollable chain reaction and serious injury.). The nanoelectrodes were carefully broken before imaging. This was carried out by moving the ITO part away from the planned imaging area until the electrooxidation of ferrocenemethanol is reached the desired steady-state current. The steady-state currents of ferrocenemethanol oxidation at a large tip-to-sample distance were used to determine the active tip radii of the resulting electrode. A home-build SECM setup composed of closed-loop piezo actuators (P625.2CD and P622.1CD, PI HERA with LVPZT Amplifier E-509 C3A, PhysikInstrumente), VA-10X patch-clamp amplifier (npi Electronic Instruments), operated under SECMx software[198] through PCIDAS1602/16 analog-digital (AD) and PCI-DDA04 DA digital-analog (DA) cards (Measurement Computing), installed on top of an inverted optical microscope Nikon MA200 was used. All SECM experiments were conducted using a two-electrode setup comprising a silver quasi-reference-counter electrode. An aqueous solution of 1 mM ferrocenemethanol in 0.1 M KCl served as the mediator. Potentiostatic polarization of the SECM tip at +0.5 V was applied to facilitate the diffusion-controlled electrooxidation of the mediator. The samples were floating. If not specified otherwise, imaging of the sample activity was carried out in a constant height feedback mode after reaching 90% of the tip current measured at a large distance. Owing to the topographic characteristics of laser-cut ITO samples, the feedback hopping mode SECM measurements were conducted by Dr. Wojciech Nogala. A retracting distance of 10 μm was employed to capture both topography and activity, shown as the closest distance slope of approach curves[199].

2.2.6 Optical microscopy

A Nikon ECLIPSE LV150 optical microscope was used for the qualitative study of the electrode architectures. The electrode widths were measured and compared with the anticipated width from the laser cutter.

2.2.7 SEM Imaging

Scanning Electron Microscope (SEM) micrographs of the electrodes were captured using a FEI Nova Nano – SEM 450 with an EDAX Octane Elect Plus EDX system. EDX mapping was performed on the elements silicon and indium. To find the width of the electrodes from SEM images, the ImageJ software was used (see **Fig. 15**).

2.2.8 Design of the measurement setup for the circular electrode array

An ITO plate consisting of 8 circular working electrodes, as constructed (diameter 1.75 mm, 2.41 mm^2 of geometrical surface area), was placed in a holder and was contacted with a custom PCB board with spring-loaded contacts and a custom 9 mm diameter PDMS (Sylgard 184, 10:1 elastomer to curing agent ratio obtained from Dow Chemicals (Midland, MI, USA)). The PCB board, PDMS well, and plastic cover was placed on top of the ITO electrode plate and fastened together to secure the setup and prevent leakage of liquids.

2.3 Results and discussions

For the readers' convenience, the results and discussion section of this chapter is divided into three parts, each corresponding to the different fabrication approaches and electrodes employed. The following sections comprehensively detail the outcomes inferred for glass capillary-sealed platinum microelectrodes, laser-cut platinum microelectrodes, as well as ITO microelectrodes and MEAs.

2.3.1 Glass capillary-sealed platinum microelectrodes

2.3.1.1 Electrochemistry

The electrodes were characterized by cycling in 1mM 1,1'ferrocenedimethanol with 0.1M potassium nitrate as a supporting electrolyte (examples provided in **Fig.11**). Out of the 50 electrodes prepared, only 15 showed optimal performances regarding the current generated, the redox processes and the shape of the graph; in simpler terms, the success rate of the fabrication of such electrodes and their reproducibility were low. It was stipulated that the noise may come from the improper electrical connection of the thin insulated Pt wires. Some of the electrodes didn't have proper disk structure due to rough surface or presence of impurities. Moreover, gluing the microwires to the copper wires with conductive silver paint as well as proper sealing of the capillary tube by hot glue was difficult. To mitigate this problem, dissolving the polyimide insulation of the platinum wire using chemical etching was also considered. A solution of 1.15 M KOH in 80% ethanol (1.28g KOH, 16.0mL ethanol, and 4.0mL water) constituted the etchant solution; an edge of the platinum wire was dipped in the solution at 70^{o}C for 5 minutes. However, the dissolution of the polyimide layer was not uniform and resulted in uncontrolled etching that gave rise to the overexposure of the platinum wire. This resulted in very high current values and uneven, non-reproducible microelectrodes.

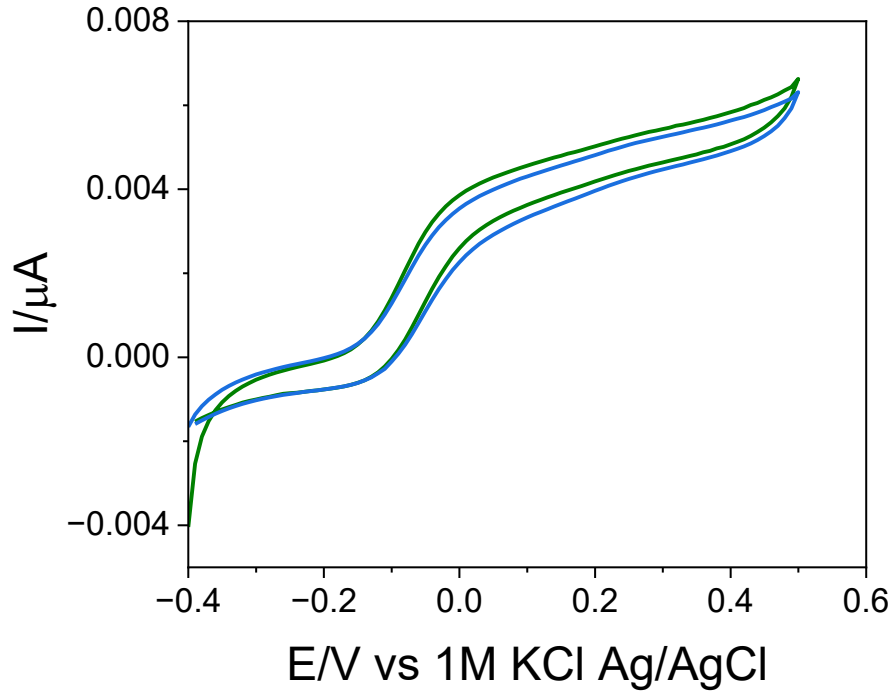

Fig.11 Cyclic voltammograms of two 25 µm (diameter) electrodes in 1 mM FcDM and 0.1 M KNO_3 (scan rate = 100mV/s)

2.3.2 Laser-cut platinum microelectrodes

2.3.2.1 Microscopic analysis

To identify the appearance of the wires after passing the laser, the electrode wires cut using different combinations of laser power, speed and other parameters were observed under an optical microscope. Most of them appeared as well-cut circular disks to the naked eye, whereas the tips appeared pointed and irregular on microscopic observation. At lower power and speed, multiple laser exposures were performed on the same wire; this melted the insulation and left the platinum core uncut. **Table 1** provides information about the responses of the insulated platinum wires to specific parameters of the laser. **Figure 12** shows the microscope images of different 25µm electrodes (80 % P and 80% S); it could be clearly observed that after a specific limit, irrespective of the parameters, the laser has caused damage to the insulation. Even though some of the electrodes seemed fine at their cross-sectional view, they might not have the expected smooth circular surface. Highly precise measurements and surface structure could be obtained with improved and widely accepted techniques like Scanning Electron Microscopy (SEM), but such analysis was not performed as the electrochemical measurements were not satisfactory.

Table 1. The responses of the insulated platinum wires to different parameters of the CO_2 laser.

Power	Speed	PPI	DPI	Inference
0 to 30	0 to 30	1500	1500	Pt wires remain uncut
30 to 35	35	1500	1500	Only insulation burnt
> 40	> 40	1500	1500	Wires are cut. However, the insulation is peeled off away from the point of dissection.

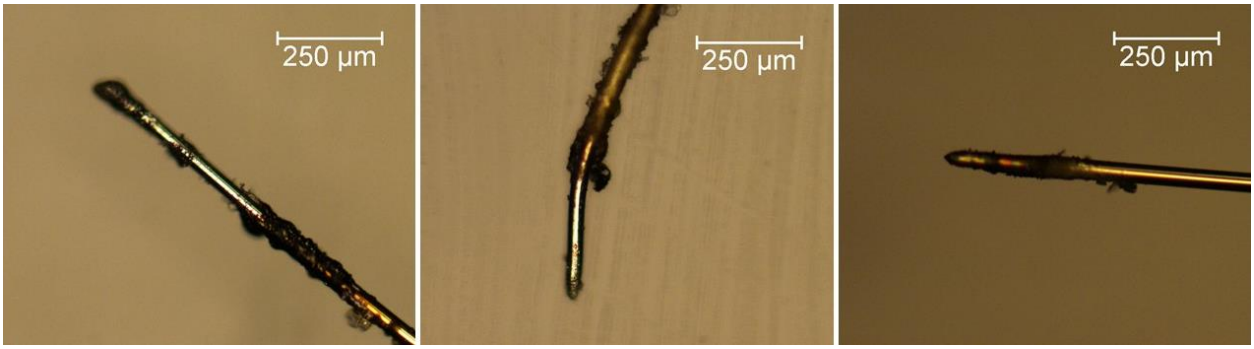

Fig.12 Microscope images of insulation damage of different 25µm electrodes (laser parameters used; power 80%, and speed 80.0).

2.3.2.2 Electrochemistry

At first, Pt microelectrodes were electrochemically cleaned by cycling in 0.5M H_2SO_4. Later, they were cycled in 1mM 1,1'-ferrocenedimethanol with 0.1M KCl as a supporting electrolyte to analyse their electrochemical signals and reproducibility. Although not at their best performances as expected, a few of the wires exhibited reasonably stabilized performances (**Fig.13 a**). The theoretical current value for a disk-shaped microelectrode for a 15µm electrode in ferrocenedimethanol should be around 1.7-2.0 nA and for a 25 µm electrode in the same conditions should be 2.9 nA. However, the experimental current values were very different from the theoretical values. Moreover, the currents between the electrodes of the same diameters that were cut with the exact parameters of the laser were very different; for example, one of the 25µm electrodes cut with a parameter of 50% laser power and 100% of the laser speed (50P 100S) had a peak current of 40nA in ferrocenedimethanol and another

electrode with same characteristics in the same solution exhibited 0.003 nA. When it comes to the case of 15µm electrodes, the peak current was around 20 times higher than the calculated value. This could result from larger exposure of the platinum wire (more than the expected circular region) due to the damage of insulation by the laser. Several batches of electrodes were prepared, and their performances were compared; it was seen that even the signals between the electrodes of the same diameters cut with the exact parameters of the laser were very different from batch to batch (**Fig.13 b**). Apart from the speed and power of the laser, the dots per inch (DPI) and pulses per inch (PPI) factors which determine the points of contact of the laser and substrate were adjusted to the maximum value (1500) so that the chances of the laser hitting our wire could be increased, but this step was of little help. The commercially available polyimide insulated platinum wires, that we used has a conductor diameter 25 µm with an insulation thickness of 5 µm. As the melting point of the polyimide insulation is very low compared to that of the platinum, the former gets burnt and peeled off easily on the application of the laser.

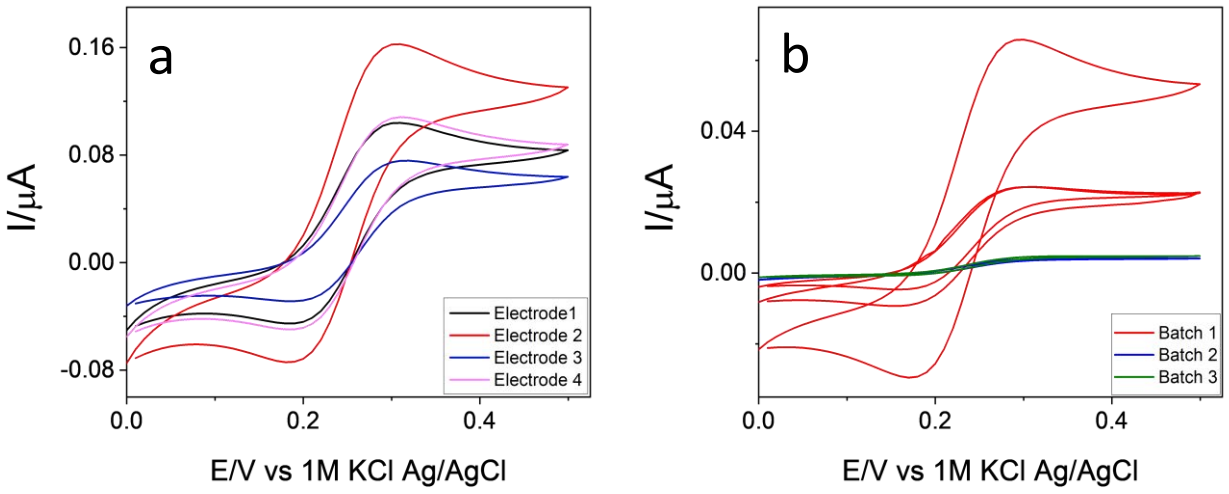

Fig.13 Cyclic voltammograms of the laser-cut Pt microelectrodes in 1mM 1, 1'-ferrocenedimethanol/0.1M KCl a) comparatively stabilized results of four platinum microelectrodes of 25 µm diameter (parameters used; power 100%, and speed 50.0), b) comparison of the cyclic voltammograms of different batches of platinum microelectrodes of 25 µm diameter (parameters used; power 80% and speed 100.0) shown in red are the signals of different electrodes of the batch 1, blue from batch 2 and green from batch 3.

Identifying the parameters that could cause no or the least damage to the insulation and offering a clean dissection of the wires is time-consuming and almost impossible for such a system. Even though there were a few promising results with the laser-cut Pt microelectrodes, the resultant electrodes were flimsy, twisted, and had uneven ends.

A fiber splicer, generally employed for cutting optical fibers, was also used as an alternate method for cutting the Pt microwires, but this did not result in a promising development. Another laser source, for example, a femtosecond laser, could be used nevertheless, this will be an expensive option and does not suit our objective of developing a low-cost electrode fabrication technique for biosensing.

2.3.3 The ITO electrodes

2.3.3.1 Microscopic analysis

The electrodes were initially examined using optical microscopy. The electrodes appeared neat and uniform when seen at low magnification. However, when viewed upon closer examination at higher magnification, cracks and irregularities are evident, particularly for the smaller electrodes (**Fig.14**). Additionally, measurements of the electrode widths indicated that the narrower electrodes were significantly wider (measuring at 39±3.5 μm) than their nominal width (25 μm).

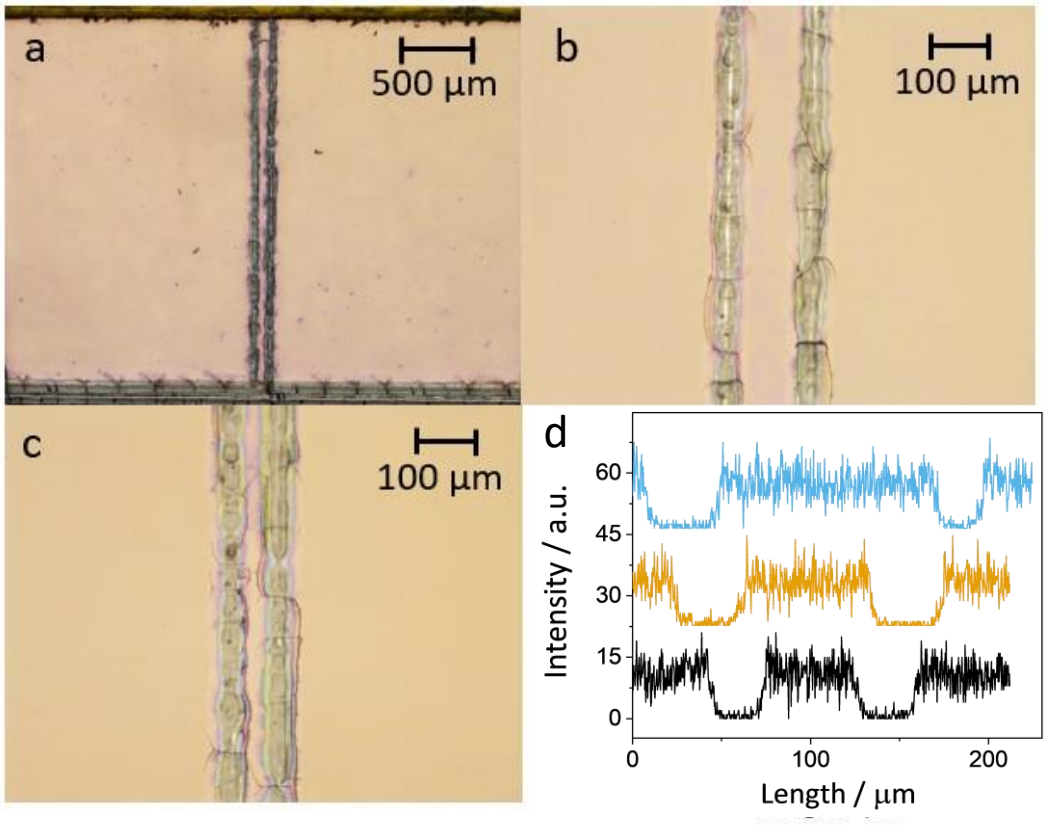

Fig.14 Microscopic image of an electrode with nominal width 100 μm a) 2.5X magnification, b) 5X magnification, c) microscopic image of an electrode with nominal width 25 μm at 5X magnification, d) EDX spectra of the ITO electrodes depicting the intensity of indium on them.

To ensure that the individual electrodes were not electrically connected to other parts of the ITO plate, a negative potential of -1.5V (vs. Ag/AgCl) was applied to the ITO working electrode for 60 seconds. This resulted in the reduction of the ITO layer. The electrode underwent a significant appearance change, indicating the disintegration of the electroactive area to metallic indium and tin. This was evident as the electrodes lost their transparency and appeared darker[200]. The reduced area was limited to the electrode, and there was no indication of any electrical connections to other parts of ITO. Observations confirmed that there are no electrical connections with any other parts of ITO.

SEM and EDX were also used to investigate the electrodes. The width of the electrodes was measured using their SEM images at various points along the length of each electrode on a plate. **Figure 15** shows that the electrode widths, as determined by SEM, are greater than their nominal widths. During EDX measurements, we focused on the elements indium and silicon. Detailed structural and morphological imaging of a 100µm electrode is provided in **Figure 16.** The EDX data clearly show that the ITO is layer eliminated along the cut when the electrodes are exposed to specific parameters of the laser. **Fig.14 d** depicts the indium signal for cross-sections of electrodes of widths 25, 50, and 100 µm.

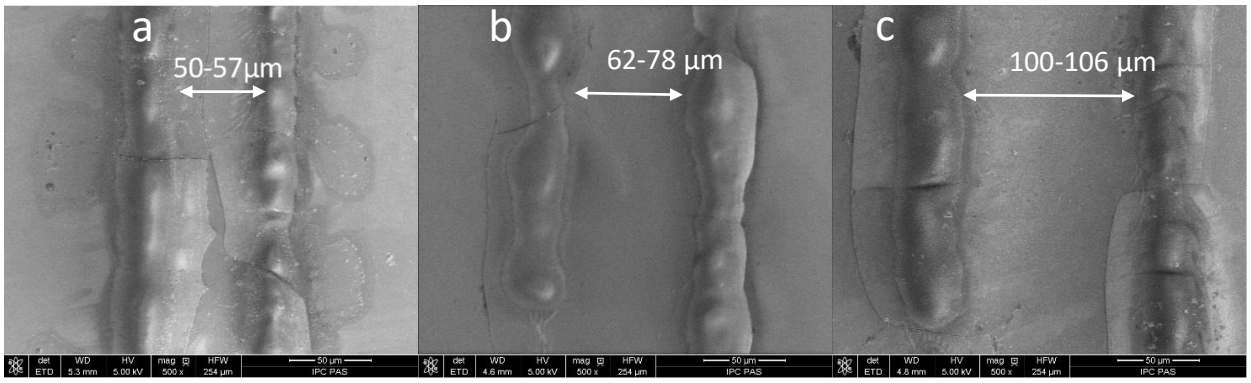

Fig.15 SEM images of the rectangular-shaped electrodes: a) 25µm, b) 50µm, c) 100µm.

2.3.3.2 Electrochemistry

Cyclic voltammetry (CV) was used to characterize the ITO microelectrodes and MEAs prepared using CO_2 laser. The rectangular electrodes of all sizes within the same plate exhibited diffusion-controlled CVs with reproducible signals. Additionally, the plate-to-plate reproducibility of their signals was quite good (14.2% for all electrodes on 5 different plates(batches)). The lack of stabilization of the signal where the limiting current should be seen, and lower inclination of the

voltammogram slope point towards resistivity of the electrode paths. The resistivity of the electrode path has a greater impact as the pattern becomes narrower. This phenomenon is particularly evident in the chosen electrode pattern because it has a high width-to-length ratio, ranging from 1:100 to 1:25, for the designs that were tested. Since even the patterns with a 1:25 ratio already produce satisfactory results, standard electrodes with a ratio of 1:1 or similar should not be affected by resistivity, even with very narrow widths. The cyclic voltammograms of electrodes of different sizes, where each set is from a single plate, are shown in **figure 17**.

The in-situ stencil fabrication followed by etching proved to be the most effective approach for producing larger circular-shaped electrodes (with a diameter of 1.75 mm and a geometrical surface area of 2.41 mm^2). This method, which involves using a laser to ablate the stencil deposited on ITO, results in structures with a larger footprint while avoiding damage to the edges. Cyclic Voltammogram of the ITO circular electrodes on different plates are provided in **figure 18.**

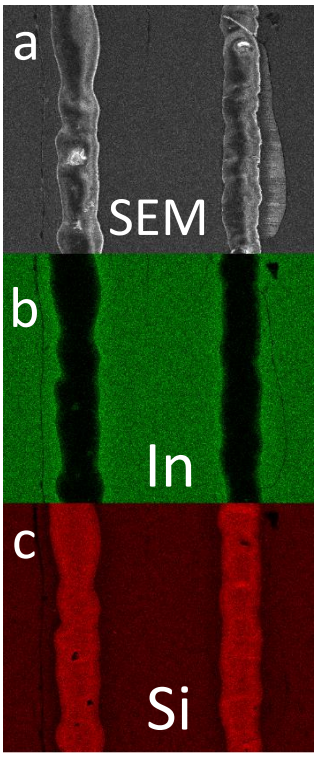

Fig.16 Detailed structural and morphological imaging of a 100μm electrode. a) an electron image (SEM image) of the electrode, b) an EDX map showing indium (green), c) an EDX map showing silicon (red).

2.3.3.3 Scanning electrochemical microscopy (SECM) analysis

The topography characteristics of the laser-cut electrodes were already exposed by optical microscopy and profilometry. These measurements were very helpful for us in choosing the hopping mode feedback imaging. The constant height SECM imaging of such samples might result in tip damage. The hopping mode SECM imaging avoids a probable collision of the SECM tip and the sample. High-resolution simultaneous topography and activity imaging are possible in this mode. When the equipment has a piezoelectric positioning set-up, the probe (tip) size frequently restricts the lateral resolution of SECM. The topography, activity, and optical images of an ITO microband isolated from the rest of the ITO slide by two laser-processed lines are shown in **figure 19**.

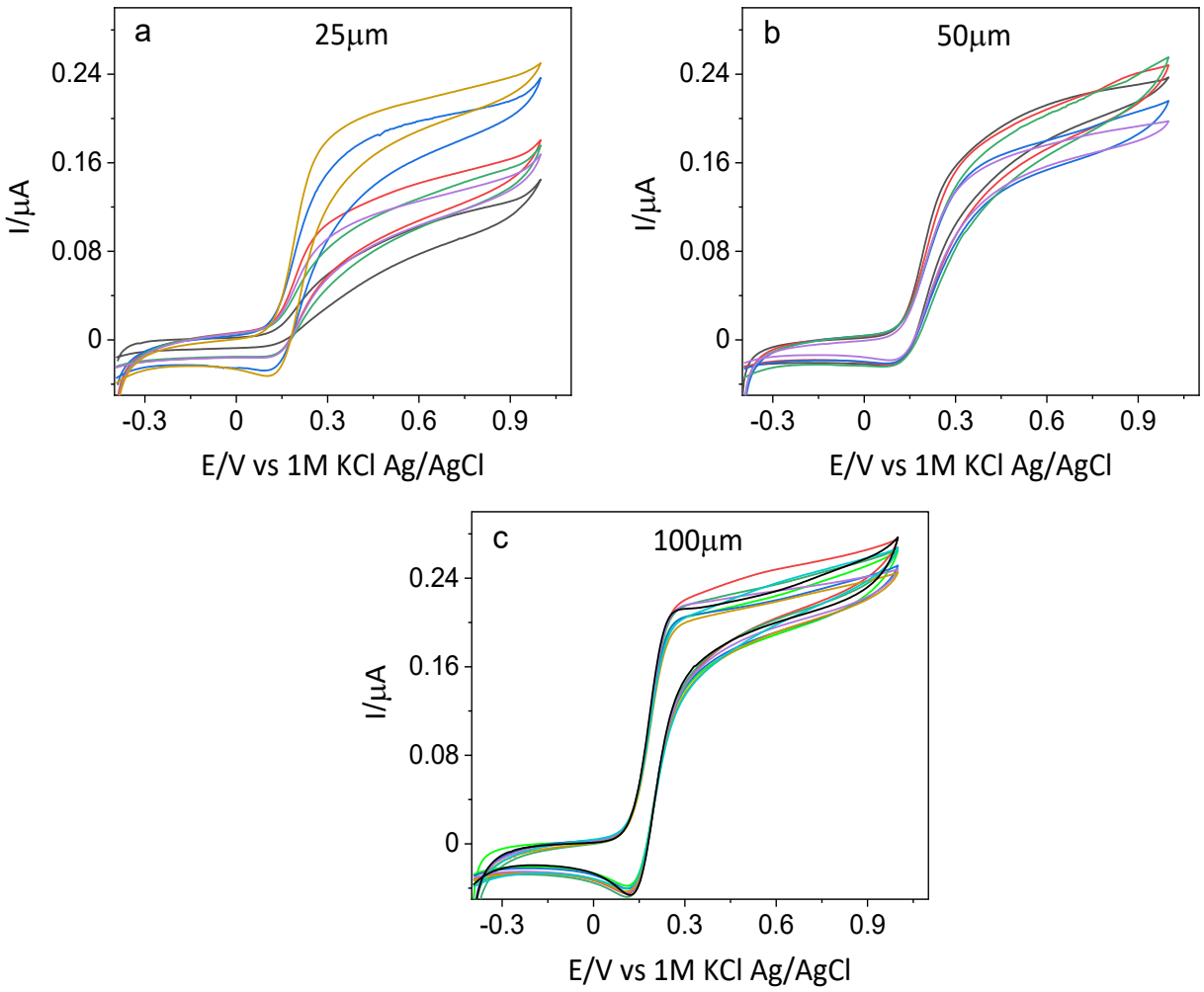

Fig.17 Cyclic voltammograms of electrodes of different sizes (a)25, (b)50 and (c)100µm width in 1 mM FcDM and 0.1 M KNO_3. Each set of electrodes comes from the same plate.

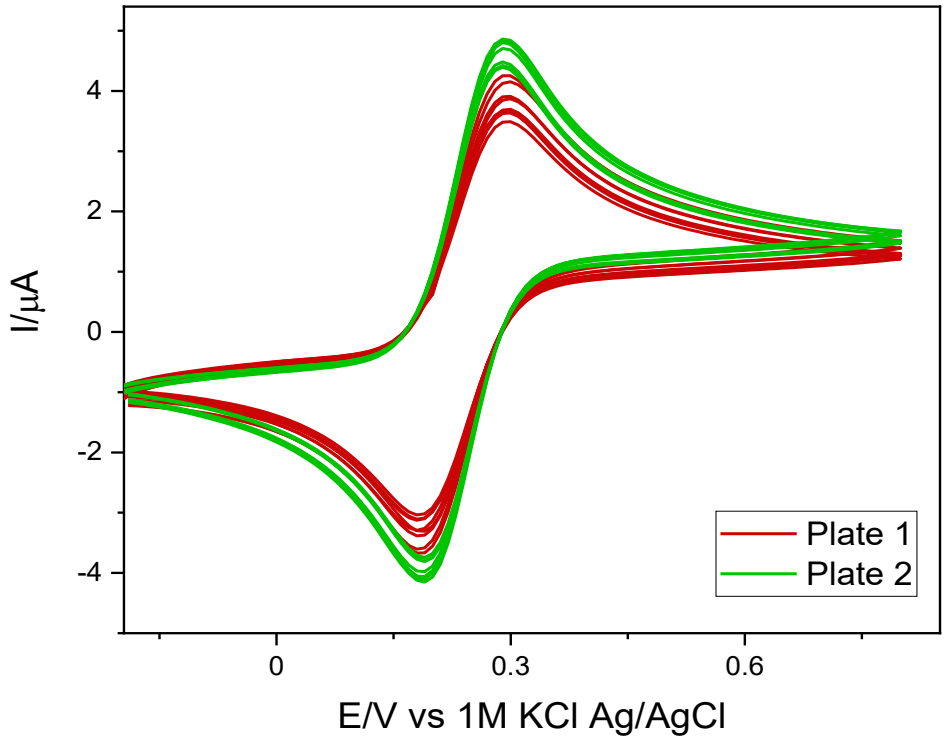

Fig.18 Cyclic Voltammogram of the ITO circular electrodes on different plates.

It is clear that the ITO layer along the laser path is effectively removed. Deactivated ITO has an uneven breadth within a range of 60 to 100 μm. As a result, the ITO microband between laser beams has a width of around 60-90 μm when the centers of the laser paths are 150 μm apart. An optical microscopy image does not show this. The optically intact regions of ITO proximate to the laser trajectories exhibit diminished charge transfer properties. The sample is recessed in the middle of the laser path while its edges protrude to about 3 μm over the ITO slide.

In the context of electrodes fabricated through laser ablation of scotch tape stencils and chemical etching, the selective etching of the ~260 nm thick ITO layer does not yield significant alterations in the topographical features of the resulting sample. The ITO structures do not protrude beyond this thickness above the glass substrate. A microelectrode with a radius of ~1.3 μm, scanning at a distance of ~3.25 μm, can be deemed sufficiently flat for constant-height SECM imaging. An SECM image of a broader etched ITO, obtained using a carbon microelectrode with Ø ~2.6 μm, illustrates a slightly elevated activity within a zone of ~30 μm width at the periphery of the etched ITO. This phenomenon may arise from the penetration of the etchant solution between the ITO and the deposited mask, where the etching agent eliminates intrinsic contaminations from the ITO surface.

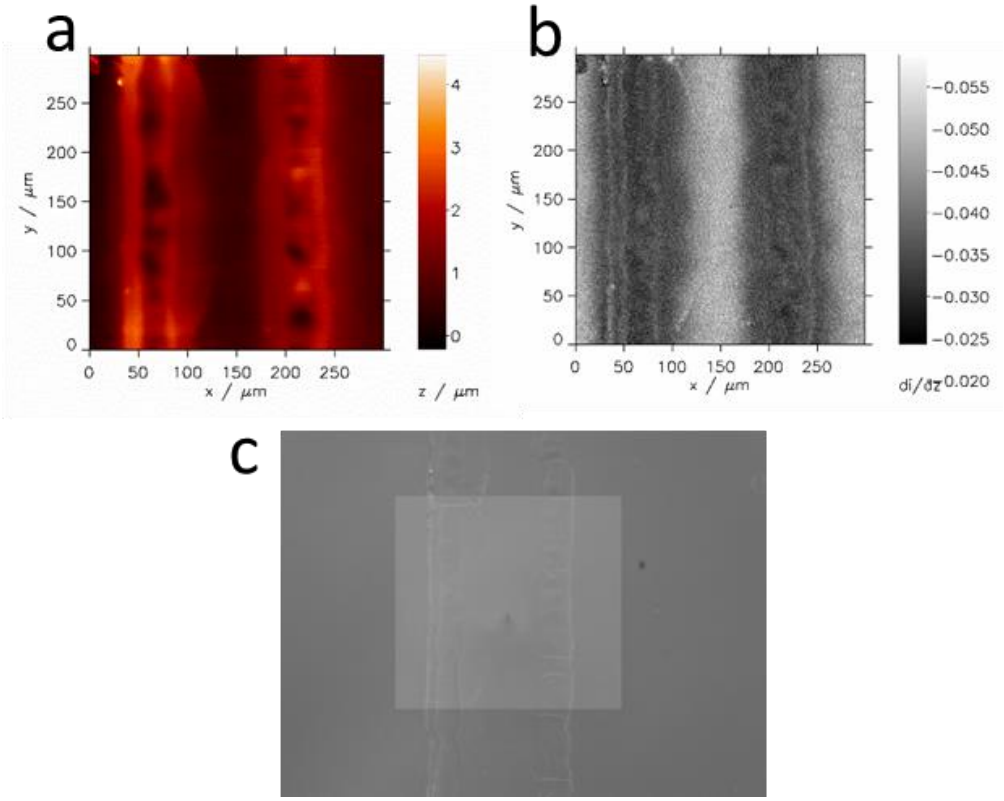

Fig. 19 Hopping mode SECM images: topography (a), activity (b) and optical micrograph (c) of ITO microband separated from remaining ITO slide by laser-cutting. Scanning area: (300 × 300) µm². Carbon microelectrode (SECM tip, Ø ca. 5.5 µm) is seen in the center of the optical image. Retracting distance: 10 µm. Effective scanning rate: 3 image pixels per second. Electrolyte: aqueous 1 mM ferrocenemethanol in 0.1 M KCl.

2.3.3.4 Reproducibility

We conducted cyclic voltammetry with electrodes from various batches in the redox probe FcDM to show the variability in their current responses. The current values at a potential of 0.29 V were plotted against electrode size. Among the three sizes tested, the 100µm wide electrodes were the most consistent and had the most uniform current ranges within each plate. Nonetheless, their increased width also signifies a greater influence of correctly positioning the insulation. However, there was less uniformity between different batches of 100µm electrodes (**Fig.20**). This deviation is likely due to manual errors during the pasting of Kapton tapes, making the length of the electrodes 10 to 15% shorter or longer. The 50µm and 25µm electrodes showed greater variability within each plate, as seen in **figure 17**.

The current value does not scale with size for 50 and 100μm wide electrodes (**Fig.20**) due to possible differences in ITO activity at the edges caused by laser ablation. Experimental verification via SECM activity and topography analysis in hopping mode feedback mode imaging confirmed that ITO in the vicinity of the laser paths is electrochemically inert. Consequently, the effective width of the active electrodes is narrower than the measurements obtained optically or through EDX and SEM.

Another factor leading to non-linearity in width scaling arises from the presence of ITO near larger electrodes. Even though these electrodes are not biased (floating), they act as local concentration cells at the open circuit potential, replenishing the substrate for the rectangular microelectrode[201]. This effect can be mitigated by selectively etching away the unnecessary ITO using the stencil method.

Figure 21 also demonstrates the reproducibility within and between the ITO plates. It displays current values extracted from CV measurements at a specific potential for individual electrodes from various batches (plates). The electrodes that are presented here are rectangular shaped with a length of 2.5 mm and come in three widths but can be tailored to different dimensions such as shorter lengths for smaller microelectrodes.

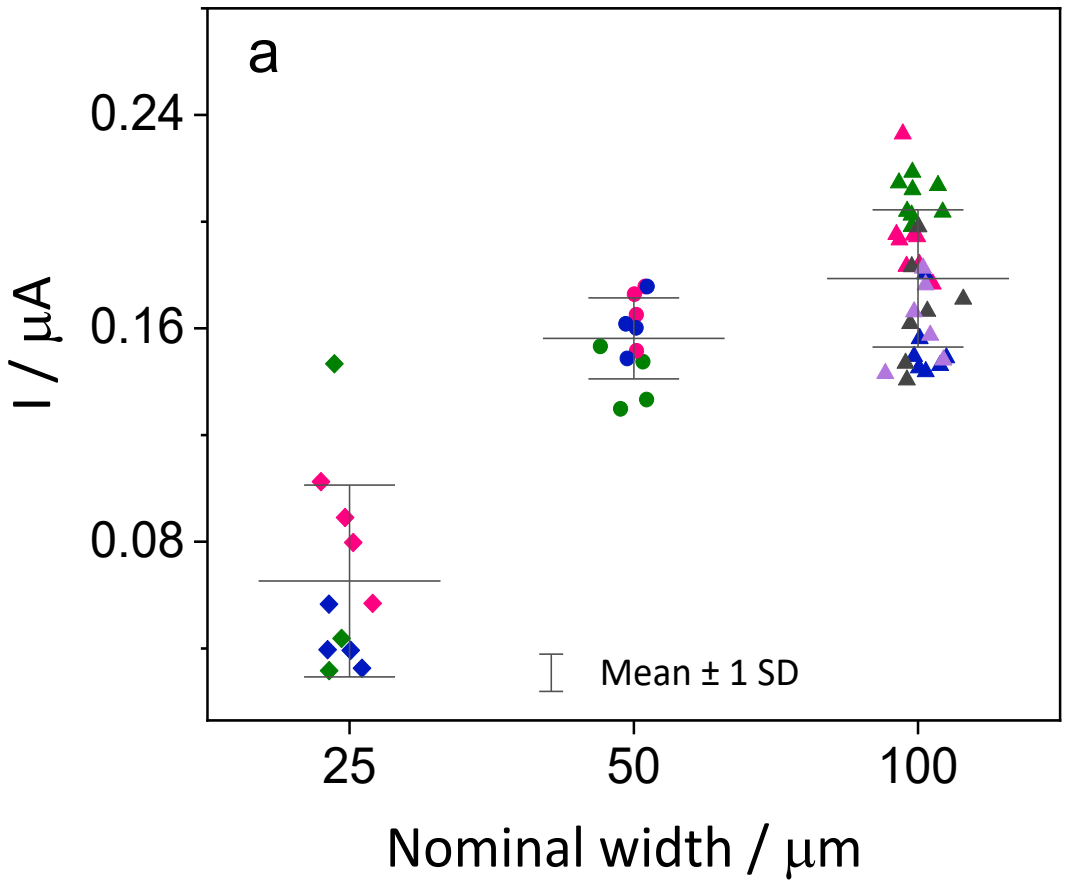

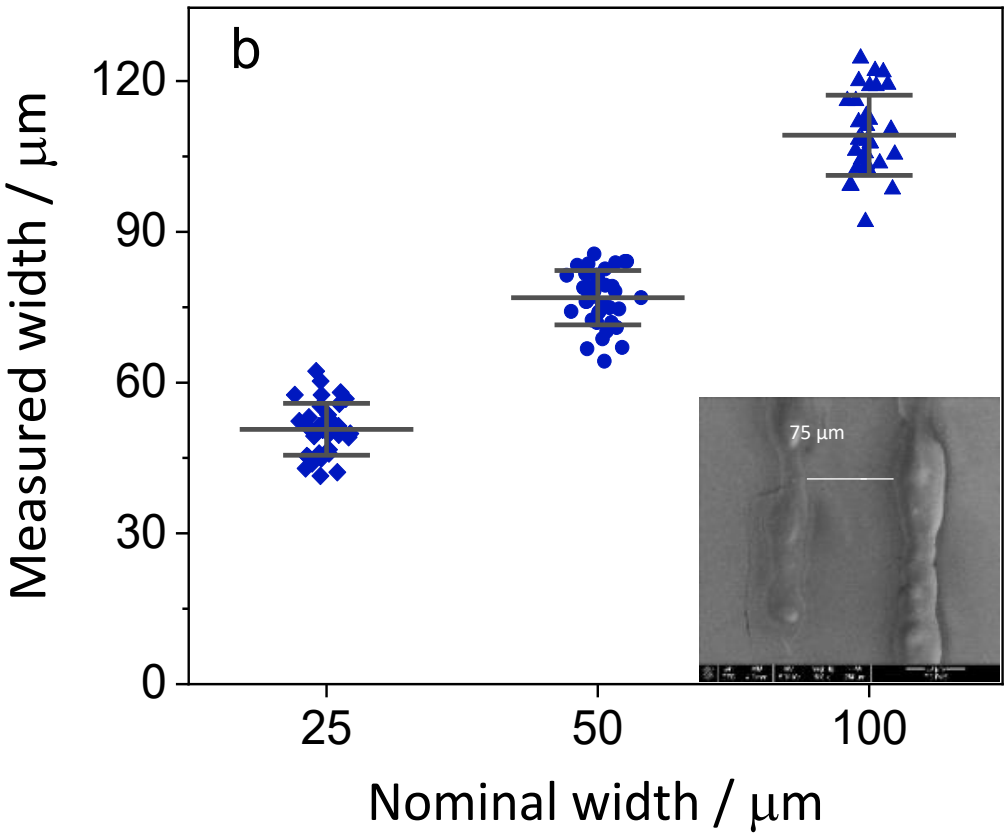

Fig.20 Reproducibility of electrode signals with respect to their nominal width are shown. a) gives the comparison of current results obtained from the cyclic voltammograms of the electrodes at 0.29 V, diamond shapes represent the 25 µm, circles the 50 µm, and triangles the 100µm wide electrodes. Each color represents a different ITO plate, b) gives the comparison of the width of the electrodes as measured by SEM technique. The diamond shapes represent 25 µm, circles the 50 µm, and triangles the 100µm wide electrodes from different plates. The inset shows an example of SEM image of an electrode with 50 µm nominal width.

2.3.3.5 Availability

While the proposed methods may not achieve the same level of precision in pattern or line width as top-end lasers (such as Yb:YAG, Nd:glass, KrF) (see **Table A1**), they offer a cost-effective alternative requiring minimal equipment investment, and can even utilize external resources. Laser plotters, like the one employed in this study, are commonly found in printing shops for tasks like stamp preparation, cutting, and engraving. To show that this technology is widely applicable, we successfully produced a few batches of electrodes using both methods at a local printing shop. Although some adjustments to power settings were necessary and a few structures had minor imperfections in the cut, these issues could likely be mitigated through optics cleaning. Nevertheless,

we were able to achieve good intra-workshop reproducibility with comparable electrochemical performance as included in **figures 22 and 23.**

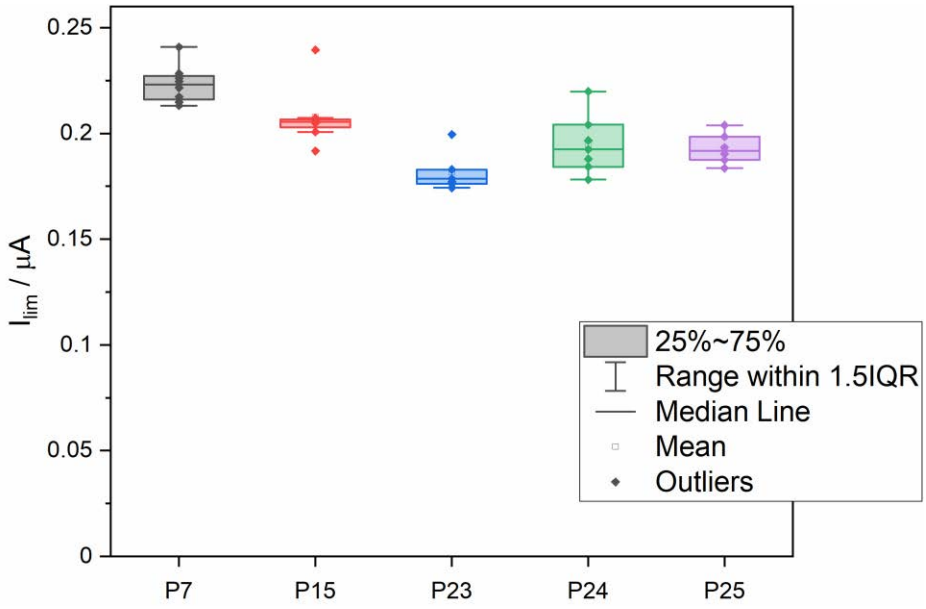

Fig. 21 Comparison of current results obtained from cyclic voltammograms of 36 electrodes at 0.29V. The numbers at the x-axis represent different ITO plates, and each point is a measurement for an individual electrode on that plate. All electrodes here have a nominal width of 100 µm.

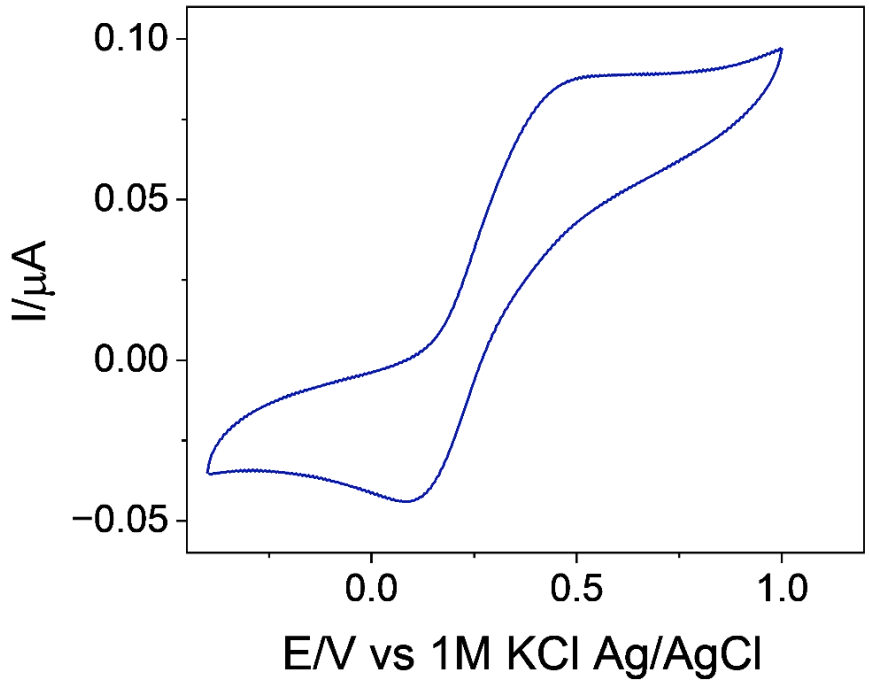

Fig.22 Cyclic voltammogram of a 100µm wide electrode prepared in a printing shop.

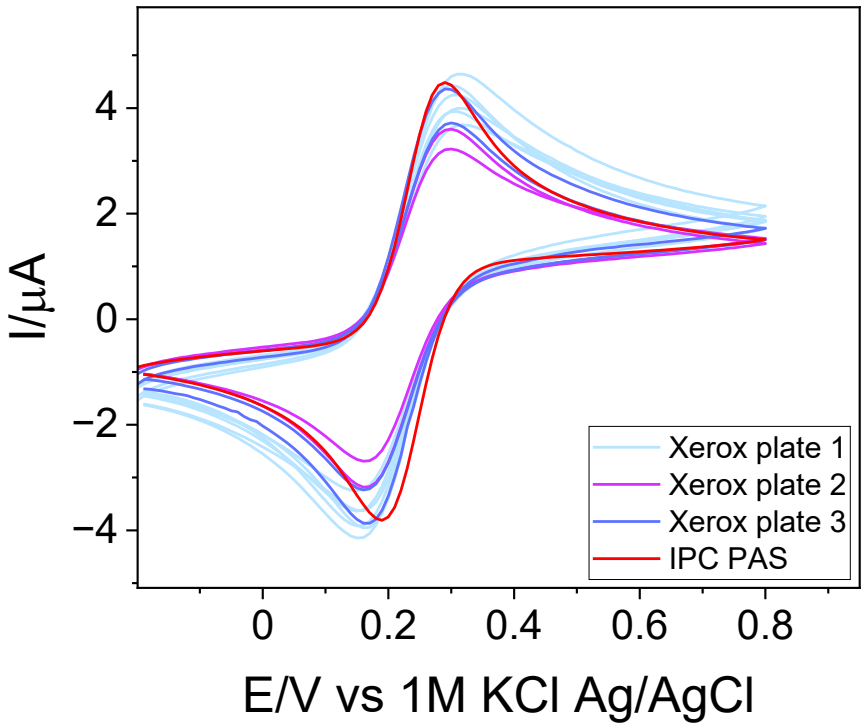

Fig.23 Comparison of cyclic voltammograms of the ITO circular electrodes on different plates prepared in a printing shop-each plate marked with a separate colour, with the electrode signal prepared in the laboratory setting (black).

2.4 Conclusions

This chapter provides a detailed description of fabrication and characterization of microelectrodes and microelectrode arrays for biosensing applications. Initially Pt microwires were used for the preparation of electrodes, but other than cyclic voltammetry and optical microscopy, no further experimental techniques were used to characterize these electrodes because of their poor performance and the optimization of the technique was time-consuming. When the laser cut Pt microelectrodes are considered, in spite of having a few positive responses, the resultant electrodes were fragile, bent, and had uneven ends. Different methods of cutting the wires, including laser treatment, also resulted in poor surface definition or damage to insulation. Overall, the methods we used to fabricate platinum microelectrodes could not be optimized to match the expected standards for sensing applications. The consistent and reliable data collected ultimately led to more meaningful ideas and proceeded to low-cost fabrication of ITO electrodes through a novel laser assisted method.

We successfully optimised the CO_2 laser cutting of ITO-coated glass plates into functional electrodes. Two separate techniques were used to prepare electrodes of different shapes and sizes. Direct patterning was used for the smaller rectangular shaped microelectrodes (smallest widths optimized

were 25, 50, and 100 μm wide), whereas in-situ stencil fabrication followed by etching was found to be the best method for the larger circular electrodes (diameter 1.75 mm, 2.41 mm^2 of geometric surface area). Direct laser ablation allowed for the fabrication of smaller features, but it resulted in edge damage, leading to a reduced electroactive area compared to measurements obtained through optical microscopy, SEM, or EDX (approximately 80 μm width active for charge transfer in 100 μm wide structures). On the other hand, the second method, involving laser ablation of the stencil deposited on ITO, produced structures with a larger footprint (minimum feature size of ~100 μm) without damaging the edges. Both methods, when combined, form a versatile toolbox for fabricating small structures through direct ablation and removing ITO from larger surfaces using the stencil method. All the fabricated electrodes and electrode arrays exhibited stable and reproducible signals. The average standard deviation for current was 7.8% within a single plate for 100 μm wide patterns and 14.2% for all electrodes across five different plates (batches) (see **Fig. 21**). Single electrodes were used repeatedly over several months without a deterioration in signal over time. These cost-effective, easily fabricated, simple, and convenient to use ITO electrodes can be employed as contemporary working electrode across various applications, including sensing, bio-sensing, EWOD, microfluidics, cell culture studies, and more. As a demonstration, the electrode arrays were utilized for characterizing cell cultures using electrochemical impedance spectroscopy (EIS) (details are provided in chapter 3).

3 Application of ITO Electrodes for Cell Culture Monitoring

The search for breakthrough technologies frequently calls for the development of novel instruments and procedures in the fields of materials science and electrochemistry. Our home-built Indium Tin Oxide (ITO) microelectrodes and microelectrode arrays (complete fabrication methods are provided in Chapter 2) provide a simple, low-cost method seeking to push the boundaries of scientific exploration and technological advancement[196].

This chapter explores the applications of ITO microelectrode arrays developed in our laboratory. Electrochemical impedance spectroscopy (EIS) is used as a tool to demonstrate their functionality. EIS has garnered much interest in the fields of electrochemistry, materials science, and other academic fields due to its capacity to investigate complex interfacial processes, electrical properties, and the dynamics of electrochemical systems[149]. It is a quick, sensitive, label-free, non-destructive electroanalytical method for examining biological processes[131,149,202]. Therefore, cell-based EIS was used to analyse the behaviour of the ITO microelectrode arrays on the attachment of cells onto their surface.

3.1 Methods

3.1.1 Routine cell culture

The HeLa and HepG2 cell lines came from the American Type Culture Collection (ATCC, Manassas, USA). The mouse hepatocytes were isolated from mouse liver tissues by Elżbieta Jarosińska. All the cell lines were cultured as a standard monolayer in the complete growth medium, supplemented with fetal bovine serum 10% v/v (FBS, Gibco), L-glutamine 1% v/v (Sigma-Aldrich), and the antibiotics: streptomycin [10,000 U ml−1] and penicillin [10 mg ml−1] 1% v/v (Sigma-Aldrich). Cultures were performed under standard conditions (37 °C, 5% CO2). Both cell lines were cultured in Dulbecco's Modified Eagle's Medium (DMEM) with low glucose content (1g/L) (Institute of Immunology and Experimental Technology, Wrocław, Poland). Using regular passages, cells were maintained in a logarithmic growth phase. 0.25% Trypsin–EDTA solution (Sigma-Aldrich) was used to detach cells from the surface.

3.1.2 Cell culture monitoring using Impedance spectroscopy

Except where otherwise specified, all impedance spectroscopy tests were carried out using a PalmSens4 potentiostat galvanostat equipped with an Electrochemical Impedance Spectroscopy (EIS)

module and PSTrace software. The Ag/AgCl (1M KCl) reference electrode, platinum wire counter electrode, and ITO working electrodes constituted the three electrodes of the electrochemical cell. A closed, temperature-controlled experiment chamber maintained at 37 °C was used to perform the measurements.

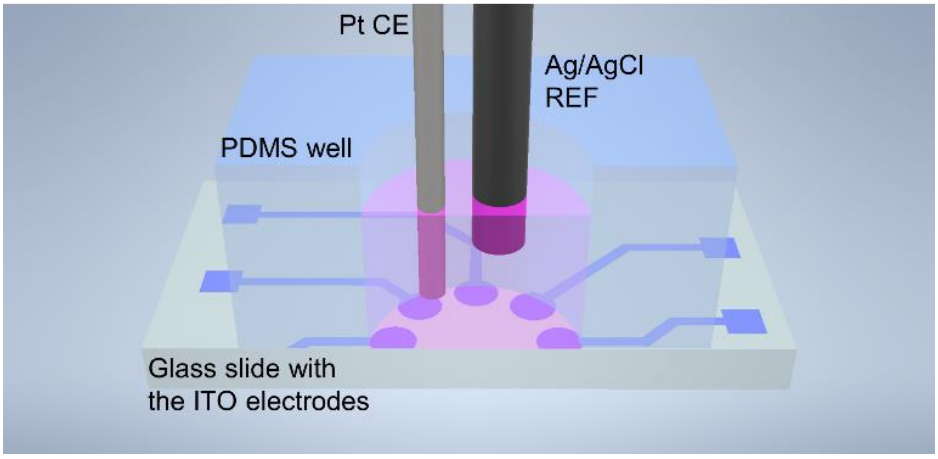

Fig. 24 Schematic representation of the measurement setup used for impedance spectroscopy of cell culture.

The cells have an adhesive character, and once they grip to the surface of the working electrode, they tend to obstruct the flow of current between the electrodes. This describes the current that passes via intercellular and accessible cell substrate space. When the cells on the electrode approach confluence, the impedance clearly fluctuates and alters at an accelerated rate[203].

Since multiple studies have shown recordings at various frequencies[203,204], impedance measurements were recorded on cells over a range of 37 frequencies so that the most suitable parameters for our system are identified. The frequency range for the experiments was selected between the margins of 10Hz and 40kHz. The initial measurements were conducted to understand behaviour of cell cultures with respect to the DMEM solution (considered as a blank solution) and determine the relative impedance change and phase angle shifts. The results of these recordings showed a noticeable rise in the impedance value ($\Delta Z \approx$ 2.5 to 4.5 kΩ) and phase angle shift ($\Delta\Phi \approx$ -10^{o}) within the frequency range of 70 to 10 kHz. This observed trend aligns with advancing insulating properties attributed to the attachment of cells to the electrode surfaces. At frequencies higher than 10 kHz, a very small phase shift ($\Delta\Phi \approx 2^{o}$), along with non-significant rise in impedance values ($\Delta Z \approx$ 30Ω) were observed. Since the highest phase angle shift and elevation of the cell impedance values relative to the blank were observed in the range of 70 to 100 Hz, the studies were carried out at 0.2 V, within this operating frequency range.

The majority of these measurements lasted only a couple of hours. The electrode well was simply filled with 150 μL of DMEM when the potentiostatic experiments first began, and impedance was recorded until the medium is stabilized. After that, 150 μL of cells with a density of 1.33 x 10^6 cells/mL were added to the medium in the well to study how the cells adhere to the electrodes and alter their surface properties. The system was then exposed to 150 μL of trypsin to observe the removal of cells from the electrode surface.

3.2 Results and discussions

3.2.1 Impedance spectroscopy

Circular electrode geometries are particularly recommended for applications involving the observation of volumetric sections (as commonly encountered in medical field applications)[159,205]. Hence, for our cell culture studies, we employed a methodology to construct an electrode array with a circular geometry, with each array featuring eight equally spaced, identical electrodes. Furthermore, circular electrodes within such an array afford a symmetrical electric field distribution due to their uniformly distributed layout. This uniformity plays a pivotal role in ensuring consistent and controlled electrical interactions with both the surrounding medium and the cells under investigation.

Potentiostatic readings were taken at a fixed potential against open circuit potential (OCP), to ensure the stability of the system. The recordings were started with only cell culture medium in the well, later when the medium was stabilized, cells were introduced to the system. The attachment of the cells to the electrode surface was then observed. Following this, trypsin was added to the well to track cell detachment from the electrodes. Any current or voltage input to the medium in the absence of cells only resulted in interfacial impedance in series with ionic solution conductivity. Real-time impedance monitoring of mouse hepatocytes cell culture is depicted in **figure 25.** Consistent signals recorded across all 8 electrodes of a circular electrode array can be observed in the graph.

As expected, the results showed lower resistance values and a more relaxed growth pattern during the impedance measurements with cell culture medium alone, compared to the impedance growth when the cells were assembling in close contact with the electrode surface. This connection formed a barrier that impedance signals had to cross before achieving solution resistance, resulting in a combination of resistive and capacitive elements. While capacitive effects were due to insulating cell membranes, resistive effects were due to the ionic properties of cytoplasm[204]. Although it was impossible to remove all electrode-attached cells within an hour of adding trypsin, it was evident that by this short time

interval, a significant portion of cells was successfully removed from the substrate contact. This was because it was possible to reduce the cell layer resistance to the point where the final signal resembled those throughout the absence of cells. For the measurements conducted, the adherence interaction did not appear to make substantial changes in the resistance component Z'. However, noticeable changes in the capacitance component Z" were observed within the measurement conditions, making Z" a more dependable variable than Z'. Therefore, this thesis explains all the experimental impedance data with respect to its capacitive component.

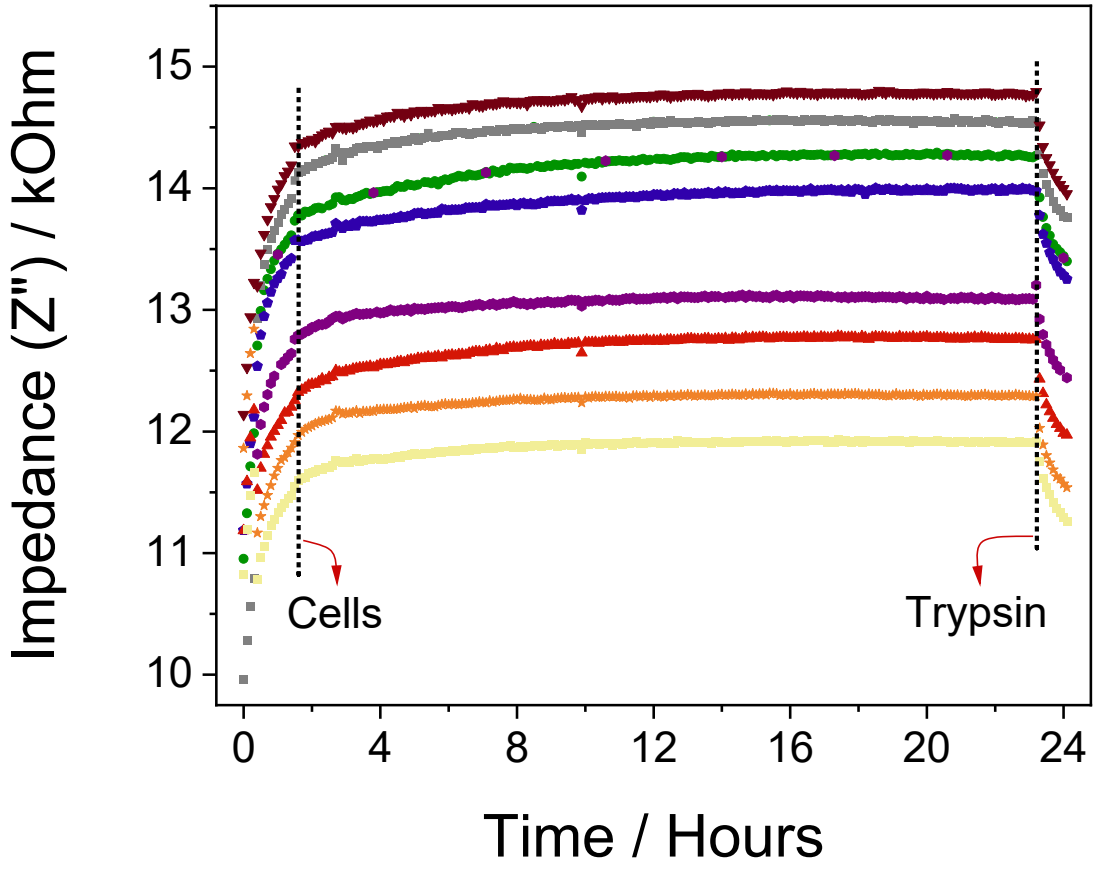

Fig.25 Impedance recording of mouse hepatocytes culture showing cell adhesion and detachment (frequency = 72.1 Hz, measurement time = 24 hours). Each colour represents a different electrode.

The cell-based EIS can also be used to perform concentration dependent studies[206]. To illustrate that the impedance measurements described here can differentiate between cell densities, two concentrations of HepG2 cells (1X 10^6 and 1X 10^8 cells/mL) were analysed. The experiments were run continuously for 2 hours without any pause while adding cells or trypsin. Although the signal for trypsin in the case of higher cell density (illustrated in pink colour) was not as expected, a clear difference was observed in the signals of both HepG2 samples (**Fig. 26**). In the case of higher density

of cells, the concentration of trypsin used was very less compared to the overall concentration of the liquid in the well. The added trypsin was not sufficient to trigger the detachment of cells immediately. In this case, a higher concentration of trypsin would have facilitated the removal of cells. To check the activity of trypsin, control experiments were conducted by recording the impedance of cell culture medium and trypsin. While the experimental set-up contained the culture medium alone, the impedance signals were growing. This is the result of attachment of amino acids, glucose or other components constituting the medium on to the electrode surface. On addition of trypsin, the impedance values began to decrease implying the removal of these adsorbed species from the electrode. This observation validated the effective functioning of trypsin as per the study's objectives (**Fig.27**). Complex experiments like continuous monitoring of the growing cell cultures can be easily conducted using such EIS techniques.

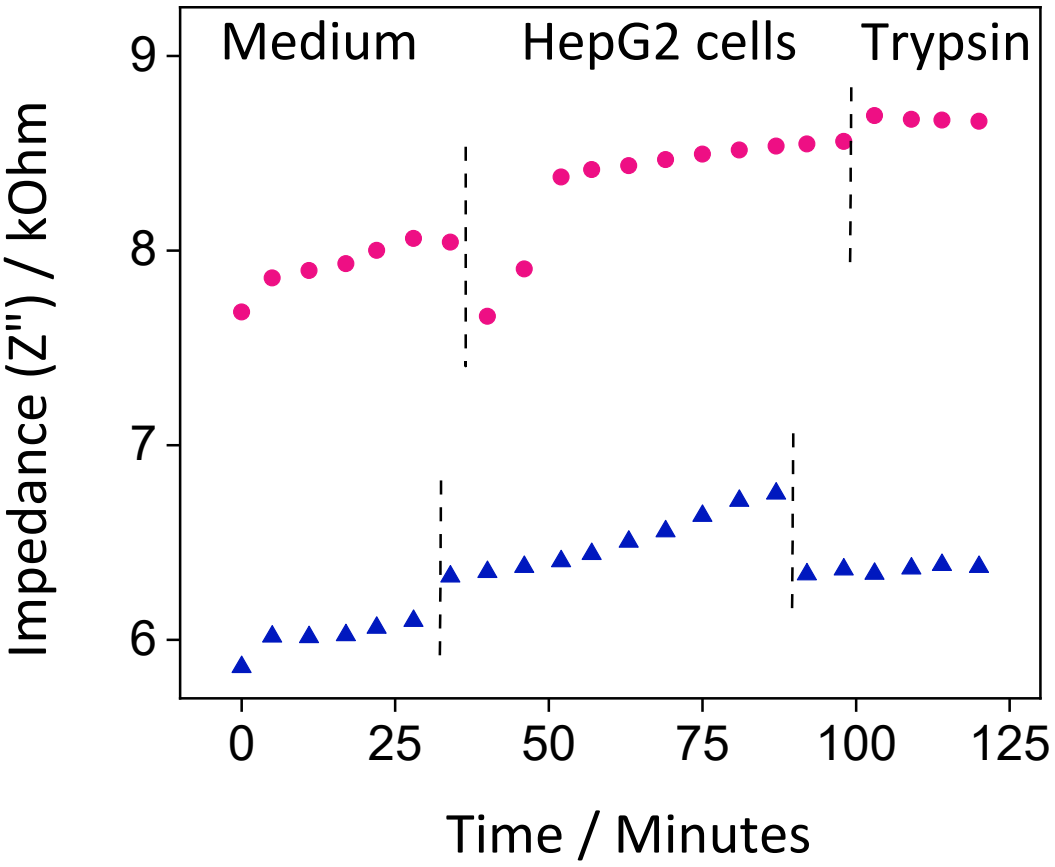

Fig. 26 Impedance evaluations for two concentrations of 2D HepG2 cell culture, with comparable signals obtained from two different measurements. The pink colour represents signals of the higher (1X 10^8 cells/mL) and the blue represents the lower concentration of cells (1X 10^6 cells/mL).

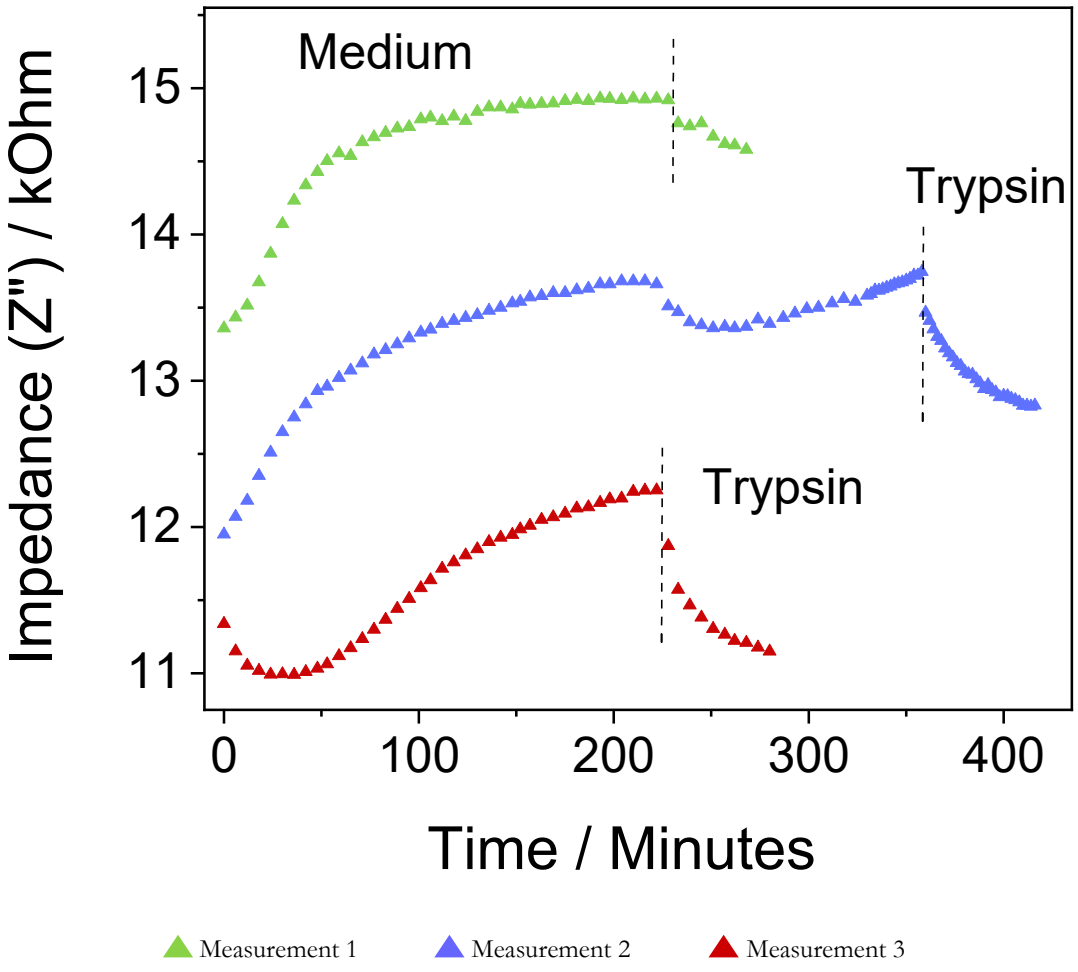

Fig.27 Control experiments conducted to monitor the activity of trypsin.

3.3 Conclusions

ITO electrodes prepared using a CO_2 laser plotter are versatile, and have the potential to serve as any conventional working electrodes. They can be applied across various fields including sensing, bio-sensing, electrowetting on dielectric (EWOD), microfluidics, cell culture studies, and beyond. Our main interest lies in bio-sensing. Microelectrode arrays prepared by the laser cutting of scotch tape stencils and chemical etching of the ITO patterns are particularly designed to suit such studies. The ITO MEAs consists of circular electrode arrays with eight identical electrodes, ensuring symmetrical electric field distribution.

Electrochemical impedance spectroscopy (EIS) serves as a rapid and potent tool for investigating biorecognition events occurring on the electrode surface, and it is equally effective in characterizing modifications to the electrode surface. Therefore, to exemplify the utility of these ITO MEAs we

employed EIS for the characterization of cell cultures. While the cells were adsorbed on the electrode surface, impedance values were increasing. This indicated the modification of surface properties of bare ITO electrodes and changing their conductivity. The capacitance component (Z'') exhibits accountable changes in the behaviour of the cell cultures, and emerges as the reliable variable. Thus far, we have successfully conducted various measurements lasting up to a duration of 24 hours. To further analyse cell viability comprehensively, the duration of these experiments will be extended to 72 hours or more. Subsequently, studies will be expanded to include cytotoxicity analysis, enabling the extraction of maximum data crucial for advanced sensing applications.

4 Mediators for glucose sensing

This chapter describes the synthesis of redox mediators for glucose biosensing. A detailed explanation of how two different approaches can be used to develop mediators for glucose biosensors is provided. One of the types of mediators used in this work is redox hydrogels based on poly (vinyl imidazole) (PVI) polymers containing cis-$Os(N\text{-}N)_2Cl_2$ redox centres. As these redox hydrogels consist of a metal part and a polymer part, they are referred to as metallopolymers. Another approach involves using Prussian Blue (PB) analogues as a mediator for the selective detection of hydrogen peroxide. The preparation methods for both mediators are very different. While the synthesis of osmium metallopolymers follows traditional techniques, PB analogues are synthesized through a novel technique based on flash light sintering (FLS). These mediators will be used to prepare easy-to-make, stable amperometric electrochemical glucose biosensors that function at low overpotential to reduce the impact of electroactive interferents. As an example, glucose sensing is performed with a PVI-bound osmium redox polymer mediator synthesized by Professor Donal Leech and co-workers at the National University of Ireland (NUI) Galway. In the case of Prussian Blue, H_2O_2 sensing is conducted with a PB sample obtained from EPFL Valais Wallis, Sion, Switzerland.

The materials used, synthetic methods, immobilization techniques and the results obtained during the preparation of both Os-PVI metallopolymer and Prussian Blue analogues are provided in the following sections of this chapter.

4.1 Osmium-based redox polymers as mediators for glucose sensing

4.1.1 Chemicals

4,4'-dimethoxy-22'-bipyridine (dmobpy), ethylene glycol, sodium dithionite, vinyl imidazole (VI), methanol, 4,4'-azobis (4-cyanopentanoic acid) (ACPA), triethylammonium phosphate (TEAP), tetrabutylammonium chloride (TBACl), glucose, glucose oxidase from Aspergillus niger (100,000-250,000 units/g solid), and glutaraldehyde solution were purchased from Sigma-Aldrich. Diethyl ether and ethanol were obtained from POCH. Azobisisobutyronitrile (AIBN) was obtained from the Warsaw University of Technology. 2,2'-bipyridine (bpy) (from Merck), $(NH_4)_2OsCl_6$ (from Alfa Aesar), and N, N'-methylenebis acrylamide (MDAA) (from Roth) were the other chemicals used. Water was filtered and deionized from a Sartorius Arium Comfort I system and a Rephile NuZar U24 water system.

4.1.2 Methods

4.1.2.1 Synthesis of osmium-based metallopolymers

In this study, a PVI-bound osmium polypyridyl complex was chosen as the metallopolymer to be used as a redox mediator for glucose sensing. The polymer, coupled with the osmium complex, can be used to wire the glucose oxidase enzyme to the working electrodes. The synthesis consists of three steps, as listed below.

Synopsis

Step 1: Syntheses of polypyridyl osmium complex ($Os(N\text{-}N)_2Cl_2$).

Step 2: Synthesis of poly (vinyl imidazole).

Step 3: Synthesis of PVI-bound osmium redox polymers.

In step 3, the $Os(N\text{-}N)_2Cl_2$ complex is combined with PVI to obtain the metallopolymer as the final product. **Scheme 2** shows a simplified reaction that represents step 3. The summary of the experiments involved in the synthesis of osmium-based redox polymers are given in **Table 2**. The following sections provide detailed descriptions of the procedures as performed at IPC, PAS.

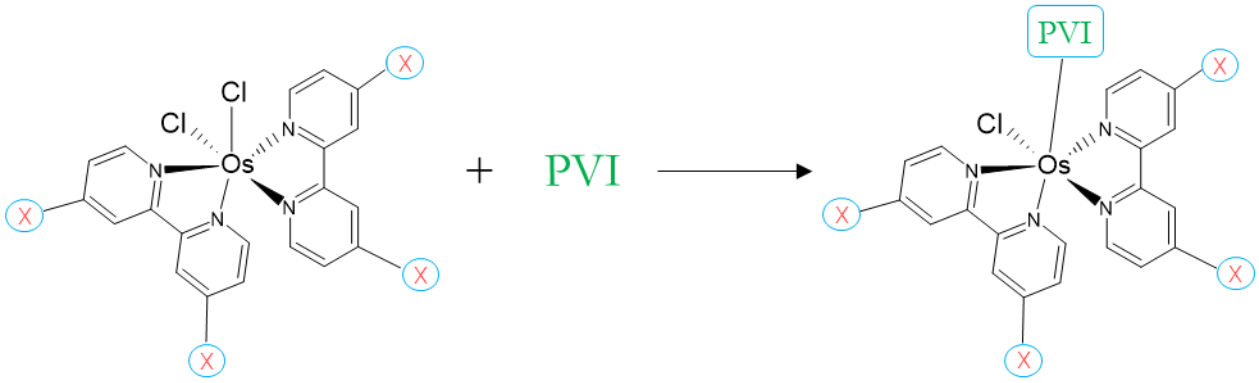

($Os(N\text{-}N)_2Cl_2$) PVI-bound osmium redox polymer

Scheme 2. A simplified reaction for the synthesis of osmium metallopolymer.

"X" can be H or methoxy group. When X = H, the ligand coordinating osmium is 2,2'-bipyridine, and the osmium complex is named dichlorobis(2,2'-bipyridine)osmium(II) by IUPAC nomenclature. This compound name can be abbreviated as $Os(bpy)_2Cl_2$. If X = OMe, the ligand is 4,4'- dimethoxy-2,2'-bipyridine, and the corresponding osmium complex is (dichlorobis(4,4'- dimethoxy-2,2'-bipyridine)osmium(II)). This IUPAC name can be abbreviated as $Os(dmobpy)_2Cl_2$. In this thesis, both

IUPAC and the abbreviated names of the above-mentioned osmium complexes are used interchangeably.

Table 2. The summary of the experiments involved in the synthesis of osmium-based redox polymers.

Compound No.	Product	Starting Materials Used	Characterizations
Osmium complexes synthesized according to step 1			
1	$Os(dmobpy)_2Cl_2$	$(NH_4)_2OsCl_6$ + 2,2'-bipyridine	CV, UV-vis spectroscopy, NMR
2	$Os(bpy)_2Cl_2$	$(NH_4)_2OsCl_6$ + 4,4'- dimethoxy-2,2'-bipyridine	CV, Elemental analysis
PVI synthesized according to step 2			
3	Crosslinked PVI	vinyl imidazole + MDAA crosslinker + ACPA initiator	^{13}C NMR
4	Linear PVI	vinyl imidazole + ACPA initiator	
5	Linear PVI	vinyl imidazole + AIBN initiator	^{1}H NMR
PVI-bound osmium redox polymers synthesized according to step 3			
6	$[Os(dmobpy)_2(PVI)_{10}Cl]^+$	5 + 1	CV, Mass spectrometry, UV-vis spectroscopy
7	$[Os(bpy)_2(PVI)_{10}Cl]^+$	5 + 2	CV, Mass spectrometry

Step 1: General Syntheses of polypyridyl osmium complexes

Cis-osmium polypyridyl complexes $Os(bpy)_2Cl_2$, and $Os(dmobpy)_2Cl_2$ were synthesized following a general procedure described by Meyer and co-workers[207]. $(NH_4)_2OsCl_6$ along with a slight excess of twice the molar equivalent of the ligand bipyridine was dissolved in ethylene glycol. The mixture was degassed by bubbling argon, and a vacuum was applied to the flask; this mixture was refluxed for one hour at 200°C. After cooling to room temperature, an excess amount of aqueous sodium dithionite was added to reduce Os(III) to Os(II). Formation of a dark brown coloured precipitate was triggered. The mixture was stirred in an ice bath for 30 to 45 minutes before filtering. The precipitate was then washed with water, followed by washing with large volumes of diethyl ether. The resulting complex is dried under a vacuum. Finally, the product was dried in the oven at 60 degrees Celsius for two days to remove any water content. The synthetic scheme for yielding $Os(bpy)_2Cl_2$ is depicted in **scheme 3**.

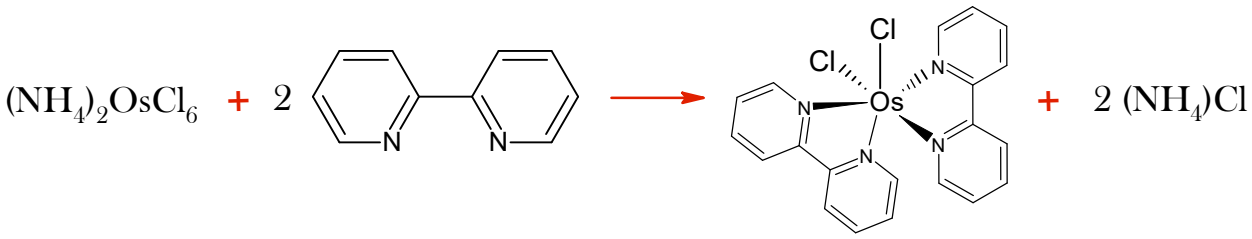

Scheme 3. Synthesis of $(Os(bpy)_2Cl_2)$.

Step 2: Synthesis of poly (vinyl imidazole)

Crosslinked PVI

In a 50mL round bottom flask, 500mg (5.31mM) of vinyl imidazole was taken and dissolved in 20.0 mL of demineralized water. To this, 441mg (2.86mM) of MDAA crosslinker was added and stirred under argon for 25 minutes at room temperature. The solution was later added with 10mg (2 weight%) of 4,4'-Azobis (4-cyanopentanoic acid). ACPA acts as an initiator for the polymerization reaction. After 15 minutes, purging of argon was stopped. The reaction pot was then sealed and refluxed in an oil bath for 24 hours at 70°C. The reaction scheme is illustrated in **scheme 4**. A curdy white precipitate was yielded. It was washed with demineralized water, filtered, dried, and ground to obtain the polymer as a fine powder. The product was characterized using solid-state ^{13}C NMR.

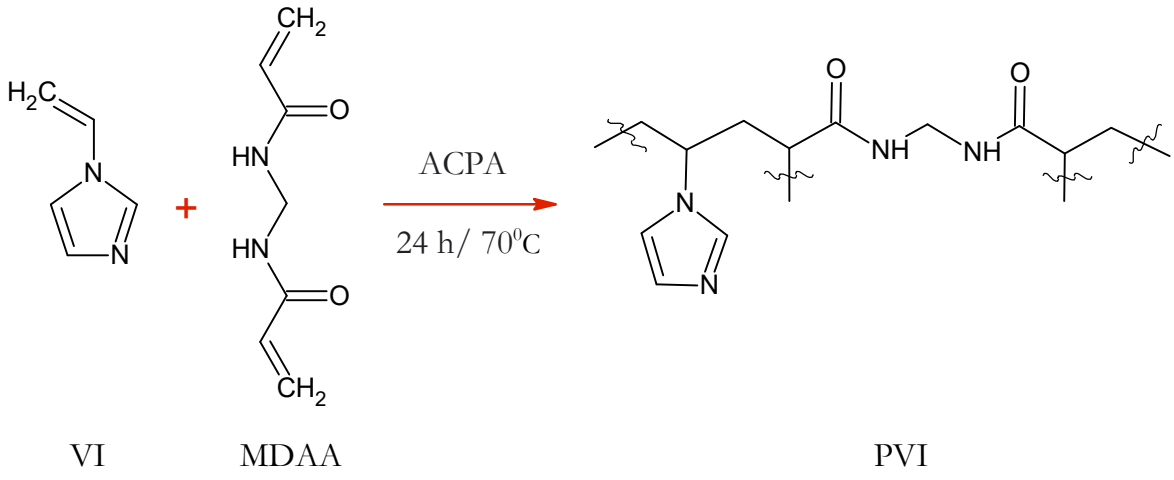

Scheme 4. Reaction for the synthesis of PVI in the presence of MDAA (crosslinker) and ACPA (initiator).

Linear PVI

Synthesis of linear PVI was conducted by two approaches;

ACPA as polymerisation initiator: In this procedure, 500mg (5.31mM) of vinyl imidazole was taken in a 50mL round bottom flask. It was dissolved in 15mL of demineralized water and stirred under argon for 10 minutes. ACPA was added to the solution (1 mol%), while the deaeration continued for another 15 minutes. The reaction pot was then sealed and refluxed in an oil bath for 24 hours at 70° C. A yellowish-cloudy solution was obtained. The proposed reaction is illustrated in **scheme 5**.

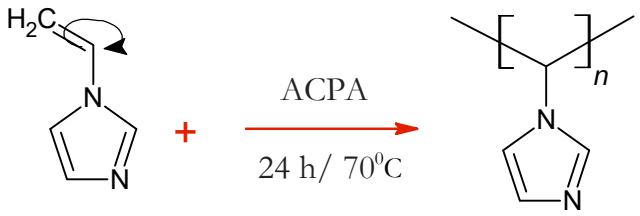

VI PVI

Scheme 5. The proposed polymerization route for the synthesis of linear PVI using ACPA as polymerisation initiator.

AIBN as polymerisation initiator: This synthesis of poly (vinyl imidazole) is a multi-step process. At first, 500mg (5.31mM) of vinyl imidazole was subjected to vacuum distillation for the removal of any inhibitor present. Bulk polymerization of the vinyl imidazole was then conducted in a well-stirred Schlenk flask by adding 1:1000 AIBN to monomer molar ratio. The reaction took place under a nitrogen atmosphere at 70°C for 2 hours. The product was dissolved in 30mL of hot methanol and undertaken fractional precipitation of polymer from methanol into large excess(600mL) of stirring diethyl ether. A white precipitate was collected after filtration and characterized using the ^{1}H NMR technique.

Step 3: Synthesis of PVI-bound osmium redox polymers

Poly (vinyl imidazole) containing cis-$Os(N\text{-}N)_2Cl_2$ redox centers with the general formula cis-$[(Os(N\text{-}N)_2(PVI)_{n+1}Cl]^+$ (n = 9) were synthesized by following the steps outlined by Forster and Vos[208]. An osmium complex with the general formula $Os(N\text{-}N)_2Cl_2$ is combined with PVI in a molar ratio of 1:10. To ensure thorough dissolution; the osmium complex was first refluxed in ethanol for 20 minutes. A ten-molar equivalent of PVI dissolved in ethanol was gradually added to the stirring complex solution in 1 ml aliquots. The mixture was allowed to reflux for three days while the reaction was continuously tracked using cyclic voltammetry. On completion of the reaction, the product was precipitated by adding the reaction mixture drop-by-drop to a solution of swirling diethyl ether. Later,

the product was vacuum-filtered and allowed to air dry at room temperature. It was further dried overnight at 50 °C in a preheated oven. The reaction scheme is as provided in **scheme 6**.

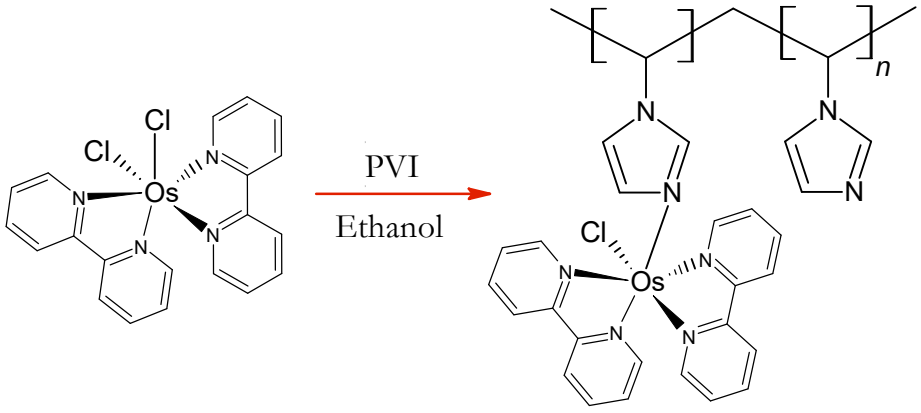

Scheme 6. Simplified reaction for the synthesis of osmium-PVI metallopolymer of formula cis $[Os(bpy)_2(PVI)_{10}Cl]^+$.

4.1.2.2 Electrochemical Measurements

All the electrochemical measurements, unless stated otherwise, were performed with a PalmSens4 potentiostat galvanostat, with an electrochemical impedance spectroscopy (EIS) module, which is controlled with the PSTrace software. A three-electrode electrochemical cell consisting of a platinum wire counter electrode and an Ag/AgCl (1M KCl) reference electrode was used, unless specified otherwise. Except where otherwise indicated, cyclic voltammetry was employed as the electrochemical characterization method for the products obtained.

Os(2,2'-bipyridine)$_2$Cl$_2$: After the complex $Os(bpy)_2Cl_2$ was dried, it was characterized using cyclic voltammetry. The measurements were recorded with GCE WE modified with the complex in CH_3CN solution with 0.1 M TEAP as supporting electrolyte at room temperature.

Os(4,4'-dimethoxy-2,2'-bipyridine)$_2$Cl$_2$: The $Os(dmobpy)_2Cl_2$ complex was electrochemically analyzed using the help of cyclic voltammetry. Different methods of CV experiments were conducted to understand the behavior of the complex: 1) measurements were performed using a glassy carbon WE modified by drop-casting the solution of the $Os(dmobpy)_2Cl_2$ in acetonitrile. After drying, these electrodes were tested either directly or with a protective layer of Nafion polymer for immobilization, 2) CV were conducted in an $Os(dmobpy)_2Cl_2$ complex solution with PBS as a supporting electrolyte, 3) aqueous solution of the complex was analyzed on screen-printed electrodes.

$[Os(dmobpy)_2(PVI)_{10}Cl]^+$: The reaction was analyzed from the start of the reaction in a solution of acetonitrile with 0.1M TBACl as electrolyte. An Ag^+/TBACl-$AgNO_3$ RE, a platinum CE and GCE WE were used for the analysis.

4.1.2.3 Elemental analysis

Elemental analysis was used to characterize the $Os(bpy)_2Cl_2$ complex. Analysis of the percentage content of the elements C, H, and N was performed in a UNICUBE automatic analyser by Elementar. The experiments were conducted by Krystyna Markucińska in the Laboratory of Elemental Analysis under the Laboratory of Bioactive Substance Analysis, Institute of Organic Chemistry, PAS. The basis of the measurement is the catalytic combustion of the analysed substance with oxygenation at the temperature of 1150 °C. Combustion gases, after having been cleaned of interfering gases (e.g. volatile chlorides), are separated on appropriate adsorption columns and subsequently determined using a thermal conductivity detector (TCD).

4.1.2.4 UV-visible spectroscopy

UV–visible spectra were recorded at room temperature on an Evolution 300 spectrophotometer (Thermo Scientific), over the spectral range 220 – 900 nm in cuvettes with an optical path of 1 cm. UV–VIS spectroscopy was used in order to characterize the osmium bipyridyl complex formation from the reaction of $(NH_4)_2OsCl_6$ and suitable ligand. The samples were dissolved in acetonitrile for UV-visible characterization. The formation of $[(Os(N\text{-}N)_2(PVI)_{10}Cl]^+$ was also monitored using the same method.

4.1.2.5 NMR spectroscopy

All NMR Liquid state NMR measurements were performed on a Bruker AVANCE II 300 MHz spectrometer equipped with a BBI 300 MHz W1 5 mm z-gradient probe with a BVT-3000 temperature controller. The solid-state experiments were conducted on a 500 MHz BRUKER AVANCE II spectrometer. The spectrometer was controlled via the TOPSPIN 3.2 program. All the NMR recordings were performed by Tomasz Ratajczyk at IPC, PAS.

4.1.2.6 Mass Spectrometry

Mass spectrometry analysis was performed using Synapt G2-S mass spectrometer (Waters) equipped with the electrospray (ESI) ion source and quadrupole-Time-of-flight (qTOF) mass analyser. Methanol (Honeywell, LC-MS Chromasolv™, purity ≥ 99.9%) was used as a solvent and mobile phase with the flow rate 100 μl/min. Sample was dissolved and injected directly into the ESI source. Injection volume was 1 μl depending on concentration. The measurement was performed in the positive ion mode with a resolving power of the TOF analyser of 30000 FWHM. The lock-spray spectrum of Leucine-enkephalin was generated by the lock-spray source and the correction was performed for the recorded spectrum. The exact mass measurement was performed within 3 mDa mass error. Nitrogen was used as desolvation and cone gas, and their flow values were set to 600 L/h and 100 L/h respectively. Desolvation gas temperature was set to 350°C. Nebulizer gas pressure was set to 5.0 bar. Capillary voltage was set to 3.0 kV, and sampling cone voltage and source offset were set to 30-50 V. The instrument was controlled and data were processed using the MassLynx V4.1 software package (Waters). All the mass spectrometry experiments were performed by **Dr. Zahra Badri in the** Mass Spectrometry Laboratory under the Laboratory of Bioactive Substance Analysis, Institute of Organic Chemistry, PAS.

4.1.2.7 Glucose sensing

Glucose sensing was performed to demonstrate the application of $[Os(bpy)_2(PVI)_{10}Cl]^+$.

Enzyme electrode preparation: Glassy carbon electrodes (GCE) of 2mm diameter were used as working electrodes for measurements using the $[Os(bpy)_2(PVI)_{10}Cl]^+$ sample obtained from NUI, Galway. The enzyme electrodes were fabricated by deposition of each components: Os(bpy)PVI redox polymer aqueous solution (5mg mL^{-1}); GOx solution (1mg mL^{-1}) in phosphate buffer, pH=5.8, glutaraldehyde solution. 3μL of Os(bpy)PVI solution was drop casted onto the GCE surface and dried at room temperature. In the next step, the electrodes were dip coated in the enzyme solution. Finally, the electrodes were coated with glutaraldehyde crosslinker by vapor deposition (for 10 minutes) and rinsed with distilled water before use.

Calibration curve: Glucose solutions of 0, 1, 3, 5, and 10 mM concentrations were prepared. Chronoamperometry was performed at +0.4 V for 30s in each solution. A calibration curve was constructed by plotting the concentration of glucose vs. average current observed for each measurement (**Fig. 40**).

4.1.3 Results and discussions

4.1.3.1 Electrochemistry

Os(2,2'-bipyridine)$_2$Cl$_2$: When the complex was cycled in TEAP, the first measurement made (**Fig.28,** measurement 1) at a scan rate of 100 mVs^{-1} was relatable to the literature results (**Fig.29** (e)). However, the next few scans in the presence and absence of oxygen, produced an extra peak during the reduction, as shown in **figure 28**. The potential window in which the reduction peak is observed holds no relevance for Os(bpy)$_2$Cl$_2$ in this study. It is possible that the reported pure compounds might also exhibit similar behaviour, but the voltammograms in the literature[168] do not include so low potentials (**Fig.29**). Clarity of the results can only be achieved with more informative characterization techniques such as NMR, mass spectrometry or XRD. The Os(bpy)$_2$Cl$_2$ complex was subjected to elemental analysis, and it was found that the synthesis was successful. The elemental composition: calculated for $C_{20}H_{16}Cl_2N_4Os$: C, 39; H, 3; N, 9.2. Observed: C, 39.78; H, 3.08; N, 9.23.

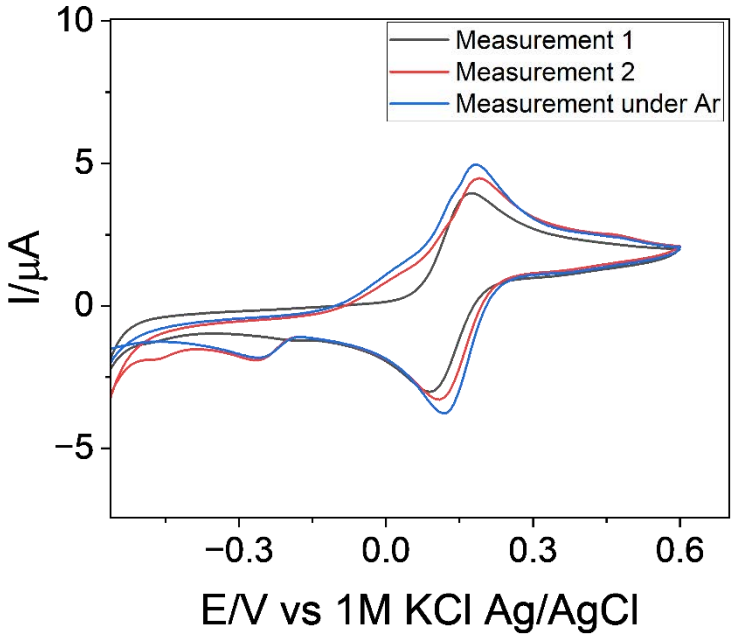

Fig. 28 Cyclic voltammograms of the Os(bpy)$_2$Cl$_2$ complex in TEAP electrolyte (scan rate = 100 mVs^{-1}).

Os(4,4'-dimethoxy-2,2'-bipyridine)$_2$Cl$_2$: The synthesis was repeated multiple times to get a stable product. These samples were subjected to CV experiments in different ways as mentioned in the methods section. **Figure 30** demonstrates the redox cycle of 3 samples of the complex (8 mg ml^{-1} aqueous solution) on commercially available screen-printed electrodes. When the two of them had similar signals, the third one showed a sharp reduction. Moreover, the former two tend to give an additional oxidation peak, which cannot be assigned to a particular reaction. It can also mark the

formation of the complex with a different conformation or an incomplete reaction (with the reaction mixture still retaining the starting materials). To observe the behaviour of the synthesized product under an inert atmosphere, the samples were cycled in the absence of oxygen.

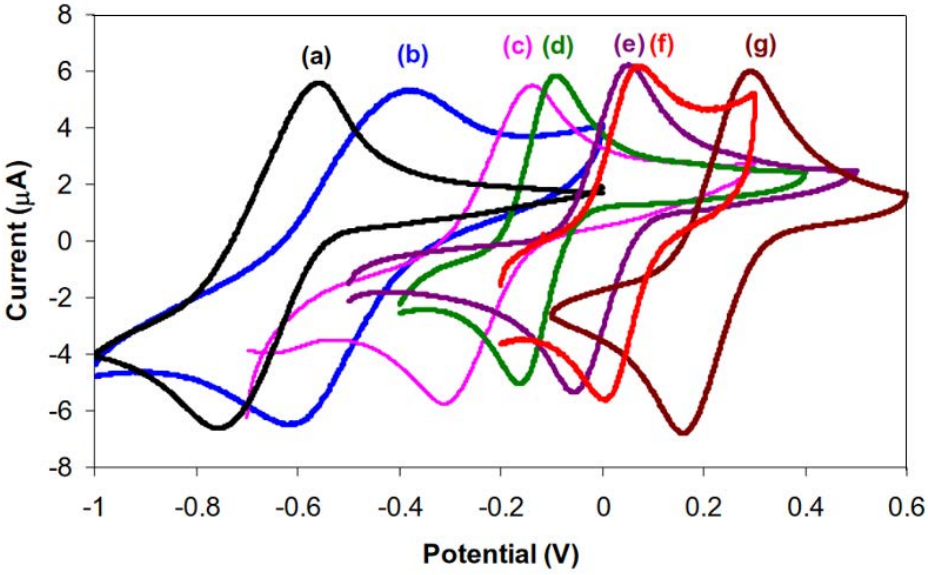

Fig.29 Cyclic voltammograms of $Os(N\text{-}N)_2Cl_2$, where N-N is 2,2'-bipyridine with the following in the 4,4' positions: (b) amino, (c) methoxy, (d) methyl, (e) H and (g) Cl, or where N-N is (a) 4,4'-dimethyl-2,2'-biimidazole and (f) 1,10-phenantroline[168]. Scans recorded at glassy carbon electrodes in 0.05 M phosphate buffer, pH 7.4 at 100 mVs^{-1}.

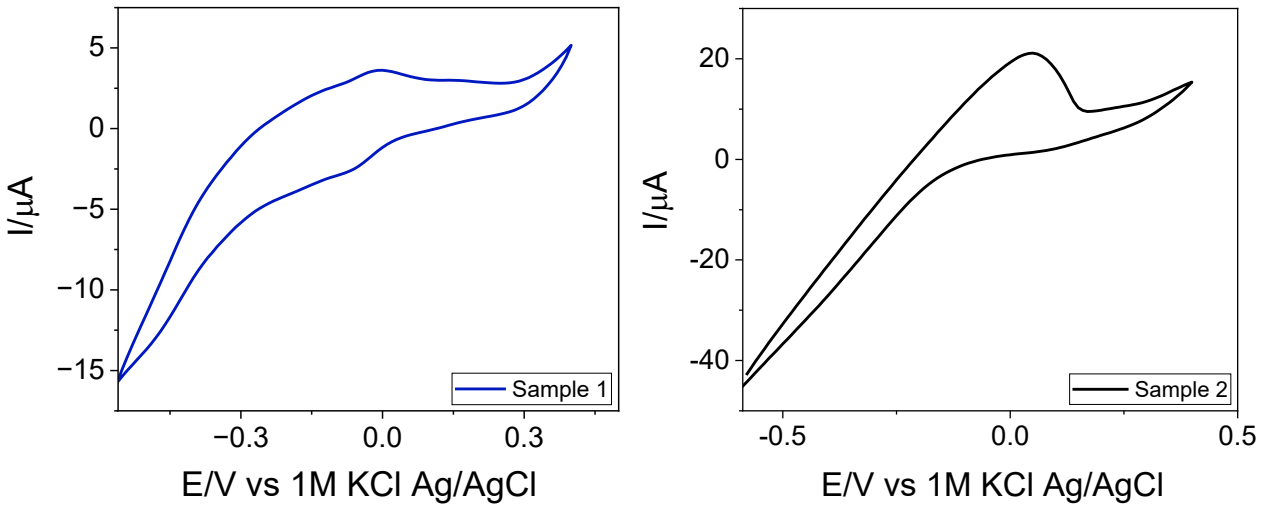

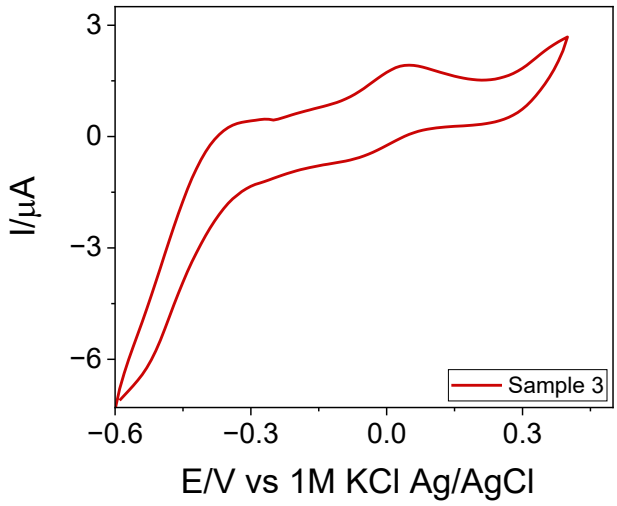

Fig.30 Cyclic voltammograms of $Os(dmobpy)_2Cl_2$ samples synthesized in IPC, PAS (scan rate = 100 mVs^{-1}).

The Cyclic Voltammetry characterization of the osmium complexes are usually carried out at low complex concentrations[169], which implies its quality and thus the sensitivity, however, the results mentioned above could not bring the best results during the characterizations. A trial was conducted by performing CV with supersaturated solutions of the three $Os(dmobpy)_2Cl_2$ complex samples synthesized. These experiments were conducted by purging argon gas. When one of the samples gave a very promising result, the rest two exhibited an additional peak (along with the overlapping peak with the best sample). **Figure 31** shows the performances of the supersaturated complex solutions in the organic medium of 0.1M TBACl in acetonitrile.

$[Os(dmobpy)_2(PVI)_{10}Cl]^+$: The coupling reaction to obtain bis-(dimethoxy2,2'-bipyridyl)-(poly-vinylimidazole)$_{10}$-chloro-osmium(II) was monitored at different time points using cyclic voltammetry. On day 1, with time, a shift of the peak positions of the reaction mixture towards negative potential was observed; this implied the beginning of the reaction. On day 3, no significant signal changes were noticed under normal air conditions as well as under an argon atmosphere. A graph depicting these CV recordings is provided in **figure 32**. This might be due to a low concentration of the reaction mixture in the electrolyte, which is not enough to produce an observable peak. The dried coupling product was also analysed using cyclic voltammograms. It was confirmed that the forward reaction did not progress.

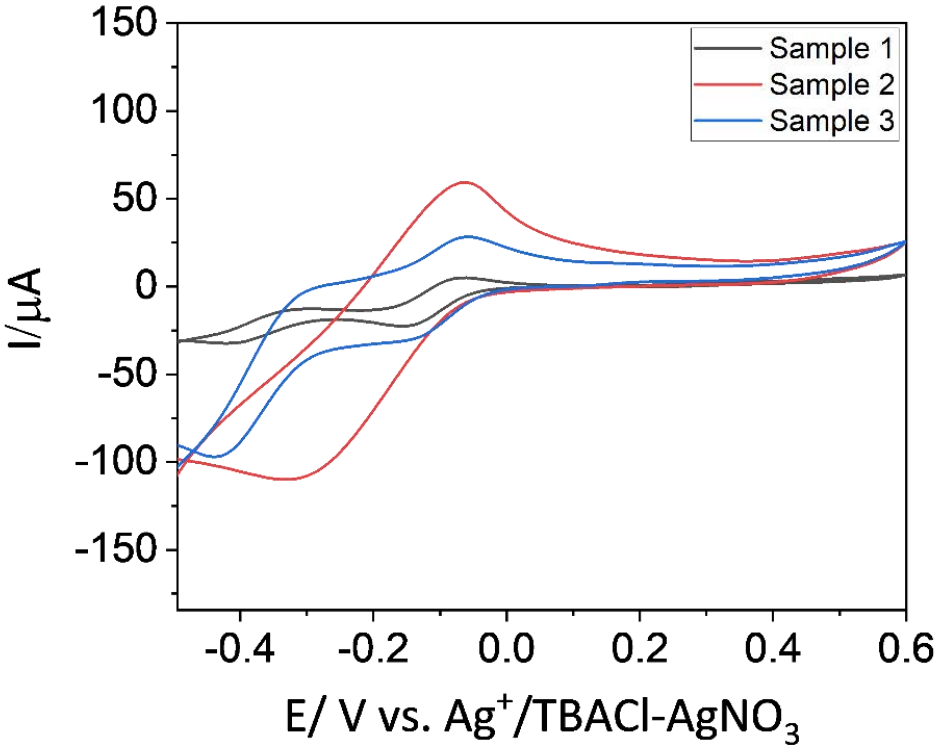

Fig. 31 The performances of supersaturated [Os(dmobpy)$_2$Cl$_2$] complex solutions in 0.1M TBACl.

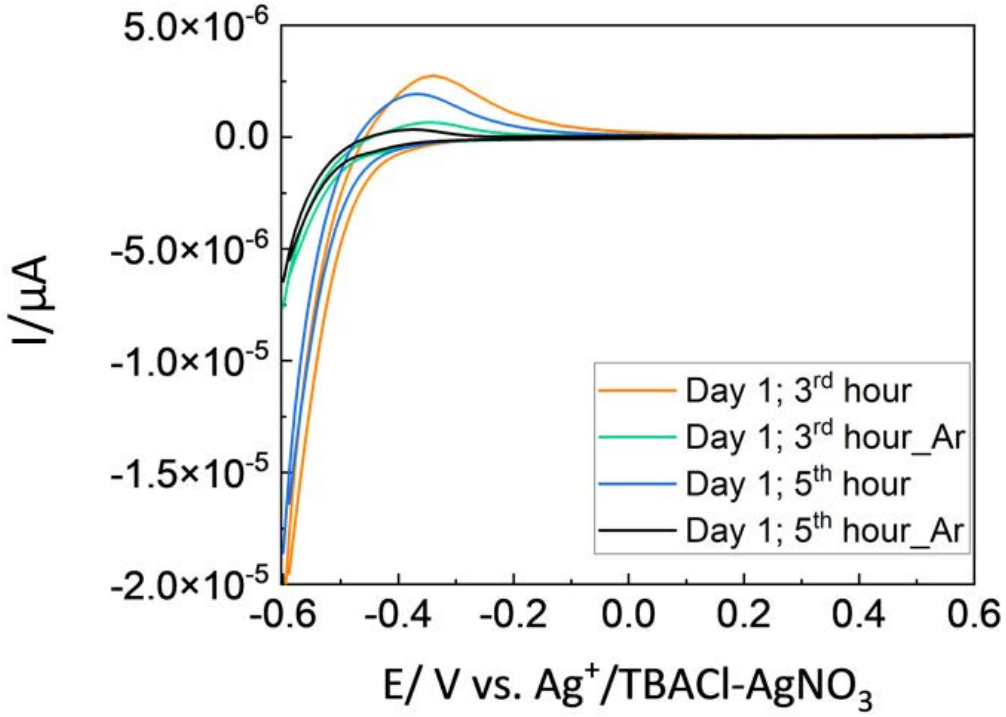

Fig.32 Progress of the coupling reaction on day 1, comparison of the reaction mixtures from 3rd hour to 5th hour.

$[Os(bpy)_2(PVI)_{10}Cl]^+$: The reaction was continuously monitored using cyclic voltammetry since the beginning. Unlike previously reported[209–211], the reaction time was not about 2 or 3 days, instead the reaction was completed over a period of 21 days. The results obtained were compared with the pure reference samples obtained from the National University of Ireland (NUI), Galway. A neat cyclic voltammogram was observed for the product synthesized in IPC, PAS. However, when compared, the signal is at a higher potential than the reference sample from the NUI, Galway (**Fig. 33**).

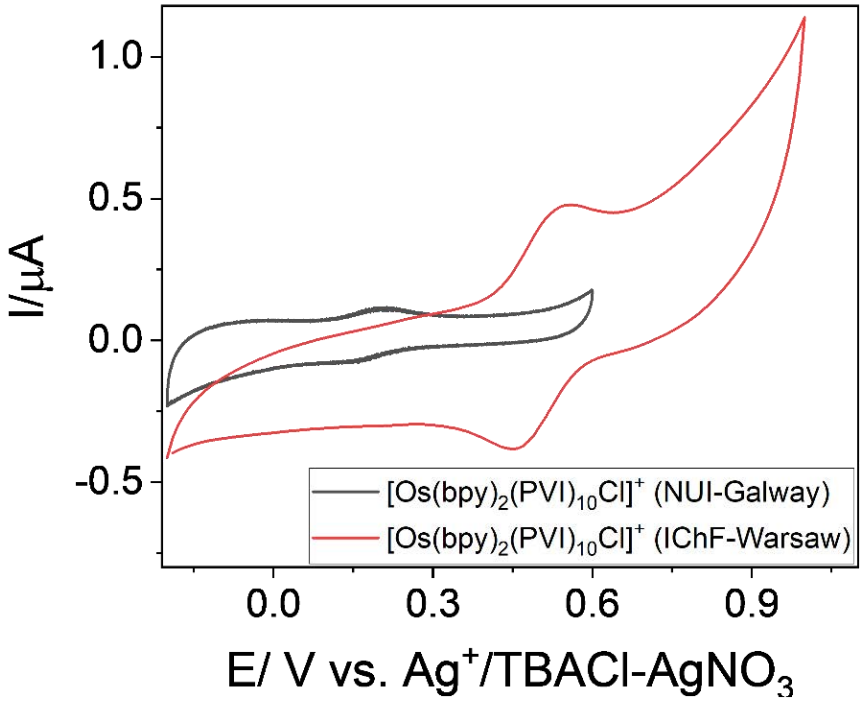

Fig. 33 The comparison of the CV of the $[Os(2,2'\text{-bipyridine})_2(PVI)_{10}Cl]^+$ synthesized at IPC, PAS and the reference sample from (NUI), Galway.

4.1.3.2 UV-visible spectroscopy

$Os(4,4'\text{-dimethoxy-}2,2'\text{-bipyridine})_2Cl_2$: To understand the progress of the reaction between $(NH_4)_2OsCl_6$ and dmobpy, UV-visible spectra of the starting materials and the products obtained were recorded. The products have two well defined peaks in range of the typical pyridine peaks of the dmobpy group[212] in the ultra violet range up-to 298 nm. While the twin peaks of the $(NH_4)_2OsCl_6$ around 350nm were found to have disappeared, and blue shifted as a single peak. **Figure 34** illustrates the absorption spectra of the starting materials and different samples of the synthesized complex. It was observed that in all the attempts, the reaction was initiated. However, the properties of the reaction mixture or products seemed to vary from sample to sample. With limited information, it was

difficult to conclude whether the expected product was formed or if the signals are from any impurity species.

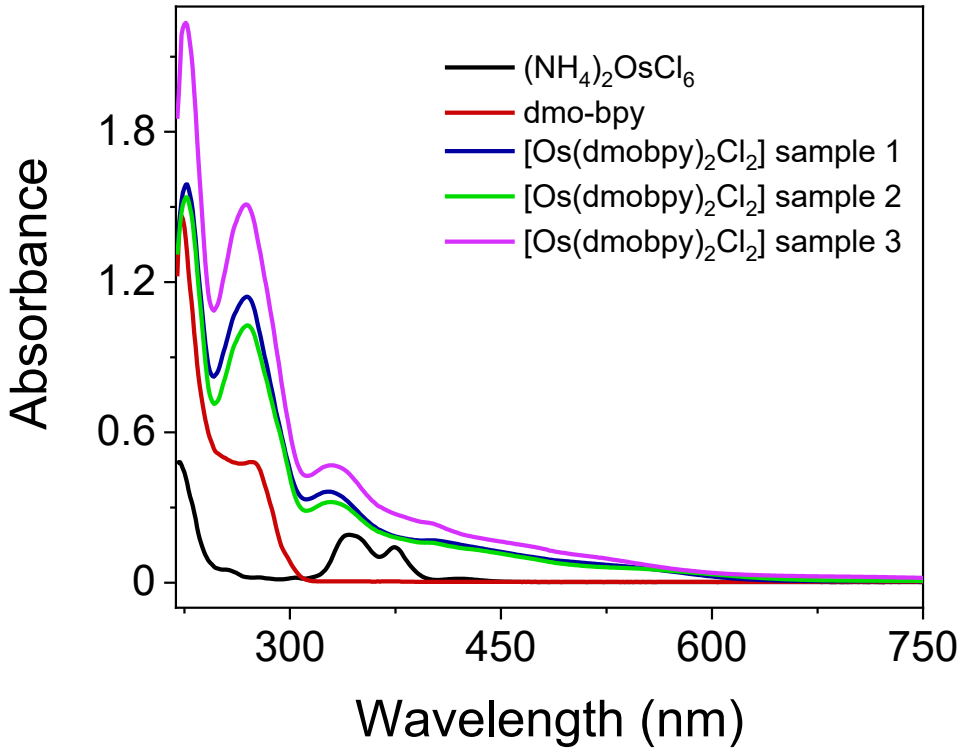

Fig.34 Absorption spectra of the starting materials and different samples of the $Os(dmobpy)_2Cl_2$ complex.

$[Os(dmobpy)_2(PVI)_{10}Cl]^+$: the synthesis of $[Os(dmobpy)_2(PVI)_{10}Cl]^+$ was analysed with the UV-visible spectroscopy. The reaction mixture, on different days of the reaction, resembled the absorption spectra of the starting osmium complex substrate. **Figure 35** shows the absorbance spectroscopy of the starting material and the reaction mixtures on different days of the reaction.

4.1.3.3 NMR

Os(4,4'-dimethoxy-2,2'-bipyridine)$_2$Cl$_2$: For detailed structure analysis, the NMR signals of the obtained osmium complex $[Os(dmobpy)_2Cl_2]$ were recorded in DMSO- d_6 ($(CD_3)_2SO$). The results obtained are not consistent with literature values. Moreover, huge peaks of the solvent and water molecules were observed in the spectrum of different samples of the complexes synthesized. **Fig. 36** shows the ^1H NMR signals for two different complex samples. In both the cases, the results indicate that the reactions were less effective. Although the signals for methoxy group (~ 4 ppm) and the aromatic rings (6.5 to 8 ppm) are visible at their characteristic δ values, the peak heights observed are insignificantly small. In the case of expected complex formation, the peaks of aromatic and methoxy

region will be well defined[212,213].

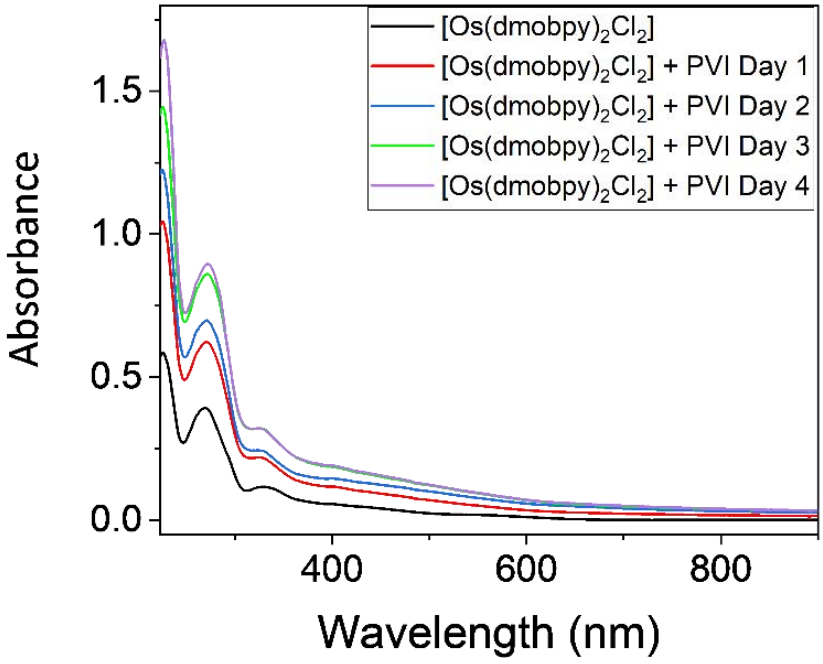

Fig. 35 UV-visible spectroscopy comparing the absorption of the starting material $Os(dmobpy)_2Cl_2$ and the reaction mixtures on different days of the reaction.

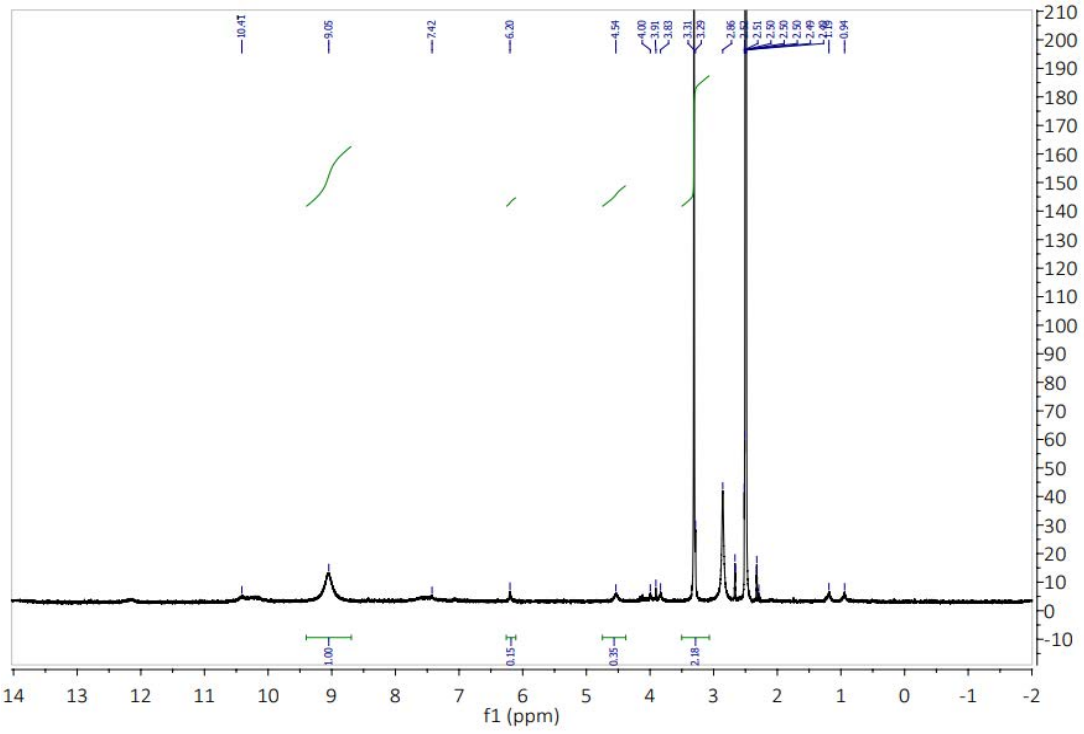

a)

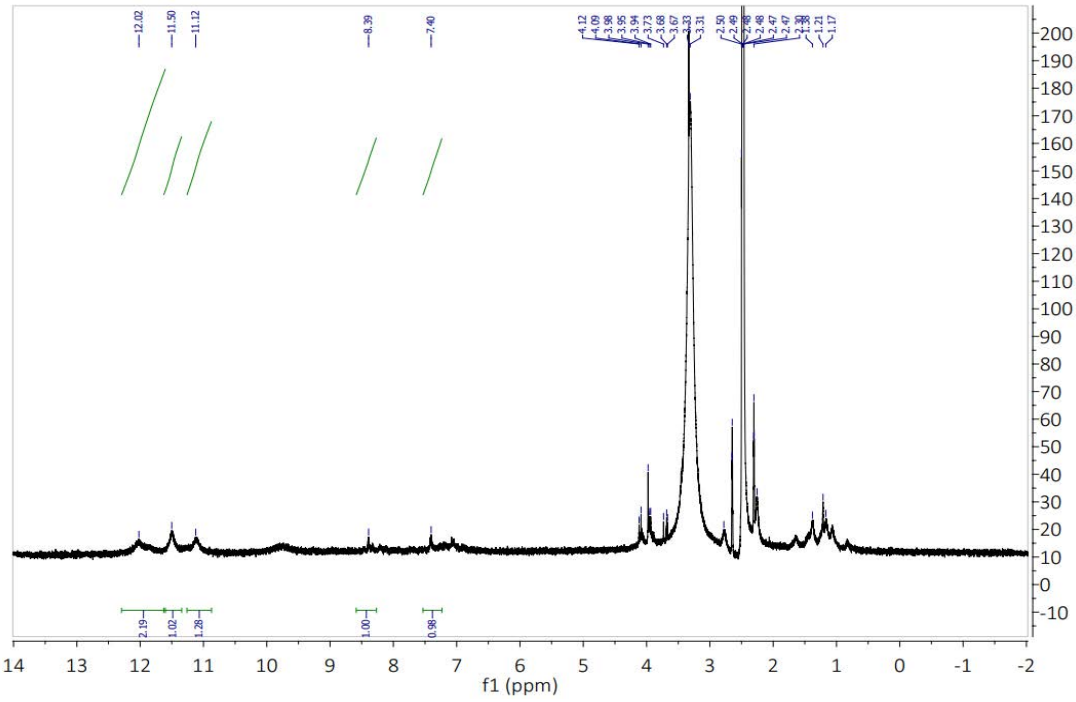

b)

Fig. 36 ^{1}H NMR spectra of a) $[Os(dmobpy)_2Cl_2]$ complex sample 1 b) $[Os(dmobpy)_2Cl_2]$ complex sample 2.

Poly (vinyl imidazole): Despite AIBN[208,210,214] or 1,1'–azobis(cyclohexanecarbonitrile)[215] being the most popular free radical initiators for the polymerization of vinyl imidazole, different synthetic methods were followed for the synthesis of poly (vinyl imidazole). Due to changes in EU regulations regarding purchase and shipping of AIBN and similar compounds other possible initiator molecules that could be employed for the respective polymerization were tested.

Usually linear PVI forms the backbone of the redox metallopolymers containing cis-$[Os(N\text{-}N)_2Cl_2]$ redox centres. Out of several alternate procedures for the preparation of the linear polymer[216–218], the use of 4,4'-azobis(4-cyano-pentanoic acid) as free radical initiator seemed promising. However, a simple reaction that combined vinyl imidazole with the initiator was not successful. Even after 30 hours since the beginning of the reaction, no significant change in appearance was noticed. It was noticed that the volume of the solvent was decreasing, but no sign of the expected product formation was observed. It was concluded that this method of linear polymerization of vinyl imidazole is not feasible under the reaction conditions as provided in this chapter.

The development of a linear PVI in one dimension is the best way to reproduce the literature results. A linear polymer structure is the most effective for electron transfer functioning of the redox polymer. Linear polymers are more flexible and they provide good accessibility of the attached functional groups. Unfortunately, constrained by the available resources, the synthesis of a crosslinked polymer seemed to be a practical solution. In a reported study, the functional monomer vinyl imidazole was combined with the crosslinker N,N'-methylenebis acrylamide (MDAA), and the free radical initiator, 4,4'-Azobis(4-cyano-pentanoic acid) to obtain a non-ionic crosslinked PVI[218]. The same procedure was followed to obtain a white precipitate. The appearance of the product was in agreement with the literature data. It was characterized using solid-state ^{13}C NMR. The recordings showed a resemblance with the reported spectrum[218] and thus confirmed the formation of the crosslinked polymer (**fig.37**).

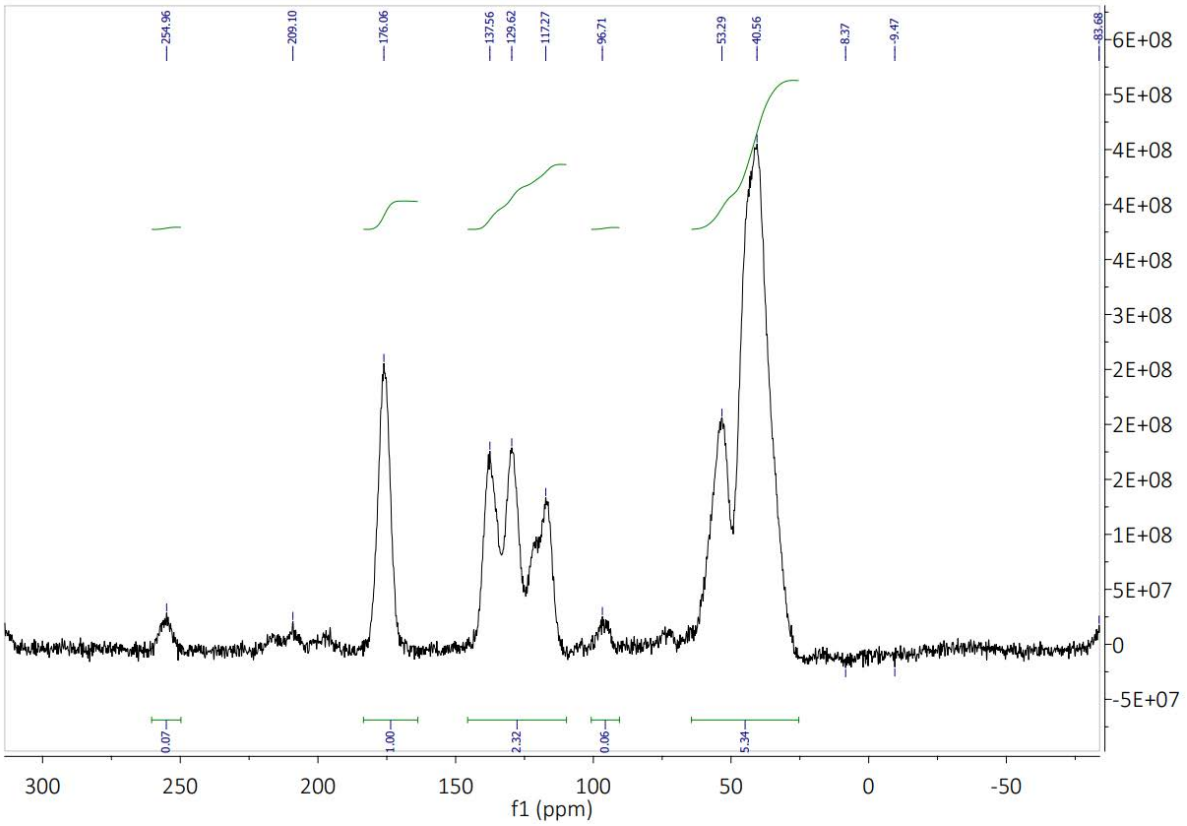

Fig. 37 The ^{13}C NMR spectrum of the synthesized crosslinked PVI

Even though crosslinked poly (vinyl imidazole) was obtained, their coupling with osmium complexes was difficult and time consuming. Despite encountering challenges in purchasing AIBN due to a change in EU regulations, a quantity of 5 mg of the initiator was obtained from the Warsaw University of Technology. Subsequently, this AIBN initiator was used to conduct a polymerization reaction,

resulting in the synthesis of linear PVI. The reported polymerization time for the procedure in general is 2 hours[209,210]. The reaction was supposed to be continued under an inert atmosphere until the mixture was solid; however, a gel-like polymer was obtained during the synthesis. After the mixture was placed at room temperature for ten minutes and dissolved in hot methanol, a white product was precipitated in diethyl ether. The undissolved polymer is the one with the highest molar mass. The remaining methanol solution was added into slight excess of stirring ether and filtered. The filtrate was collected, washed with ether, and the process was continued to obtain PVI with subsequent lower molar masses. Generally, the 1st precipitate (with a molar mass of ~100kDa) is used in making the Osmium-PVI metallopolymer. The formation of PVI was confirmed with NMR spectroscopy. **Figure 38** shows the comparison of the NMR spectra of the reported PVI to the VI polymerization product. The formation of poly (vinyl imidazole) was confirmed. The recording of the spectrum of the wet product showed the presence of a considerable amount of monomer, whereas the signals from the dried sample show a minute ratio of the monomer. The obtained PVI was used for coupling with ([Os(2,2'- bipyridine)$_2$Cl$_2$]) to get a metallopolymer.

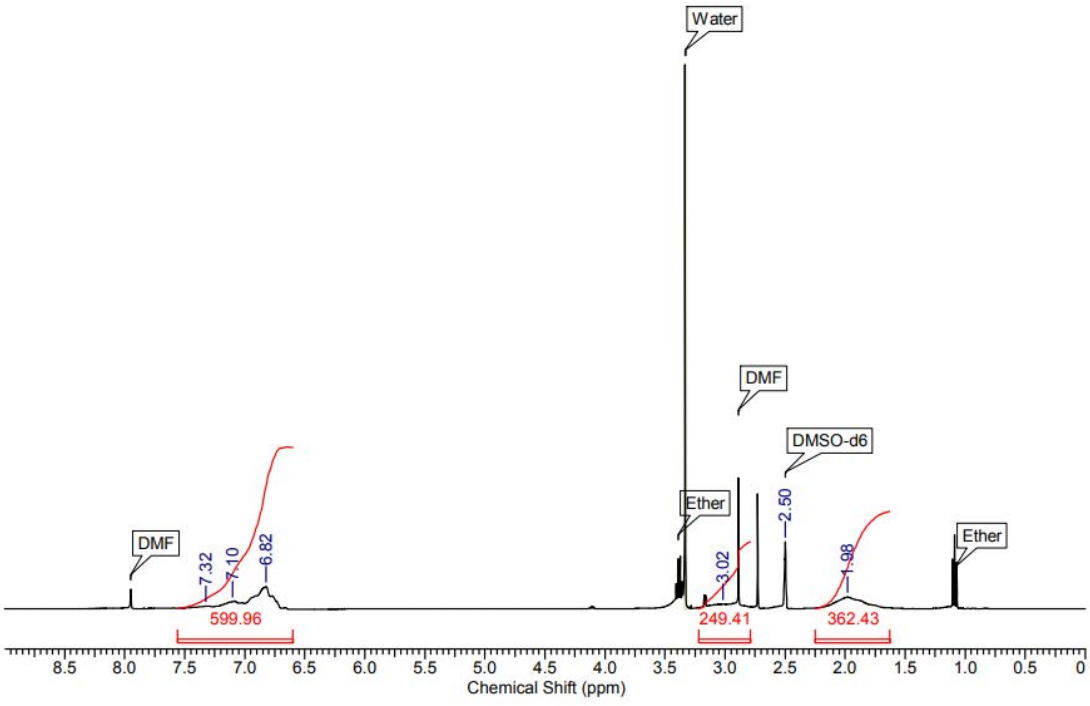

a)

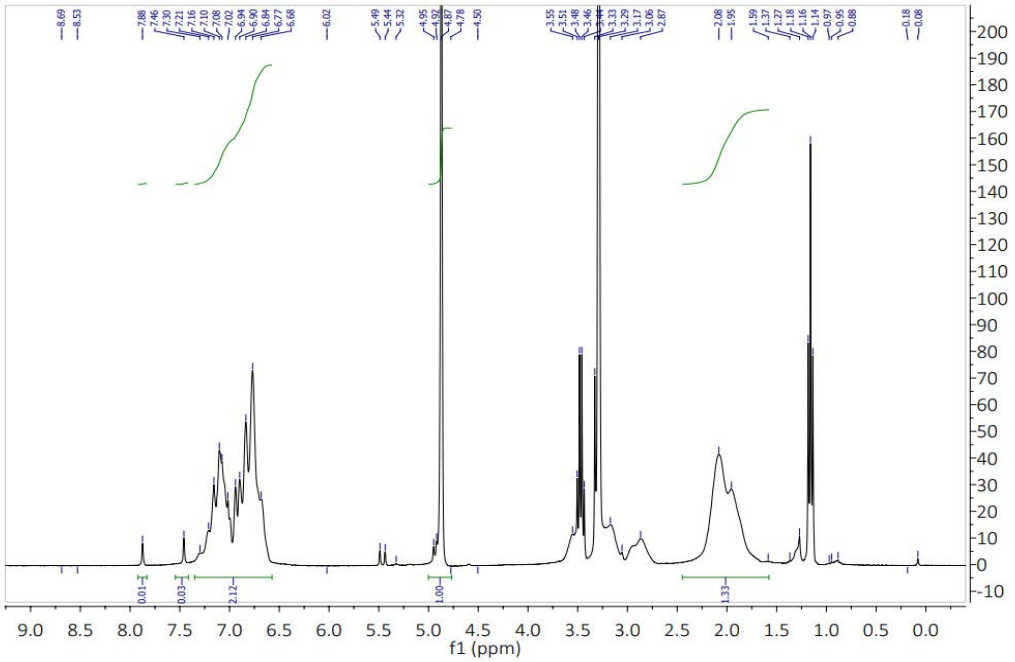

b)

Fig. 38 a) ^{1}H NMR (400 MHz, DMSO-d6) spectrum of PVI synthesized by radical polymerization in DMF as reported by Fan *et al.,*. The analyte contains a small amount of DMF and diethyl ether[219]. b) ^{1}H NMR (400 MHz, methanol-d4) spectrum of the synthesized PVI (solvent peaks are deleted).

4.1.3.4 Mass Spectrometry

High-resolution mass spectrometry was used to characterize $[Os(bpy)_2(PVI)_{10}Cl]^+$ and compare it with the reference sample obtained from NUI, Galway. Considering the major fragment peaks, the spectra were not very similar. With minimal to no fragmentation, the ESI-MS uses the soft positive ionization method to produce multiply charged molecule ions.

In the case of the reference sample (NUI, Galway), the molecular ion ($[Os(bpy)_2Cl_2]^+$) of the redox polymer under examination was consistently the base peak (m/z value, 574.03). Around this m/z value, sub-peaks are observed; these peaks can be attributed to the presence of the osmium isotopes. The ^{192}Os is the most abundant, followed by ^{190}Os, ^{189}Os, and ^{188}Os. The ^{191}Os is unstable, and this explains the absence of the peak at 573.03 m/z below the main peak (574.03 m/z). The next significant peak is observed at 607.10 m/z at a mass difference of 33 amu. This can be due to the coordination of $Os(bpy)_2Cl_2$ fragment with the protonated methanol that is used as the solvent during the mass spectrometry analysis. A very small peak at an m/z value of 633.12 corresponding to $C_{25}H_{22}N_6ClOs$

can also be seen in **figure 39a**. This resembles the base peak of the sample synthesized at IPC, PAS (**Fig. 39 b**). The signals suggest that a significant amount of an adduct of $Os(bpy)_2Cl^+$ ion and the vinyl imidazole monomer ($C_5H_6N_2$, molecular weight 94.117 $g \cdot mol^{-1}$) is formed. A similar fragment corresponding to $C_{25}H_{22}N_6ClOs$ with an osmium-192 isotope can be spotted at 635.12 m/z, and at 539.06 m/z, the peak for $^{192}Os(bpy)_2Cl^+$ is observed. An insignificant peak (<10 % intensity) is visible at 574.03 m/z indicating the traces of the desired product. The data shows that the coupling reaction did not give the redox metallopolymer we are interested in.

4.1.3.5 Glucose sensing

The $[Os(bpy)_2(PVI)_{10}Cl]^+$ from NUI, Galway was used for glucose sensing to understand the response of the stable redox polymer. A calibration curve was prepared by plotting average glucose oxidation current as a function of glucose concentration (**Fig. 40**). The methods were optimized and the signals obtained were reproducible. The same measurements were conducted using the $[Os(bpy)_2(PVI)_{10}Cl]^+$ sample synthesized at IPC, PAS. However, in this case the synthetic procedure needs to be modified for better results. From **fig. 33** it can be seen that the oxidation peak potential for the synthesized product is shifted by ~ 0.350 V. Moreover, the procedure needs to be improved regarding the functioning potential of the sensor because the applied measurement potential (+0.4 V) is already high and the idea is to perform glucose sensing at low oxidation potentials.

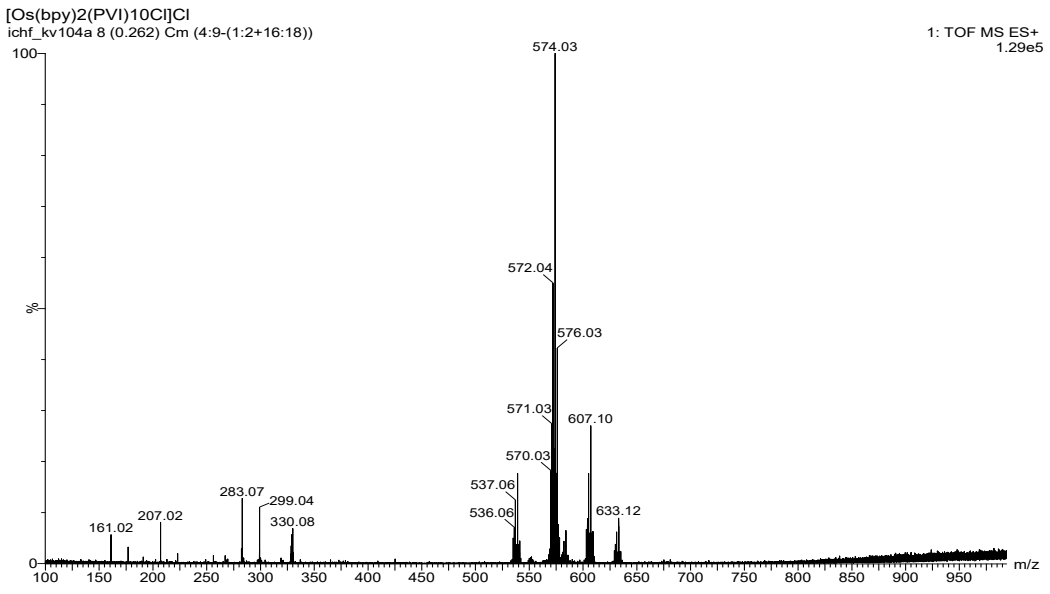

a)

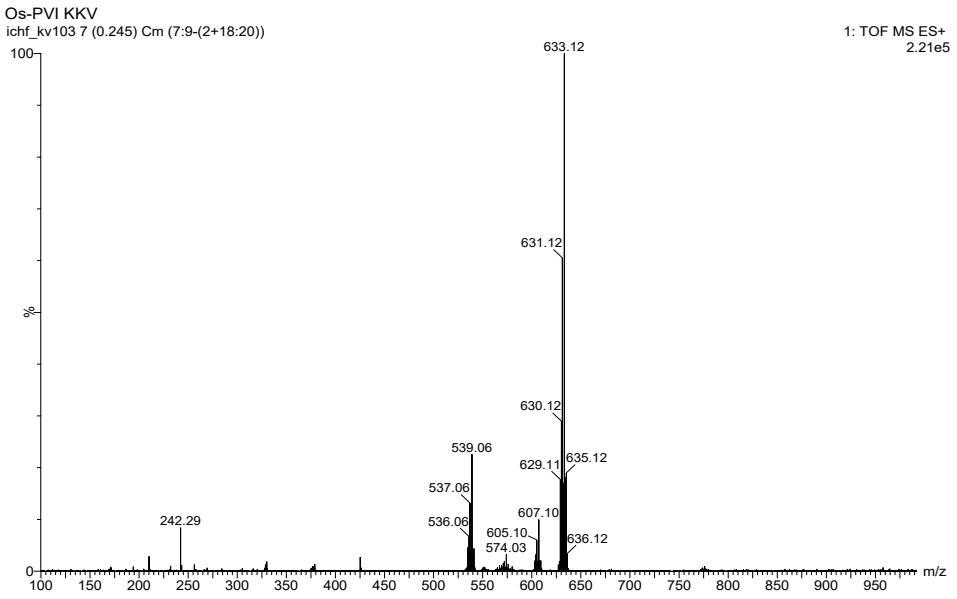

b)

Fig. 39 Mass spectrometry results for $[Os(bpy)_2(PVI)_{10}Cl]^+$, a) reference sample obtained from NUI, Galway b) metallopolymer synthesized at IPC, PAS.

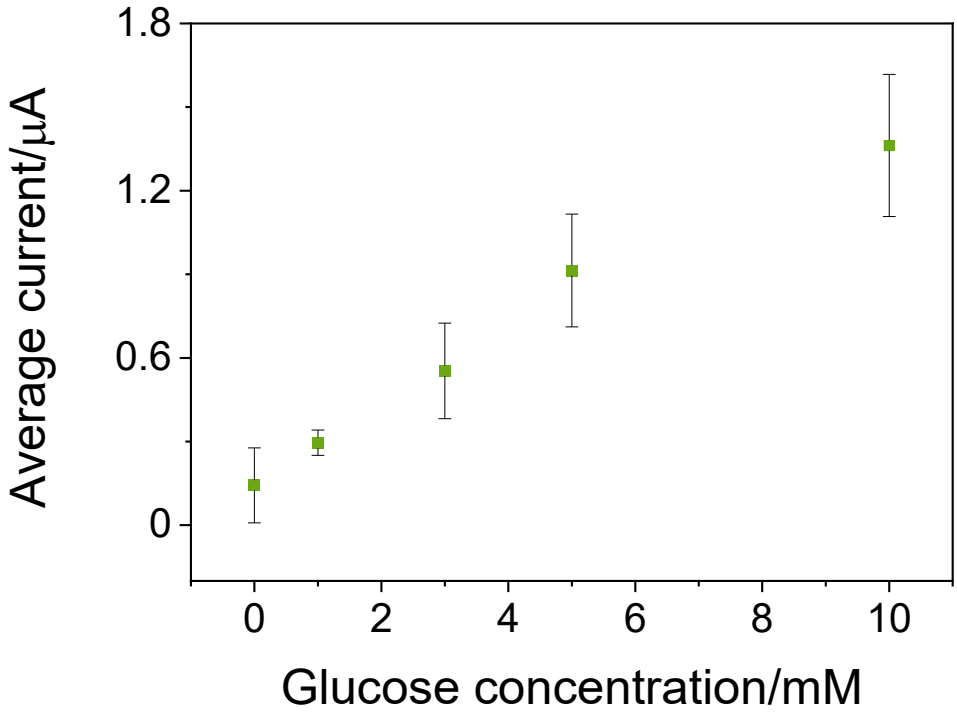

Fig. 40 Average glucose oxidation current as a function of glucose concentration. Measurements were made at +0.4 V at room temperature (pH= 5.8). The enzyme electrodes were prepared with Os(bpy)PVI redox polymer aqueous solution, GOx solution in phosphate buffer, pH=5.8, and glutaraldehyde solution.

4.1.4 Conclusions

After continuous unsuccessful efforts, it was observed that the synthesis of $Os(dmobpy)_2Cl_2$ is a very difficult process as the complexation is challenging. 4,4'-dimethoxy-2,2'-bipyridine is a bulky ligand, this steric hindrance can prevent the ligand from coordinating effectively with the Os(II) centre, reducing the reaction yield. A range of cis-osmium polypyridyl complexes can be synthesized following a similar procedure[208]. In terms of spatial orientation, selecting a smaller ligand can effectively help the coordination process. Apart from this, each complex has a different level of solubility depending on the substitutions made to the polypyridyl ligand. To a large extent, it can be seen that the solubility declines as ligand substituents become more electron-donating. For instance, $Os(dmobpy)_2Cl_2$ has a lower solubility in acetonitrile than Os(4,4'-dimethyl-2,2'-bipyridine)$_2Cl_2$ and $Os(bpy)_2Cl_2$ has the maximum solubility among the three. Thus, the synthesis was repeated by replacing the coordinating ligand with $Os(bpy)_2Cl_2$. The product obtained was also coupled with linear poly (vinyl imidazole).

Based on the cyclic voltammetry, mass spectrometry, NMR, and absorption spectroscopy data, it was concluded that the $[Os(bpy)_2(PVI)_{10}Cl]^+$ synthesis was unsuccessful. Although there was a trait of product formation, there is a chance that an isomer of the desired redox complex is formed, or a polymer with a slightly different molar mass, or a mixture of the copolymer is formed. Apart from the above-mentioned possibilities, the reaction product might also have some adduct impurities like oxygen-containing $Os(bpy)_2$ intermediate complexes such as $OsO_2(bpy)_2Cl_2$ and $[OsO_2(bpy)]Cl_2$, as reported by Calhoun *et al.,*[213].

On average, the whole synthesis process (consisting three-step) can take up to 30 days. Thus, optimization of the products can be time-consuming and frequently difficult. Moreover, contaminations during $Os(bpy)_2Cl_2$ synthesis will result in poor yields and a completely different Os complex, which will lead to a contaminated osmium-loaded poly (vinyl imidazole). During the synthesis, it is difficult to distinguish the oxygen-containing $Os(bpy)_2$ molecule apart from its original counterpart[213]. Especially with our lack of experience in this field and unclear literature descriptions, achieving an on-demand well-established metallopolymer structure was challenging. Therefore, the procedures for the synthesis should be optimized to get pure and stable osmium-based redox polymers to be employed in glucose sensing.

4.2 Shades of Prussian blue: Photonic curing for the synthesis of mixed hexacyanoferrates

4.2.1 Chemicals

Potassium hexacyanoferrate(II) trihydrate ($K_4[Fe(CN)_6]\cdot 3H_2O$), Potassium ferricyanide ($K_3[Fe(CN)_6]$), potassium hexacyanocobaltate(III) ($K_3[Co(CN)_6]$), Cobalt(II) nitrate ($Co(NO_3)_2$), Cobalt(II) sulphate ($CoSO_4$), Sodium ferrocyanide decahydrate ($Na_4Fe(CN)_6$), Nickel(II) dichloride ($NiCl_2$), Nickel(II) nitrate ($Ni(NO_3)_2$), hydrochloric acid (HCl, 37 wt %), potassium chloride (KCl), PBS and Na_2HPO_4 were purchased from Sigma-Aldrich. NaH_2PO_4 was purchased from Chempur. All solutions were prepared from ultrapure water (18.2 MΩ cm) that was produced with a Milli-Q plus 185 (Merck Millipore). Nafion solution (5 wt %) were provided by DuPont. ITO glass substrates were obtained from Delta Technologies (Loveland, CO, USA).

4.2.2 Methods

4.2.2.1 Electrodeposition of Prussian Blue

A solution of 2 mM $FeCl_3$ and 2 mM $K_3[Fe(CN)_6]$ was prepared in deionised water with 0.1 M KCl and 0.1 M HCl as supporting electrolytes. The electrochemical deposition of Prussian Blue was performed based on the method outlined by Karyakin[220–222]. GCEs of 2mm diameter were used as working electrodes and they were cleaned by polishing with alumina powder before use. The electrode surface was subjected to chronoamperometry at 0.4 V vs Ag/AgCl for 100 s. The Prussian blue layer formed in this process was activated in a solution of 0.1M KCl by cycling in the potential range between –50 to 350 mV vs. Ag/AgCl at a scan rate of $50 mVs^{-1}$ (No. of scans=50).

In order to increase the electroactive surface, electrodeposition experiments were also performed on GCE WE electrodes modified with carbon nanoparticles and graphite particles suspended in a polysilicate matrix.

4.2.2.2 Flash light sintering (FLS) or Photonic Curing

Flash light sintering (FLS) was conducted at the Laboratory of Physical and Analytical Electrochemistry, EPFL Valais Wallis, Sion, Switzerland. Different Prussian blue analogues were synthesized from the solutions of inorganic salts (100mM). Aqueous solutions of the starting materials were prepared in 1M HCl. The reactant solutions were drop casted on ITO plates and products are

directly obtained on them. A PulseForge 1300 photonic curing system (Novacentrix, USA) equipped with a xenon flash lamp is the instrument used for the synthesis. The lamp charging voltage was set to 600 V, and the distance between the light source and the substrate was maintained at 6mm. FLS was carried out in an oxygen atmosphere managed by a chamber that has a quartz glass window. The solution samples were placed in the chamber and exposed to the flash light (a single flash comprised of 13 μpulses with 5 overlaps). Every single pulse had a shot energy density of 10.86 ± 0.19 J cm^{-2} of 20 ms. This spike in the energy pushes the reaction forward to yield the product.

4.2.2.3 Electrochemical measurements

All the electrochemical characterizations were conducted at room temperature in a 3-electrode cell using a PalmSens 4 potentiostat/ galvanostat, controlled with PSTrace software. The electrochemical cell consisted of a platinum wire counter electrode (CE), Ag/AgCl (1 M KCl) reference electrode (RE). For the PB analogue samples prepared through FLS method, the working electrodes (WE) were directly prepared on ITO plates through photonic curing. Through this, thin films of Prussian blue analogues were obtained on ITO WEs. The synthesized Prussian blue analogues were first characterized using the cyclic voltammetry (CV) technique. The measurements were conducted in two pH conditions, at first the samples were cycled in 1M KCl, 5 mM HCl (pH 2.5), and later in phosphate buffer (pH 7.4).

4.2.2.4 H_2O_2 sensing

H_2O_2 sensing was performed to demonstrate the application of Prussian Blue. Glassy carbon electrodes (GCE) of 2mm diameter were used as WEs for measurements with the Prussian Blue sample synthesized by the FLS. The electrodes were modified by drop casting aqueous solution of Prussian Blue. The sensor layer was immobilized with Nafion.

Calibration curve: Thirteen different concentrations of H_2O_2 ranging from 20mM to 5μM (0, 5 μM, 10 μM, 25 μM, 50 μM, 75 μM, 0.1 mM, 0.25 mM, 0.5 mM, 0.75 mM, 3 mM, 5 mM, 10 mM, 20 mM) were prepared in PBS (pH=5.8). Chronoamperometric characterization was conducted at –0.5 V for 30 seconds in each of the solutions. A calibration curve was constructed by plotting Prussian Blue reduction current as a function of H_2O_2 concentration (**Fig. 46**).

4.2.3 Results and discussions

4.2.3.1 Prussian Blue

Traditional methods like chemical or electrochemical deposition are useful for the synthesis of Prussian Blue. Nevertheless, these procedures yield unstable PB complex structures, thereby restricting their electrochemical properties. The experiments to reproduce literature results showed that irrespective of the preparation procedure (chemical and electrochemical methods, or deposition on carbon nanoparticles coated electrodes) and the post-treatment chosen (cycling in KCl, heating) the material, although showing very good initial performance, loses activity with each measurement performed in solution without K^+ ions (**Fig. 41**). To overcome these difficulties associated with the common practices, a novel, fast and flexible FLS technique was used for the preparation of PB thin films as reported by Silva *et al.,*[179]. The resultant product of the FLS method significantly simplifies the electrode modification process as no additional post-processing is necessary. It was observed that Prussian Blue obtained from this photo-assisted method exhibits similar stability to other methods, except when cycled in H_2O_2.

Prussian Blue is known as one of the most effective hydrogen peroxide transducer[180]. Unfortunately, the complex suffers lack of stability during long-term continuous monitoring, particularly in neutral and alkaline solutions.

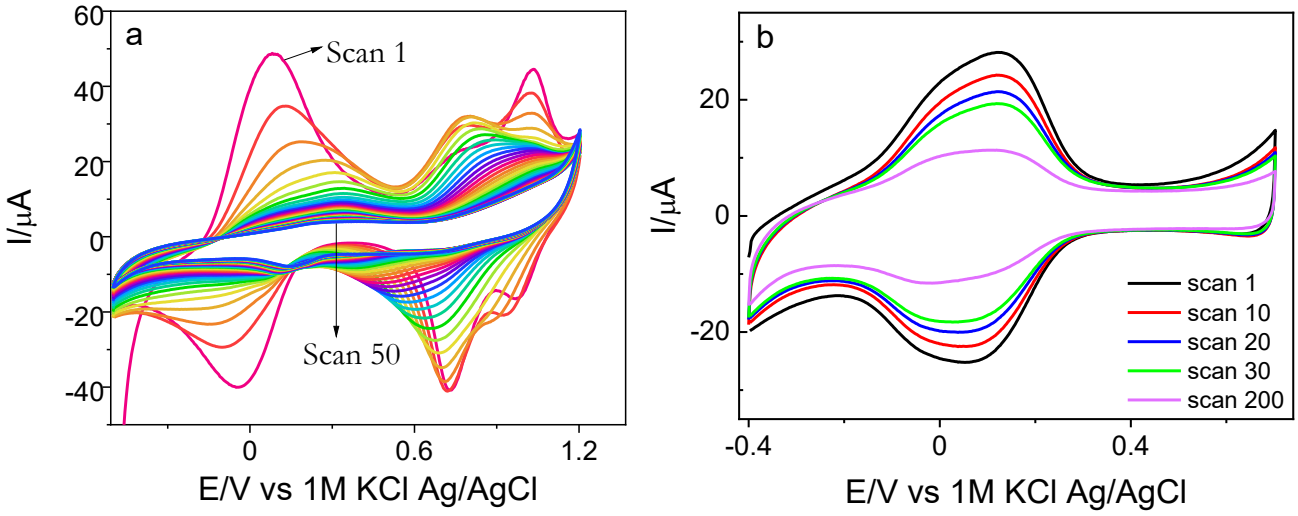

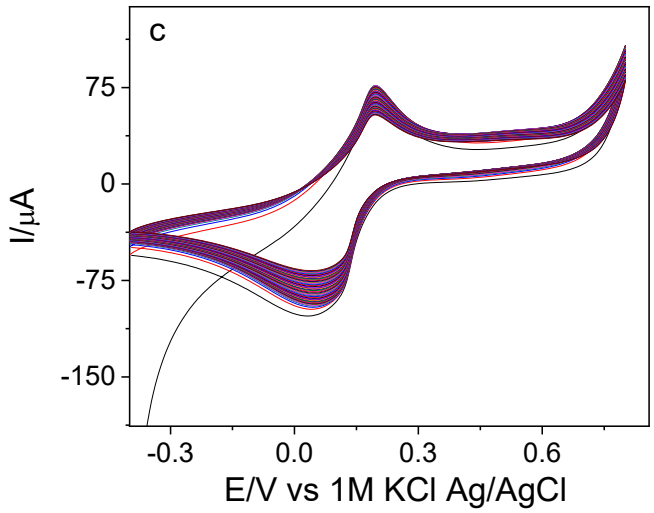

Fig.41 a) Signals of electrochemically deposited PB (on GCE); loss of intensity with prolonged scanning in phosphate buffer (a medium without K+ ions, pH=7.4) was observed, b) Performance of chemically deposited PB (on GCE) showing the lack of signal stability; the electrode was modified with graphite microparticles coated with PB and measured in PBS (pH=7.4), c) Performance of PB synthesized by photonic curing(on GCE); electrode modified with PB (sample obtained from EPFL, Valais Wallis, Switzerland) and Nafion in PBS shows much stable signals.

4.2.3.2 Prussian Blue Analogues (Mixed Hexacyanoferrates)

Mixed Hexacyanoferrates were synthesized using the method developed at EPFL, Valais Wallis, Switzerland[179]. Flash Light Sintering was employed as the synthetic method. It is a fast and flexible method that uses photon energy which is based on photothermal effect. The solutions of reagents that can yield the nickel, cobalt and sodium analogues of classic Prussian Blue were prepared. Trials were performed with 14 different sample solutions and the best ones were chosen. In most of the cases, the reaction was conducted by combining a metal salt with $K_4Fe(CN)_6$ or $K_3Fe(CN)_6$. The combination of reactants used in this study are:

a) $K_3Co(CN)_6$ with $K_4Fe(CN)_6$,

b) $K_3Co(CN)_6$ with $K_3Fe(CN)_6$,

c) $Co(NO_3)_2$ with $K_4Fe(CN)_6$,

d) $Co(NO_3)_2$ with $K_3Fe(CN)_6$,

e) $CoSO_4$ with $K_4Fe(CN)_6$,

f) $CoSO_4$ with $K_3Fe(CN)_6$,

g) $Na_4Fe(CN)_6$ with $K_4Fe(CN)_6$,

h) $Na_4Fe(CN)_6$ with $K_3Fe(CN)_6$,

i) $NiCl_2$ with $K_4Fe(CN)_6$,

j) $NiCl_2$ with $K_3Fe(CN)_6$,

k)$Ni(NO_3)_2$ with $K_4Fe(CN)_6$,

l) $Ni(NO_3)_2$ with $K_3Fe(CN)_6$.

In a couple of cases like m) $K_3Co(CN)_6$, and n) $Na_4Fe(CN)_6$, single complex was used as starting material to obtain the product.

All samples were first checked for reproducibility through measurement in 1M KCl, 5 mM HCl (pH 2.5) at 10mV/s. Long-time electrochemical characterizations were also performed by cycling the products in sodium phosphate buffer at pH 7.4, as Prussian blue tends to lose stability in pH above 7.0 and in solutions without potassium, because of leakage of ferric ions from the crystal structure[177,223,224]. It was noted that different results were obtained on new and used ITO substrates. Choosing the most suitable substrate material is important for the reaction progress. Apart from this, it was seen that the properties of the flash also influence the final electrochemical signals. Results confirmed that some flashes were not successful and reproducibility can be obtained when preparing samples in batches. The samples were flashed in batches of 6.

The products based on $Co(NO_3)_2$, as well as the ones from $CoSO_4$ were first discarded from future studies due to unsatisfactory signals obtained for all prepared samples. The modifications based on $NiCl_2$, the combination of $Na_4Fe(CN)_6$ with $K_4Fe(CN)_6$ and the solution of $K_3Co(CN)_6$ provided most promising results. The $Ni(NO_3)_2$ based modifications exhibited medium stability. The other products lost signal after just few scans, the synthesis of potassium–cobalt hexacyanoferrate by the combination of $K_3Co(CN)_6$ and $K_3Fe(CN)_6$ is a good example for this. 7 of these combinations were selected for future studies and 18 samples for each of them were prepared and analysed. **Fig. 42** provides the reproducible cyclic voltammograms of the $NiCl_2$ based mixed hexacyanoferrates.

Based on the above-mentioned studies the most reproducible samples were chosen for further analysis. In the next step one of the respective hexacyanoferrate samples were subjected to slow scan in 1M KCl, 5 mM HCl solution (scan rate=1 mVs^{-1}) at pH 2.5. One of the samples were subjected for long term cycling in phosphate buffer at pH 7.4. **Figure. 43-45** illustrates the cyclic voltammograms of the most promising mixed hexacyanoferrates synthesized so far.

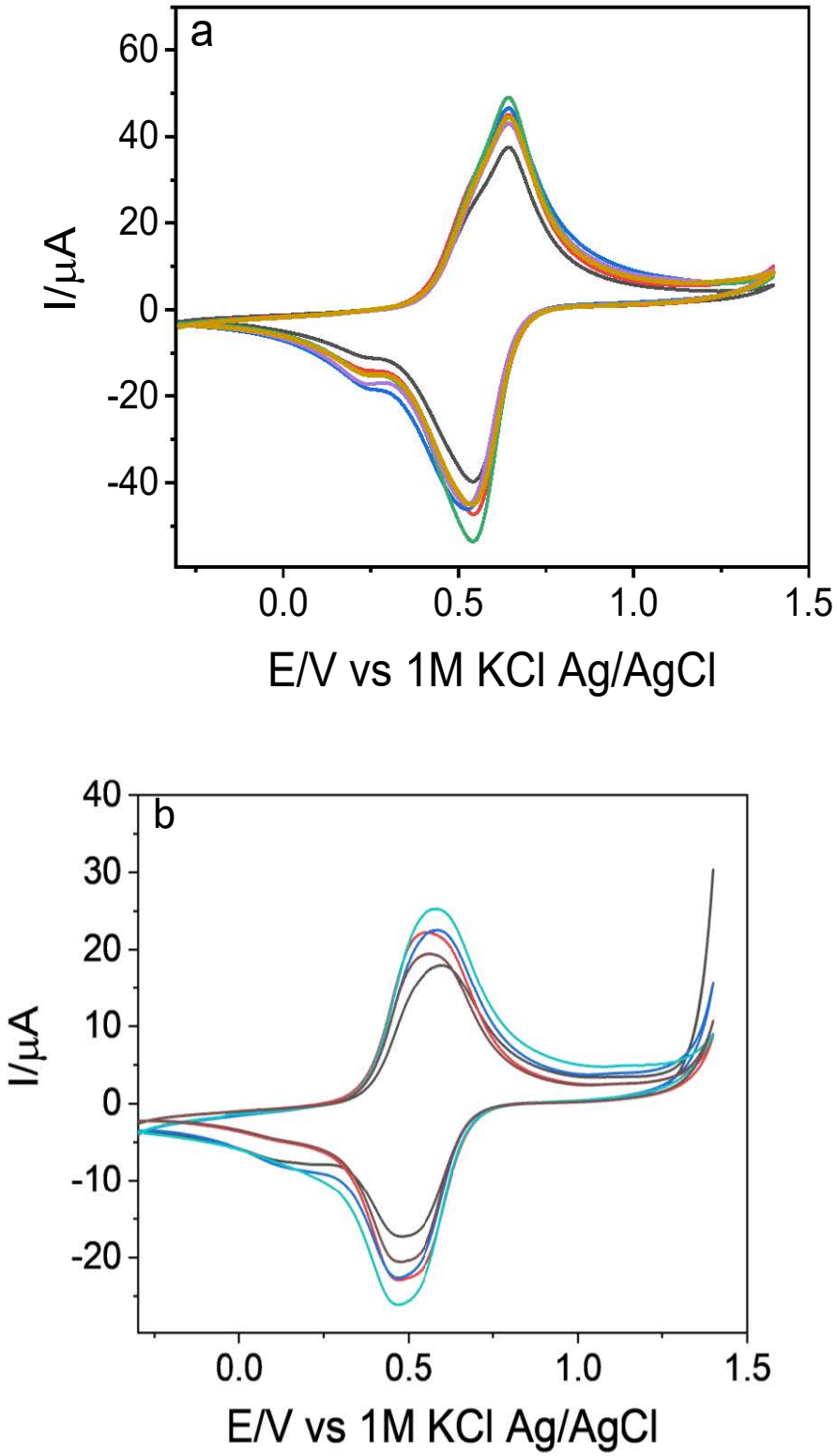

Fig. 42 Cyclic voltammogram of modifications a) $NiCl_2$ with $K_4Fe(CN)_6$ and b) $NiCl_2$ with $K_3Fe(CN)_6$ in 1M KCl, 5 mM HCl (pH 2.5) at $10mVs^{-1}$. Each colour represents a different sample of the same composition.

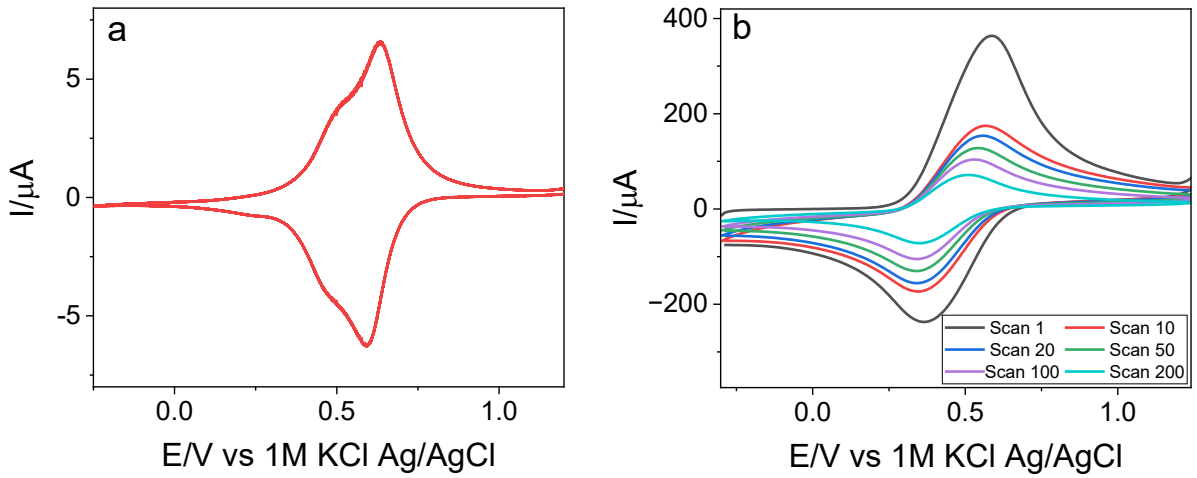

Fig. 43 Cyclic voltammogram of potassium–nickel hexacyanoferrate, the product from the combination $NiCl_2$ with $K_4Fe(CN)_6$ a) scanned in 1M KCl, 5 mM HCl (scan rate=1mVs^{-1}, pH 2.5) and b) long-term stability studies of the same combination in phosphate buffer at 100 mVs^{-1} (pH 7.4).

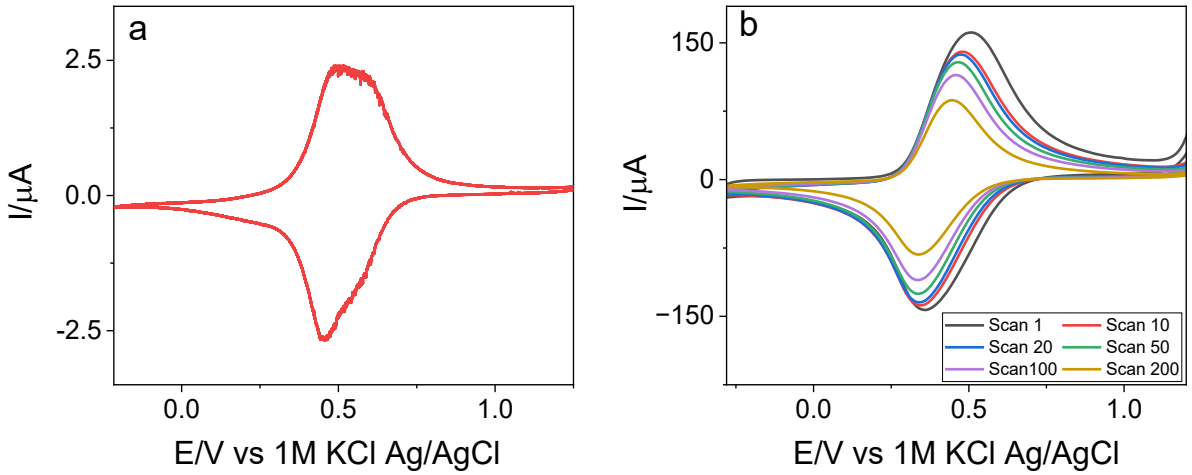

Fig. 44 Cyclic voltammogram of potassium–nickel hexacyanoferrate, the product from the combination $NiCl_2$ with $K_3Fe(CN)_6$ a) scanned in 1M KCl, 5 mM HCl (scan rate=1mVs^{-1}, pH 2.5) and b) long-term stability studies of the same combination in phosphate buffer at 100 mVs^{-1} (pH 7.4).

4.2.3.3 H_2O_2 sensing

H_2O_2 sensing was conducted using Prussian Blue to analyse the sensitivity and linear range of the sample. The PB samples synthesized using photonic curing were used for the measurements. The half-wave potential of the H_2O_2 reduction matches closely with the Prussian Blue/Prussian White redox potential. When a reduction potential is applied to PB-based sensors, it underdoes reduction,

forming Prussian White. The Prussian White catalyse the reduction of H_2O_2 to hydroxyl ions, while oxidising itself to Prussian Blue. The concentration of H_2O_2 is proportional to the amount of Prussian Blue used[175,225,226]. A calibration curve was prepared by plotting Prussian Blue reduction current as a function of H_2O_2 concentration (**Fig. 46**). The results were optimized and the signals were reproducible. As expected, it was observed that current values were decreasing with increasing H_2O_2 concentration. These measurements serve as a control experiment for analyzing the signals of the Prussian Blue analogues obtained through the FLS method.

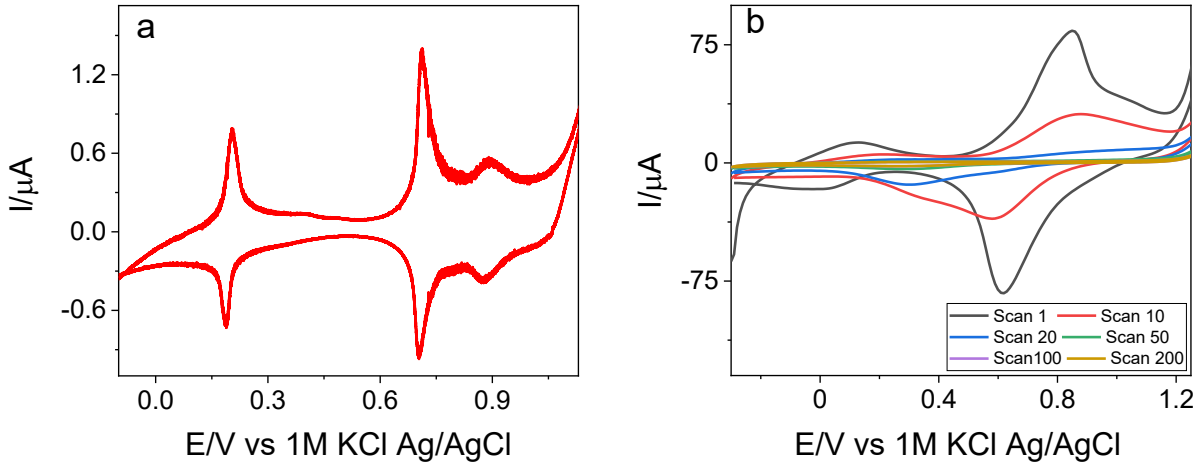

Fig. 45 Cyclic voltammogram of sodium–iron hexacyanoferrate, the product of the combination $Na_4Fe(CN)_6$ and $K_4Fe(CN)_6$ a) scanned in 1M KCl, 5 mM HCl (scan rate=1mVs^{-1}, pH 2.5) and b) long-term stability studies of the same combination in phosphate buffer at 100 mVs^{-1} (pH 7.4).

The PB analogues synthesized at EPFL were subjected to initial CV characterizations in the presence and absence of H_2O_2. Cyclic voltammetry is performed before chronoamperometry measurements to characterize the electrochemical behaviour of the sensor and to determine the optimum potential range for H_2O_2 detection. An example of these measurements is provided in **fig. 47**. The graph compares the voltammograms of potassium nickel hexacyanoferrate (obtained from the combination of $K_4Fe(CN)_6$ and $NiCl_2$) in PBS (0 mM H_2O_2) to that in 20 mM H_2O_2. The scan results in PBS (0mM H_2O_2) show peaks with a redox potential cantered at 0.539 V vs. Ag/AgCl (1 M KCl); which is similar to the previously reported values for the nickel hexacyanoferrate[227,228]. In the presence of H_2O_2, the half-wave potential recorded is slightly positive shifted (0.03 V) in comparison to the redox potential in the absence of H_2O_2. The cause of this shift is unknown at present. When cycled in 20mM H_2O_2, the complex displayed a single oxidation peak at 0.569 V. In the presence of H_2O_2, an increase in current response was observed at anodic potentials as shown in **fig. 47**.

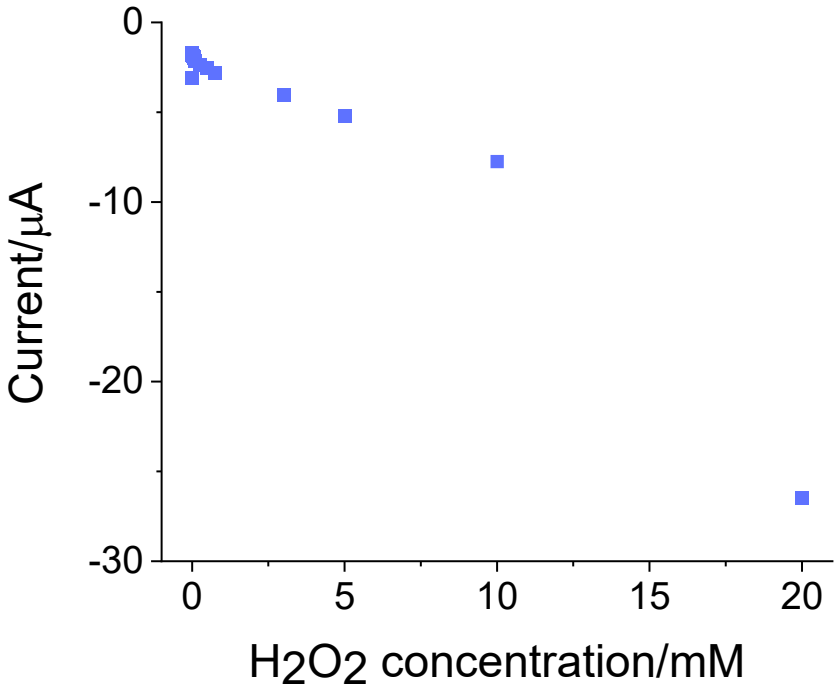

Fig. 46 Prussian Blue reduction current as a function of H_2O_2 concentration. Measurements were made at -0.5 V at room temperature in PBS (pH= 5.8). The sensor electrodes were prepared with aqueous solution of Prussian Blue (FLS) and Nafion.

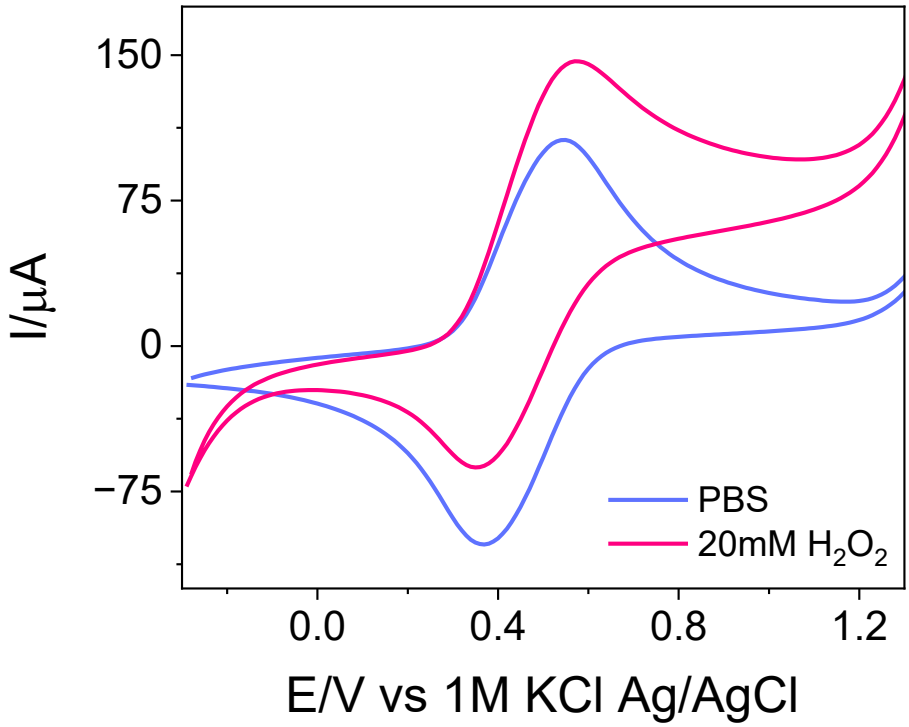

Fig. 47 Preliminary cyclic voltammetry experiments of potassium nickel hexacyanoferrate (obtained from the combination of $K_4Fe(CN)_6$ and $NiCl_2$) for H_2O_2 sensing. The results in PBS (0 mM H_2O_2) and 20 mM H_2O_2 are presented.

4.2.4 Conclusions

Flash light sintering is identified as most suitable synthetic method for this study concerned with Prussian blue analogues. Recognizing the higher stability of mixed hexacyanoferrates, a total of 14 different reactant combinations were investigated, out of which 7 products showed positive reaction progress. Unfortunately, the stability displayed by some of them is similar as observed with other methods. Although the signals of potassium–cobalt hexacyanoferrate obtained from the reaction of $K_3Co(CN)_6$ seemed good at the beginning, the complex characteristics were not reproducible. In terms of electrochemical performances, the samples based on nickel, especially blends of $NiCl_2$ exhibited the best results. However, the potential for the detection of hydrogen peroxide might be too high for our application.

The mixed hexacyanoferrates were prepared as thin films on the ITO plates, and their primary characterization was conducted for the qualitative analysis. It was reported that PB films can be synthesized in situ on porous substrates like titanium[179]. Therefore, to prepare samples for quantitative and physical characterizations, Prussian Blue analogues were synthesized on titanium substrate. It was noted that higher concentrations of solutions should be used for such rough surfaces. More experiments should be performed to achieve high yield. In the future, synthetic methods will be modified for improvement.

H_2O_2 sensing was performed with the Prussian Blue complex (from the FLS method). The calibration curves of hydrogen peroxide detection were constructed, and sensitivity was studied. These control measurements will be used as a standard to assess the sensitivity of the Prussian Blue analogues in H_2O_2 sensing. Preliminary experiments have been conducted in this regard. Detailed electrochemical analysis of the Prussian Blue analogues will be conducted to study their sensitivity and stability in different ionic conditions. Material characterizations will be conducted with the help of powder X-Ray diffraction, XPS spectra, FT-IR, Raman and EDX spectroscopy. Once the formation of stable PB analogues are confirmed, they will be used as mediators for glucose sensing in simple solutions. Finally, sensing will be performed in biologically active systems like cell cultures.

5 Summary

This thesis explores the significance of electrochemistry as a powerful analytical tool to investigate cellular processes. It underscores its advantages, including its non-intrusive character, high sensitivity, cost-effectiveness, and wide-ranging applicability. Electrochemical biosensing based on cell cultures has the potential to transform the fields of medicine, biotechnology, and environmental science by offering a rapid, accurate, and ethical alternative to animal testing. The long-term objective of this research is to develop a multielectrode design integrated into a cell culturing dish. This device will incorporate electrodes at various points of the 3D cell culture scaffold, thus allowing amperometric and potentiometric analysis of biological processes. Although microelectrode arrays are among the basic tools in electrophysiology, their full potential for the analysis of cell activities is rather unexplored. Microelectrode arrays integrated in a 3D scaffold would provide an adaptable platform for this purpose. Models of this nature have the capability to replicate the in vivo environment, encompassing the histological, physiological, and functional attributes of the relevant tissues far more effectively than conventional planar cultures.

Herein, I have presented the development of different components of the final device. The research has successfully developed low-cost ITO (indium tin oxide) microelectrodes and microelectrode arrays for biosensing applications. The versatility and stable performances of these electrodes, as well as the use of EIS to characterise cell cultures, are described. Additionally, this work investigates the synthesis of osmium polypyridyl complexes, Prussian blue analogues and their potential use as mediators for glucose sensing.

The first chapter serves as a general introduction highlighting the importance of cell culture-based biosensing. The second chapter portrays the electrode fabrication techniques. Initially, insulated platinum microwires were employed for electrode preparation, but their poor performance and challenging optimisation led to their replacement. Functional microelectrodes and MEAs were successfully prepared from ITO-coated glass plates with a CO_2 laser plotter. These lasers are readily accessible (commonly found in printing shops), simple to upkeep, and user-friendly. Two distinct techniques were employed: direct patterning for smaller rectangular microelectrodes and in-situ stencil fabrication, followed by etching for larger circular MEAs. While direct laser ablation allowed the definition of smaller structures, it resulted in edge damage, reducing the electroactive area. In contrast, the stencil method produced larger structures without edge damage. All fabricated electrodes and

electrode arrays exhibited stable and reproducible signals with low standard deviations for current. This ensured their cost-effectiveness, simplicity, and reliability for various applications.

The ITO electrodes can be applied across fields such as sensing, bio-sensing, electrowetting on dielectric (EWOD), microfluidics, and cell culture studies. In particular, my focus is on bio-sensing, utilising cell cultures for viability studies through glucose sensing. To illustrate the practicality of these ITO electrodes, we utilised electrochemical impedance spectroscopy (EIS). In the third chapter, we delve into the use of circular microelectrode arrays for the characterisation of HeLa and HepG2 cell cultures. The impedance recordings revealed notable differences in conductivity variations and surface modifications of the electrodes due to cell culture responses. It was found that the attachment of cells to the electrodes creates a barrier to the passage of alternating current. This results in the variation of impedance; as the adhesion increases, the growth of impedance was clearly observed.

Biosensing using ITO electrodes will be performed with a focus on developing a glucose sensor as a versatile platform adaptable for lactate and glutamate measurements. Chapter 4 contains the synthesis of electron mediators for glucose sensing. Electron mediators are used in glucose sensing to allow the effective flow of electrons between the electrode and the glucose oxidase enzyme. They enhance the sensor's sensitivity and enable precise monitoring of glucose levels. They also expand the detection range and reduce interference from other substances, improving the overall reliability and performance of glucose sensors. Simultaneously, two approaches are employed in the preparation of electron mediators. One of the mediators is a mediating redox hydrogel that consists of Os polymer complexes of general formula cis-$[(Os(N\text{-}N)_2(PVI)_{n+1}Cl]^+$ (n = 9). Synthesis of Prussian blue analogues using flash light sintering is the other approach. Although certain products appear promising, additional stability testing and optimisation of synthetic processes are required for better outcomes.

In conclusion, this research discusses the possibilities of electrochemistry in advancing biosensing in cellular studies. The successful development of ITO microelectrodes and microelectrode arrays was achieved through CO_2 laser cutting. An example of the application of these electrodes is depicted with simple EIS measurements. This, combined with ongoing efforts in synthesising electron mediators and characterisation, promises exciting prospects for biosensing applications.

6 Future Outlook

The findings presented in this thesis offer opportunities for further exploration as discrete research problems. Each chapter outlined herein introduces simplified approaches to conducting experiments in their respective domains. Additionally, they pave the way for generating numerous ideas in the pursuit of developing efficient, cost-effective and user-friendly biosensing devices. This section serves as a bridge between the accomplishments detailed in earlier sections and the exciting possibilities that lie ahead.

6.1 Advancements in Electrode Fabrication and expanding Applications

The versatility of ITO electrodes prepared using CO_2 laser cutting is a promising aspect of our research. These electrodes are poised to become ubiquitous in diverse research domains, driven by their simplicity, cost-effectiveness, and reliability. Looking ahead, we foresee their application expanding across various fields, such as electrowetting on dielectric (EWOD), microfluidics, neurostimulation research, and even beyond the fields of biosensing. Exploring novel materials and modification of fabrication methods could unlock new possibilities, enhancing the utility, versatility, stability, and performance of electrodes.

6.2 Integration of Multielectrode Designs

One of the key objectives of our research is the development of a multielectrode design integrated into a cell culturing dish. This ambitious goal remains at the forefront of our vision. As we continue to refine this technology, we anticipate that it will revolutionise the utilisation of 3D cell cultures. The current challenges associated with analysing intricate 3D structures and the complete absence of automation options are limiting the full realisation of this technology. Our envisioned device, incorporating electrodes at multiple points within the scaffold, holds the key to unprecedented insights into biological processes. Continued research will focus on perfecting this integration, ensuring seamless communication between the electrodes and the living biological entities. Moreover, the future of cellular biosensing is inherently interdisciplinary. We anticipate fostering collaborations with researchers from diverse fields, including biology, chemistry, materials science, and medicine.

6.3 Technological advancements, commercialisation and impact

As technology continues to advance at a rapid pace, we will remain at the forefront of adopting cutting-edge techniques and tools. Emerging technologies in data analysis and machine learning will

be leveraged to extract deeper insights from our biosensing experiments. These advancements will further refine our understanding of cellular processes.

The practical applications of our research hold immense potential for commercialisation. We envision the development of user-friendly biosensing platforms that can be readily adopted in research laboratories, clinical settings, and individual uses. The impact of our work extends beyond the academic sphere, with the potential to improve healthcare, diagnostics, and environmental monitoring.

In conclusion, this thesis represents a stepping stone toward shaping the future of biosensing technologies. The journey thus far, marked by advancements in electrode fabrication, electron mediator synthesis, and cellular response characterisation, is driven by the conviction that our work will continue to advance scientific knowledge. As we forge ahead, we remain committed to pushing the boundaries of cellular biosensing, unlocking new frontiers, and making a meaningful impact on the world of science and technology. I believe we stand on the brink of transformative discoveries, unlocking the secrets of cellular processes and ushering in an era of innovative, ethical, and precise biosensing technologies that will redefine the landscape of scientific inquiry.

7 Appendix

Table A1. Comparison of different laser ablation methods for fabrication of ITO structures[196] (adapted from Kappalakandy Valapil et al., 2023).

Laser type	**Yb:YAG 1,030 nm**	**Yb:YAG 1,030 nm**	**Nd:glass 1,056 nm**	**KrF excimer laser 248 nm**	**CO_2 10.6μm Direct ablation**	**CO_2 10.6μm Stencil ablation**
Model	LXR 100–1030, Luxinar GmbH, Germany	TruMicro2000 system,TRUMPF	femtoREGEN, Spectra-Physics, Inc	Coherent Variolas COMPex Pro 205F	GCC C180II, New Taipei City, Taiwan	GCC C180II, New Taipei City, Taiwan
Power	100 W	20 W	N/A	20 W	30W	30W
Min size of the ablated path	~2μm	~4μm	~10μm	~100μm	~50μm	~100μm
Min. feature width	~2μm	~2μm	N/A	~200μm	~50μm	~100μm
Cost of the laser	~200 000 EUR	High	High	High	12 000 EUR gross	12 000 EUR gross
Availability	Research units	Research units	Research units	Research units	Xerox shops	Xerox shops
Conservation of electrochemical properties	Not tested but resistivity for the patterns in which the ablated section became insulating increased from RS = 3.8 to 200 Ω/sq	Not tested	Not tested	Not tested	Yes	Yes
Reference	[229]	[230]	[231]	[232]	This work	This work

8 References

1. Segeritz CP, Vallier L. Cell Culture. In: *Basic Science Methods for Clinical Researchers*. Elsevier; 2017:151-172. doi:10.1016/B978-0-12-803077-6.00009-6

2. Harrison RG. Observations on the living developing nerve fiber. *Proceedings of the Society for Experimental Biology and Medicine*. 1906;4(1):140-143. doi:10.3181/00379727-4-98

3. Torsvik A, Stieber D, Enger PØ, et al. U-251 revisited: genetic drift and phenotypic consequences of long-term cultures of glioblastoma cells. *Cancer Med*. 2014;3(4):812-824. doi:10.1002/cam4.219

4. Gupta N, Renugopalakrishnan V, Liepmann D, Paulmurugan R, Malhotra BD. Cell-based biosensors: Recent trends, challenges and future perspectives. *Biosensors and Bioelectronics*. 2019;141:111435. doi:10.1016/j.bios.2019.111435

5. Pan C, Kumar C, Bohl S, Klingmueller U, Mann M. Comparative Proteomic Phenotyping of Cell Lines and Primary Cells to Assess Preservation of Cell Type-specific Functions. *Molecular & Cellular Proteomics*. 2009;8(3):443-450. doi:10.1074/mcp.M800258-MCP200

6. Richter M, Piwocka O, Musielak M, Piotrowski I, Suchorska WM, Trzeciak T. From Donor to the Lab: A Fascinating Journey of Primary Cell Lines. *Frontiers in Cell and Developmental Biology*. 2021;9. doi:10.3389/fcell.2021.711381

7. Stacey G. Primary Cell Cultures and Immortal Cell Lines. In: *eLS*. John Wiley & Sons, Ltd; 2006. doi:https://doi.org/10.1038/npg.els.0003960

8. Victorelli S, Passos JF. Telomeres and Cell Senescence - Size Matters Not. *EBioMedicine*. 2017;21:14-20. doi:10.1016/j.ebiom.2017.03.027

9. Hayflick L. The limited in vitro lifetime of human diploid cell strains. *Exp Cell Res*. 1965;37:614-636. doi:10.1016/0014-4827(65)90211-9

10. Burnet M. *Intrinsic Mutagenesis*. Springer Netherlands; 1974. doi:10.1007/978-94-011-6606-5

11. Jensen C, Teng Y. Is It Time to Start Transitioning From 2D to 3D Cell Culture? *Frontiers in Molecular Biosciences*. 2020;7. Accessed April 3, 2023. https://www.frontiersin.org/articles/10.3389/fmolb.2020.00033

12. Edmondson R, Broglie JJ, Adcock AF, Yang L. Three-dimensional cell culture systems and their applications in drug discovery and cell-based biosensors. *Assay Drug Dev Technol*. 2014;12(4):207-218. doi:10.1089/adt.2014.573

13. Brajša K. Three-dimensional cell cultures as a new tool in drug discovery. *Period Biol*. 2016;118(1):59-65. doi:10.18054/pb.2016.118.1.3940

14. Kapałczyńska M, Kolenda T, Przybyła W, et al. 2D and 3D cell cultures – a comparison of different types of cancer cell cultures. *aoms*. 2018;14(4):910-919. doi:10.5114/aoms.2016.63743

15. Cacciamali A, Villa R, Dotti S. 3D Cell Cultures: Evolution of an Ancient Tool for New Applications. *Front Physiol*. 2022;13:836480. doi:10.3389/fphys.2022.836480

16. Golikov MV, Valuev-Elliston VT, Smirnova OA, Ivanov AV. Review on the Use of Cell Cultures to Study Metabolism, Transport, and Accumulation of Flavonoids: From Mono-Cultures to Co-Culture Systems. *Mol Biol*. 2022;56(5):629-637. doi:10.1134/S0026893322050077

17. Gonzales GB, Van Camp J, Vissenaekens H, Raes K, Smagghe G, Grootaert C. Review on the Use of Cell Cultures to Study Metabolism, Transport, and Accumulation of Flavonoids: From Mono-Cultures to Co-Culture Systems. *Comprehensive Reviews in Food Science and Food Safety*. 2015;14(6):741-754. doi:10.1111/1541-4337.12158

18. Halama A. Metabolomics in cell culture—A strategy to study crucial metabolic pathways in cancer development and the response to treatment. *Archives of Biochemistry and Biophysics*. 2014;564:100-109. doi:10.1016/j.abb.2014.09.002

19. Kamiloglu S, Sari G, Ozdal T, Capanoglu E. Guidelines for cell viability assays. *Food Frontiers*. 2020;1(3):332-349.

20. Hanks JH, Wallace JH. Determination of Cell Viability. *Experimental Biology and Medicine*. 1958;98(1):188-192. doi:10.3181/00379727-98-23985

21. Sart S, Ronteix G, Jain S, Amselem G, Baroud CN. Cell Culture in Microfluidic Droplets. *Chem Rev*. 2022;122(7):7061-7096. doi:10.1021/acs.chemrev.1c00666

22. Legut M, Gajic Z, Guarino M, et al. A genome-scale screen for synthetic drivers of T cell proliferation. *Nature*. 2022;603(7902):728-735. doi:10.1038/s41586-022-04494-7

23. Mohammadi M, Bagheri L, Badreldin A, et al. Biological Effects of Gyrophoric Acid and Other Lichen Derived Metabolites, on Cell Proliferation, Apoptosis and Cell Signaling pathways. *Chemico-Biological Interactions*. 2022;351:109768. doi:10.1016/j.cbi.2021.109768

24. Friedl P, Sahai E, Weiss S, Yamada KM. New dimensions in cell migration. *Nat Rev Mol Cell Biol*. 2012;13(11):743-747. doi:10.1038/nrm3459

25. Isomursu A, Park KY, Hou J, et al. Directed cell migration towards softer environments. *Nat Mater*. 2022;21(9):1081-1090. doi:10.1038/s41563-022-01294-2

26. Juriga D, Kalman EE, Toth K, et al. Analysis of Three-Dimensional Cell Migration in Dopamine-Modified Poly(aspartic acid)-Based Hydrogels. *Gels*. 2022;8(2):65. doi:10.3390/gels8020065

27. Yap L, Tay HG, Nguyen MTX, Tjin MS, Tryggvason K. Laminins in Cellular Differentiation. *Trends in Cell Biology*. 2019;29(12):987-1000. doi:10.1016/j.tcb.2019.10.001

28. Marniemi J, Parkki MG. Radiochemical assay of glutathione S-epoxide transferase and its enhancement by phenobarbital in rat liver in vivo. *Biochem Pharmacol*. 1975;24(17):1569-1572. doi:10.1016/0006-2952(75)90080-5

29. Veres A, Faust AL, Bushnell HL, et al. Charting cellular identity during human in vitro β-cell differentiation. *Nature*. 2019;569(7756):368-373. doi:10.1038/s41586-019-1168-5

30. Sies H. Oxidative stress: oxidants and antioxidants. *Exp Physiol*. 1997;82(2):291-295. doi:10.1113/expphysiol.1997.sp004024

31. Halliwell B, Gutteridge JMC. *Free Radicals in Biology and Medicine*. 5th ed. Oxford University Press; 2015. doi:10.1093/acprof:oso/9780198717478.001.0001

32. Sies H. On the history of oxidative stress: Concept and some aspects of current development. *Current Opinion in Toxicology*. 2018;7:122-126. doi:10.1016/j.cotox.2018.01.002

33. Janiszewska M, Primi MC, Izard T. Cell adhesion in cancer: Beyond the migration of single cells. *Journal of Biological Chemistry*. 2020;295(8):2495-2505. doi:10.1074/jbc.REV119.007759

34. Zanetti C, Spitz S, Berger E, et al. Monitoring the neurotransmitter release of human midbrain organoids using a redox cycling microsensor as a novel tool for personalized Parkinson's disease modelling and drug screening. *Analyst*. 2021;146(7):2358-2367. doi:10.1039/D0AN02206C

35. Bajaj S, Bagley JA, Sommer C, et al. Neurotransmitter signaling regulates distinct phases of multimodal human interneuron migration. *The EMBO Journal*. 2021;40(23):e108714. doi:10.15252/embj.2021108714

36. Keighron JD, Wang Y, Cans AS. Electrochemistry of Single-Vesicle Events. *Annual Review of Analytical Chemistry*. 2020;13(1):159-181. doi:10.1146/annurev-anchem-061417-010032

37. Maïno NG. *Development of New Volcano-Shaped Microelectrodes for Single Cell Electrochemistry, Electrophysiology and Impedance Studies*. EPFL; 2023. doi:10.5075/epfl-thesis-9769

38. Bucher ES, Wightman RM. Electrochemical Analysis of Neurotransmitters. *Annual Review of Analytical Chemistry*. 2015;8(1):239-261. doi:10.1146/annurev-anchem-071114-040426

39. Nam S, Stowers R, Lou J, Xia Y, Chaudhuri O. Varying PEG density to control stress relaxation in alginate-PEG hydrogels for 3D cell culture studies. *Biomaterials*. 2019;200:15-24. doi:10.1016/j.biomaterials.2019.02.004

40. Mirbagheri M, Adibnia V, R. Hughes B, D. Waldman S, Banquy X, Kun Hwang D. Advanced cell culture platforms: a growing quest for emulating natural tissues. *Materials Horizons*. 2019;6(1):45-71. doi:10.1039/C8MH00803E

41. Li H, Ning S, Ghandi M, et al. The landscape of cancer cell line metabolism. *Nat Med*. 2019;25(5):850-860. doi:10.1038/s41591-019-0404-8

42. Hartmann FJ, Mrdjen D, McCaffrey E, et al. Single-cell metabolic profiling of human cytotoxic T cells. *Nat Biotechnol*. 2021;39(2):186-197. doi:10.1038/s41587-020-0651-8

43. Amoêdo ND, Valencia JP, Rodrigues MF, Galina A, Rumjanek FD. How does the metabolism of tumour cells differ from that of normal cells. *Biosci Rep*. 2013;33(6):e00080. doi:10.1042/BSR20130066

44. Rampersad SN. Multiple applications of Alamar Blue as an indicator of metabolic function and cellular health in cell viability bioassays. *Sensors (Basel)*. 2012;12(9):12347-12360. doi:10.3390/s120912347

45. Sumantran VN. Cellular chemosensitivity assays: an overview. *Methods Mol Biol*. 2011;731:219-236. doi:10.1007/978-1-61779-080-5_19

46. Li Q, Nan K, Le Floch P, et al. Cyborg Organoids: Implantation of Nanoelectronics via Organogenesis for Tissue-Wide Electrophysiology. *Nano Lett*. 2019;19(8):5781-5789. doi:10.1021/acs.nanolett.9b02512

47. Jomova K, Raptova R, Alomar SY, et al. Reactive oxygen species, toxicity, oxidative stress, and antioxidants: chronic diseases and aging. *Arch Toxicol*. 2023;97(10):2499-2574. doi:10.1007/s00204-023-03562-9

48. Alrashidi H, Eaton S, Heales S. Biochemical characterization of proliferative and differentiated SH-SY5Y cell line as a model for Parkinson's disease. *Neurochemistry International*. 2021;145:105009. doi:10.1016/j.neuint.2021.105009

49. Li P, Zhang F, Li Y, et al. Isoginkgetin treatment attenuated lipopolysaccharide-induced monoamine neurotransmitter deficiency and depression-like behaviors through downregulating p38/NF-κB signaling pathway and suppressing microglia-induced apoptosis. *J Psychopharmacol*. 2021;35(10):1285-1299. doi:10.1177/02698811211032473

50. Voleti R, Bali S, Guerrero J, et al. Evaluation of the tert-butyl group as a probe for NMR studies of macromolecular complexes. *J Biomol NMR*. 2021;75(8-9):347-363. doi:10.1007/s10858-021-00380-y

51. Bard AJ, Faulkner LR. *Electrochemical Methods: Fundamentals and Applications*. 2nd ed. Wiley; 2001.

52. Hibbert DB. Introduction to electrochemistry. In: Hibbert DB, ed. *Introduction to Electrochemistry*. Macmillan Physical Science Series. Macmillan Education UK; 1993:1-10. doi:10.1007/978-1-349-22721-1_1

53. Brett CMA, Brett AMO. *Electrochemistry: Principles, Methods, and Applications*. Oxford University Press; 1993.

54. Brett CMA. Electrochemistry. In: *Reference Module in Chemistry, Molecular Sciences and Chemical Engineering*. Elsevier; 2014. doi:10.1016/B978-0-12-409547-2.10742-5

55. Wang J. *Analytical Electrochemistry*. John Wiley & Sons; 2023.

56. Oliveira M, Conceição P, Kant K, Ainla A, Diéguez L. Electrochemical Sensing in 3D Cell Culture Models: New Tools for Developing Better Cancer Diagnostics and Treatments. *Cancers*. 2021;13(6):1381. doi:10.3390/cancers13061381

57. Nagel B, Dellweg H, Gierasch LM. Glossary for chemists of terms used in biotechnology (IUPAC Recommendations 1992). *Pure and Applied Chemistry*. 1992;64(1):143-168. doi:10.1351/pac199264010143

58. Bhatia AK, Dewangan S. Biosensors: Detection of biomolecules by biosensors. In: *Handbook of Biomolecules*. Elsevier; 2023:259-274. doi:10.1016/B978-0-323-91684-4.00029-3

59. Bhalla N, Jolly P, Formisano N, Estrela P. Introduction to biosensors. Estrela P, ed. *Essays in Biochemistry*. 2016;60(1):1-8. doi:10.1042/EBC20150001

60. Clark Jr. LC, Lyons C. Electrode Systems for Continuous Monitoring in Cardiovascular Surgery. *Annals of the New York Academy of Sciences*. 1962;102(1):29-45. doi:10.1111/j.1749-6632.1962.tb13623.x

61. Abdulbari HA, Basheer EAM. Electrochemical Biosensors: Electrode Development, Materials, Design, and Fabrication. *ChemBioEng Reviews*. 2017;4(2):92-105. doi:10.1002/cben.201600009

62. Pan T, Lu D, Xin H, Li B. Biophotonic probes for bio-detection and imaging. *Light Sci Appl*. 2021;10(1):124. doi:10.1038/s41377-021-00561-2

63. Sung KE, Beebe DJ. Microfluidic 3D models of cancer. *Adv Drug Deliv Rev*. 2014;79-80:68-78. doi:10.1016/j.addr.2014.07.002

64. Charwat V, Schütze K, Holnthoner W, et al. Potential and limitations of microscopy and Raman spectroscopy for live-cell analysis of 3D cell cultures. *Journal of Biotechnology*. 2015;205:70-81. doi:10.1016/j.jbiotec.2015.02.007

65. Singh S, Kumar V, Dhanjal DS, Datta S, Prasad R, Singh J. Biological Biosensors for Monitoring and Diagnosis. In: Singh J, Vyas A, Wang S, Prasad R, eds. *Microbial Biotechnology: Basic Research and Applications*. Environmental and Microbial Biotechnology. Springer; 2020:317-335. doi:10.1007/978-981-15-2817-0_14

66. Hashem A, Hossain MAM, Marlinda AR, Mamun MA, Simarani K, Johan MR. Nanomaterials based electrochemical nucleic acid biosensors for environmental monitoring: A review. *Applied Surface Science Advances*. 2021;4:100064. doi:10.1016/j.apsadv.2021.100064

67. Modena MM, Chawla K, Misun PM, Hierlemann A. Smart Cell-Culture Systems: Integration of Sensors and Actuators into Microphysiological Systems. *ACS Chem Biol*. 2018;13(7):1767-1784. doi:10.1021/acschembio.7b01029

68. Valapil KK, Jarosińska E, Filipiak MS, Mazurkiewicz W, Nery EW. Guidelines on the development of sensors and application of data analysis tools for potentiometric electronic tongues. *Electronic Tongues: Fundamentals and recent advances*. Published online November 1, 2021. doi:10.1088/978-0-7503-3687-1ch3

69. Podrażka M, Bączyńska E, Kundys M, Jeleń PS, Witkowska Nery E. Electronic Tongue—A Tool for All Tastes? *Biosensors*. 2018;8(1):3. doi:10.3390/bios8010003

70. Zhang Z, Ma C, Xu Q, Zhu JJ. Recent progress in electrochemiluminescence microscopy analysis of single cells. *Analyst*. 2022;147(13):2884-2894. doi:10.1039/D2AN00709F

71. Podrażka M, Witkowska Nery E, Henares TG, Jönsson-Niedziółka M, Arrigan DWM. Ion Transfer Voltammetry with an Electrochemical Pen. *Anal Chem*. 2020;92(24):15997-16004. doi:10.1021/acs.analchem.0c03530

72. Shlosberg Y, Spungin D, Schuster G, Berman-Frank I, Adir N. Trichodesmium erythraeum produces a higher photocurrent than other cyanobacterial species in bio-photo electrochemical cells. *Biochimica et Biophysica Acta (BBA) - Bioenergetics*. 2022;1863(8):148910. doi:10.1016/j.bbabio.2022.148910

73. Liu L, Choi S. Enhanced biophotoelectricity generation in cyanobacterial biophotovoltaics with intracellularly biosynthesized gold nanoparticles. *Journal of Power Sources*. 2021;506:230251. doi:10.1016/j.jpowsour.2021.230251

74. Mazurkiewicz W, Małolepszy A, Witkowska Nery E. Comparison of Carbon Nanomaterials for Simultaneous Detection of Neurotransmitters in the Presence of Interfering Species. *ChemElectroChem*. 2022;9(15):e202200330. doi:10.1002/celc.202200330

75. Kundys-Siedlecka M, Bączyńska E, Jönsson-Niedziółka M. Electrochemical Detection of Dopamine and Serotonin in the Presence of Interferences in a Rotating Droplet System. *Anal Chem*. 2019;91(16):10908-10913. doi:10.1021/acs.analchem.9b02967

76. Boonkaew S, Dettlaff A, Sobaszek M, Bogdanowicz R, Jönsson-Niedziółka M. Electrochemical determination of neurotransmitter serotonin using boron/nitrogen co-doped diamond-graphene nanowall-structured particles. *Journal of Electroanalytical Chemistry*. 2022;926:116938. doi:10.1016/j.jelechem.2022.116938

77. da Rocha AM, Creech J, Thonn E, Mironov S, Herron TJ. Detection of Drug-Induced Torsades de Pointes Arrhythmia Mechanisms Using hiPSC-CM Syncytial Monolayers in a High-Throughput Screening Voltage Sensitive Dye Assay. *Toxicological Sciences*. 2020;173(2):402-415. doi:10.1093/toxsci/kfz235

78. Goshi N, Morgan RK, Lein PJ, Seker E. A primary neural cell culture model to study neuron, astrocyte, and microglia interactions in neuroinflammation. *Journal of Neuroinflammation*. 2020;17(1):155. doi:10.1186/s12974-020-01819-z

79. Gross GW, Gopal KV. Emerging Histiotypic Properties of Cultured Neuronal Networks. In: Taketani M, Baudry M, eds. *Advances in Network Electrophysiology*. Springer US; 2006:193-214. doi:10.1007/0-387-25858-2_8

80. Bagheri Hashkavayi A, Hashemnia S, Osfouri S. Investigations of antioxidant potential and protective effect of Acanthophora algae on DNA damage: An electrochemical approach. *Microchemical Journal*. 2020;159:105455. doi:10.1016/j.microc.2020.105455

81. Barciszewska AM, Giel-Pietraszuk M, Perrigue PM, Naskręt-Barciszewska M. Total DNA Methylation Changes Reflect Random Oxidative DNA Damage in Gliomas. *Cells*. 2019;8(9):1065. doi:10.3390/cells8091065

82. Singh S, Saha Podder P, Russo M, Henry C, Cinti S. Tailored point-of-care biosensors for liquid biopsy in the field of oncology. *Lab on a Chip*. 2023;23(1):44-61. doi:10.1039/D2LC00666A

83. Lomae A, Preechakasedkit P, Hanpanich O, et al. Label free electrochemical DNA biosensor for COVID-19 diagnosis. *Talanta*. 2023;253:123992. doi:10.1016/j.talanta.2022.123992

84. Khezri B, Beladi Mousavi SM, Krejčová L, Heger Z, Sofer Z, Pumera M. Ultrafast Electrochemical Trigger Drug Delivery Mechanism for Nanographene Micromachines. *Advanced Functional Materials*. 2019;29(4):1806696. doi:10.1002/adfm.201806696

85. Foroughi MM, Jahani S. Investigation of a high-sensitive electrochemical DNA biosensor for determination of Idarubicin and studies of DNA-binding properties. *Microchemical Journal*. 2022;179:107546. doi:10.1016/j.microc.2022.107546

86. Zhu B, Li X, Zhou L, Su B. An Overview of Wearable and Implantable Electrochemical Glucose Sensors. *Electroanalysis*. 2022;34(2):237-245. doi:10.1002/elan.202100273

87. Kar A, Ahamad N, Dewani M, Awasthi L, Patil R, Banerjee R. Wearable and implantable devices for drug delivery: Applications and challenges. *Biomaterials*. 2022;283:121435. doi:10.1016/j.biomaterials.2022.121435

88. Chiorcea-Paquim AM, Oliveira-Brett AM. Amyloid beta peptides electrochemistry: A review. *Current Opinion in Electrochemistry*. 2022;31:100837. doi:10.1016/j.coelec.2021.100837

89. Joshi PN, Mervinetsky E, Solomon O, Chen YJ, Yitzchaik S, Friedler A. Electrochemical biosensors based on peptide-kinase interactions at the kinase docking site. *Biosensors and Bioelectronics*. 2022;207:114177. doi:10.1016/j.bios.2022.114177

90. Wiloch MZ, Jönsson-Niedziółka M. Very small changes in the peptide sequence alter the redox properties of Aβ(11–16)-Cu(II) and pAβ(11–16)-Cu(II) β-amyloid complexes. *Journal of Electroanalytical Chemistry*. 2022;922:116746. doi:10.1016/j.jelechem.2022.116746

91. Wiloch MZ, Baran N, Jönsson-Niedziółka M. The Influence of Coordination Mode on the Redox Properties of Copper Complexes with Aβ(3-16) and Its Pyroglutamate Counterpart pAβ(3-16). *ChemElectroChem*. 2022;9(17):e202200623. doi:10.1002/celc.202200623

92. Kannan P, Maiyalagan T, Marsili E, et al. Highly active 3-dimensional cobalt oxide nanostructures on the flexible carbon substrates for enzymeless glucose sensing. *Analyst*. 2017;142(22):4299-4307. doi:10.1039/C7AN01084B

93. Filipiak MS, Vetter D, Thodkar K, Gutiérrez-Sanz O, Jönsson-Niedziółka M, Tarasov A. Electron transfer from FAD-dependent glucose dehydrogenase to single-sheet graphene electrodes. *Electrochimica Acta*. 2020;330:134998. doi:10.1016/j.electacta.2019.134998

94. Nery EW, Kubota LT. Evaluation of enzyme immobilization methods for paper-based devices—A glucose oxidase study. *Journal of Pharmaceutical and Biomedical Analysis*. 2016;117:551-559. doi:10.1016/j.jpba.2015.08.041

95. Ucar A, González-Fernández E, Staderini M, et al. Miniaturisation of a peptide-based electrochemical protease activity sensor using platinum microelectrodes. *Analyst*. 2020;145(3):975-982. doi:10.1039/C9AN02321F

96. J. Ronkainen N, Brian Halsall H, R. Heineman W. Electrochemical biosensors. *Chemical Society Reviews*. 2010;39(5):1747-1763. doi:Miniaturisation of a peptide-based electrochemical protease activity sensor using platinum microelectrodes

97. Juska VB, Pemble ME. A Critical Review of Electrochemical Glucose Sensing: Evolution of Biosensor Platforms Based on Advanced Nanosystems. *Sensors*. 2020;20(21):6013. doi:10.3390/s20216013

98. Moussa S, Mauzeroll J. Review—Microelectrodes: An Overview of Probe Development and Bioelectrochemistry Applications from 2013 to 2018. *J Electrochem Soc*. 2019;166(6):G25. doi:10.1149/2.0741906jes

99. Lakard S, Pavel IA, Lakard B. Electrochemical Biosensing of Dopamine Neurotransmitter: A Review. *Biosensors*. 2021;11(6):179. doi:10.3390/bios11060179

100. O'Neill RD, Chang SC, Lowry JP, McNeil CJ. Comparisons of platinum, gold, palladium and glassy carbon as electrode materials in the design of biosensors for glutamate. *Biosensors and Bioelectronics*. 2004;19(11):1521-1528. doi:10.1016/j.bios.2003.12.004

101. Yu H, Yu J, Li L, et al. Recent Progress of the Practical Applications of the Platinum Nanoparticle-Based Electrochemistry Biosensors. *Frontiers in Chemistry*. 2021;9. Accessed May 8, 2023. https://www.frontiersin.org/articles/10.3389/fchem.2021.677876

102. Sharma S, Kumar A, Singh N, Kaur D. Excellent room temperature ammonia gas sensing properties of n-MoS2/p-CuO heterojunction nanoworms. *Sensors and Actuators B: Chemical*. 2018;275:499-507. doi:10.1016/j.snb.2018.08.046

103. Celebanska A, Filipiak MS, Lesniewski A, Jubete E, Opallo M. Nanocarbon electrode prepared from oppositely charged nanoparticles and nanotubes for low-potential thiocholine oxidation. *Electrochimica Acta*. 2015;176:249-254. doi:10.1016/j.electacta.2015.06.143

104. Huang L, Zaman S, Tian X, Wang Z, Fang W, Xia BY. Advanced Platinum-Based Oxygen Reduction Electrocatalysts for Fuel Cells. *Acc Chem Res*. 2021;54(2):311-322. doi:10.1021/acs.accounts.0c00488

105. Kloke A, Von Stetten F, Zengerle R, Kerzenmacher S. Strategies for the Fabrication of Porous Platinum Electrodes. *Advanced Materials*. 2011;23(43):4976-5008. doi:10.1002/adma.201102182

106. Zhang S, Chen M, Zhao X, et al. Advanced Noncarbon Materials as Catalyst Supports and Non-noble Electrocatalysts for Fuel Cells and Metal–Air Batteries. *Electrochem Energ Rev*. 2021;4(2):336-381. doi:10.1007/s41918-020-00085-0

107. Anuar NS, Basirun WJ, Shalauddin Md, Akhter S. A dopamine electrochemical sensor based on a platinum–silver graphene nanocomposite modified electrode. *RSC Adv*. 2020;10(29):17336-17344. doi:10.1039/C9RA11056A

108. Boehler C, Vieira DM, Egert U, Asplund M. NanoPt—A Nanostructured Electrode Coating for Neural Recording and Microstimulation. *ACS Appl Mater Interfaces*. 2020;12(13):14855-14865. doi:10.1021/acsami.9b22798

109. Liu Q, Wang W, Reynolds MF, et al. Micrometer-sized electrically programmable shape-memory actuators for low-power microrobotics. *Sci Robot*. 2021;6(52):eabe6663. doi:10.1126/scirobotics.abe6663

110. Hussain S, Erikson H, Kongi N, et al. Oxygen reduction reaction on nanostructured Pt-based electrocatalysts: A review. *International Journal of Hydrogen Energy*. 2020;45(56):31775-31797. doi:10.1016/j.ijhydene.2020.08.215

111. Grabiec P, Domanski K, Szmigiel D, Hodgins D. Electrode array design and fabrication for implantable systems. In: *Implantable Sensor Systems for Medical Applications*. Elsevier; 2013:150-182. doi:10.1533/9780857096289.1.150

112. Gudmundsson JT, Lundin D. Introduction to magnetron sputtering. In: *High Power Impulse Magnetron Sputtering*. Elsevier; 2020:1-48. doi:10.1016/B978-0-12-812454-3.00006-1

113. Fu K, Zeng L, Liu J, et al. Magnetron sputtering a high-performance catalyst for ultra-low-Pt loading PEMFCs. *Journal of Alloys and Compounds*. 2020;815:152374. doi:10.1016/j.jallcom.2019.152374

114. Stadler A. Transparent Conducting Oxides—An Up-To-Date Overview. *Materials*. 2012;5(12):661-683. doi:10.3390/ma5040661

115. Aydın EB, Sezgintürk MK. Indium tin oxide (ITO): A promising material in biosensing technology. *TrAC Trends in Analytical Chemistry*. 2017;97:309-315. doi:https://doi.org/10.1016/j.trac.2017.09.021

116. Granqvist CG, Hultåker A. Transparent and conducting ITO films: New developments and applications. *Thin Solid Films*. 2002;411(1):1-5. doi:10.1016/S0040-6090(02)00163-3

117. Huang X, Shi W, Li J, Bao N, Yu C, Gu H. Determination of salivary uric acid by using poly(3,4-ethylenedioxythipohene) and graphene oxide in a disposable paper-based analytical device. *Analytica Chimica Acta*. 2020;1103:75-83. doi:10.1016/j.aca.2019.12.057

118. Lee HB, Jin WY, Ovhal MM, Kumar N, Kang JW. Flexible transparent conducting electrodes based on metal meshes for organic optoelectronic device applications: A review. *Journal of Materials Chemistry C*. 2019;7(5):1087-1110. doi:10.1039/c8tc04423f

119. Zhuang Z, Iida D, Kirilenko P, Velazquez-Rizo M, Ohkawa K. Optimal ITO transparent conductive layers for InGaN-based amber/red light-emitting diodes. *Opt Express*. 2020;28(8):12311-12321. doi:10.1364/OE.389725

120. Chinky, Kumar P, Sharma V, Malik P, Raina KK. Nano particles induced vertical alignment of liquid crystal for display devices with augmented morphological and electro-optical characteristics. *Journal of Molecular Structure*. 2019;1196:866-873. doi:10.1016/j.molstruc.2019.06.045

121. Lucarelli G, Brown TM. Development of Highly Bendable Transparent Window Electrodes Based on MoOx, SnO2, and Au Dielectric/Metal/Dielectric Stacks: Application to Indium Tin Oxide (ITO)-Free Perovskite Solar Cells. *Frontiers in Materials*. 2019;6(December):1-11. doi:10.3389/fmats.2019.00310

122. Si M, Andler J, Lyu X, et al. Indium–Tin-Oxide Transistors with One Nanometer Thick Channel and Ferroelectric Gating. *ACS Nano*. 2020;14(9):11542-11547. doi:10.1021/acsnano.0c03978

123. Zhou JY, Bai JL, Zhao H, et al. Gas sensing enhancing mechanism via doping-induced oxygen vacancies for gas sensors based on indium tin oxide nanotubes. *Sensors and Actuators B: Chemical*. 2018;265:273-284. doi:10.1016/j.snb.2018.03.008

124. Zhang D, Tavakoliyaraki A, Wu Y, van Swaaij RACMM, Zeman M. Influence of ITO deposition and post annealing on HIT solar cell structures. *Energy Procedia*. 2011;8:207-213. doi:10.1016/j.egypro.2011.06.125

125. Sierros KA, Morris NJ, Ramji K, Cairns DR. Stress–corrosion cracking of indium tin oxide coated polyethylene terephthalate for flexible optoelectronic devices. *Thin Solid Films*. 2009;517(8):2590-2595. doi:10.1016/j.tsf.2008.10.031

126. Pratheesh Kumar S, Elangovan S, Mohanraj R, Sathya Narayanan V. Significance of continuous wave and pulsed wave laser in direct metal deposition. *Materials Today: Proceedings*. 2021;46:8086-8096. doi:10.1016/j.matpr.2021.03.041

127. Assuncao E, Williams S. Comparison of continuous wave and pulsed wave laser welding effects. *Optics and Lasers in Engineering*. 2013;51(6):674-680. doi:10.1016/j.optlaseng.2013.01.007

128. Nee AYC, ed. *Handbook of Manufacturing Engineering and Technology*. Springer London; 2015. doi:10.1007/978-1-4471-4670-4

129. Nam VB, Giang TT, Koo S, Rho J, Lee D. Laser digital patterning of conductive electrodes using metal oxide nanomaterials. *Nano Convergence*. 2020;7(1). doi:10.1186/s40580-020-00232-9

130. Kim JH, Jeon KA, Kim GH, Lee SY. Electrical, structural, and optical properties of ITO thin films prepared at room temperature by pulsed laser deposition. *Applied Surface Science*. 2006;252(13):4834-4837. doi:10.1016/j.apsusc.2005.07.134

131. Mokhtarifar N, Goldschmidtboeing F, Woias P. ITO/Glass as Extended-Gate of FET: A Low-Cost Method for Differential pH-Sensing in Alkaline Solutions. *Journal of The Electrochemical Society*. 2019;166(12):B896-B902. doi:10.1149/2.0401912jes

132. Reinhardt HM, Maier P, Kim HC, Rhinow D, Hampp N. Nanostructured Transparent Conductive Electrodes for Applications in Harsh Environments Fabricated via Nanosecond Laser-Induced Periodic Surface Structures (LIPSS) in Indium–Tin Oxide Films on Glass. *Advanced Materials Interfaces*. 2019;6(16):1-6. doi:10.1002/admi.201900401

133. Kundys M, Nejbauer M, Jönsson-Niedziolka M, Adamiak W. Generation–Collection Electrochemistry Inside a Rotating Droplet. *Anal Chem*. 2017;89(15):8057-8063. doi:10.1021/acs.analchem.7b01533

134. Chen W, Ackerson P, Molian P. CO2 laser welding of galvanized steel sheets using vent holes. *Materials & Design*. 2009;30(2):245-251. doi:10.1016/j.matdes.2008.05.009

135. Liu HB, Gong HQ. Templateless prototyping of polydimethylsiloxane microfluidic structures using a pulsed CO 2 laser. *Journal of Micromechanics and Microengineering*. 2009;19(3):037002. doi:10.1088/0960-1317/19/3/037002

136. Speller NC, Morbioli GG, Cato ME, et al. Cutting edge microfluidics: Xurography and a microwave. *Sensors and Actuators B: Chemical*. 2019;291:250-256. doi:10.1016/j.snb.2019.04.004

137. Radonić V, Birgermajer S, Podunavac I, Djisalov M, Gadjanski I, Kitić G. Microfluidic sensor based on composite left-right handed transmission line. *Electronics (Switzerland)*. 2019;8(12). doi:10.3390/electronics8121475

138. Chitnis G, Ding Z, Chang CL, Savran CA, Ziaie B. Laser-treated hydrophobic paper: An inexpensive microfluidic platform. *Lab on a Chip*. 2011;11(6):1161-1165. doi:10.1039/c0lc00512f

139. Rashiku M, Bhattacharya S. Fabrication Techniques for Paper-Based Micro fl uidic Devices. In: *Paper Microfluidics*. ; 2019:29-45. doi:https://doi.org/10.1007/978-981-15-0489-1_3

140. Deshmukh S, Jakobczyk P, Ficek M, Ryl J, Geng D, Bogdanowicz R. Tuning the Laser-Induced Processing of 3D Porous Graphenic Nanostructures by Boron-Doped Diamond Particles for Flexible Microsupercapacitors. *Adv Funct Materials*. 2022;32(36):2206097. doi:10.1002/adfm.202206097

141. Ge L, Hong Q, Li H, Liu C, Li F. Direct-Laser-Writing of Metal Sulfide-Graphene Nanocomposite Photoelectrode toward Sensitive Photoelectrochemical Sensing. *Advanced Functional Materials*. 2019;29(38):1-10. doi:10.1002/adfm.201904000

142. Pingarrón JM, Labuda J, Barek J, et al. Terminology of electrochemical methods of analysis (IUPAC Recommendations 2019). *Pure and Applied Chemistry*. 2020;92(4):641-694. doi:10.1515/pac-2018-0109

143. Madkour PDLH. Electrochemical Methods- Chapter 11. Accessed August 15, 2023. https://www.academia.edu/14750477/Electrochemical_Methods_Chapter_11

144. Borland LM, Michael AC. An Introduction to Electrochemical Methods in Neuroscience. In: Michael AC, Borland LM, eds. *Electrochemical Methods for Neuroscience*. Frontiers in Neuroengineering. CRC Press/Taylor & Francis; 2007. Accessed April 25, 2023. http://www.ncbi.nlm.nih.gov/books/NBK1845/

145. Smutok O, Katz E. Biosensors: Electrochemical Devices—General Concepts and Performance. *Biosensors*. 2022;13(1):44. doi:10.3390/bios13010044

146. Bobacka J, Ivaska A, Lewenstam A. Potentiometric Ion Sensors. *Chem Rev*. 2008;108(2):329-351. doi:10.1021/cr068100w

147. Dzyadevych S, Jaffrezic-Renault N. 6 - Conductometric biosensors. In: Schaudies RP, ed. *Biological Identification*. Woodhead Publishing; 2014:153-193. doi:10.1533/9780857099167.2.153

148. Lorenz W, Schulze KD. Zur anwendung der transformations—impedanzspektrometrie. *Journal of Electroanalytical Chemistry and Interfacial Electrochemistry*. 1975;65(1):141-153. doi:10.1016/0368-1874(75)85112-4

149. Magar HS, Hassan RYA, Mulchandani A. Electrochemical Impedance Spectroscopy (EIS): Principles, Construction, and Biosensing Applications. *Sensors*. 2021;21(19):6578. doi:10.3390/s21196578

150. Wang S, Zhang J, Gharbi O, Vivier V, Gao M, Orazem ME. Electrochemical impedance spectroscopy. *Nat Rev Methods Primers*. 2021;1(1):41. doi:10.1038/s43586-021-00039-w

151. Lasia A. Introduction. In: *Electrochemical Impedance Spectroscopy and Its Applications*. Springer New York; 2014:1-5. doi:10.1007/978-1-4614-8933-7_1

152. Gabrielli C. Once upon a time there was EIS. *Electrochimica Acta*. 2020;331:135324. doi:10.1016/j.electacta.2019.135324

153. Lazanas ACh, Prodromidis MI. Electrochemical Impedance Spectroscopy─A Tutorial. *ACS Meas Sci Au*. 2023;3(3):162-193. doi:10.1021/acsmeasuresciau.2c00070

154. O. Laschuk N, Bradley Easton E, V. Zenkina O. Reducing the resistance for the use of electrochemical impedance spectroscopy analysis in materials chemistry. *RSC Advances*. 2021;11(45):27925-27936. doi:10.1039/D1RA03785D

155. Meddings N, Heinrich M, Overney F, et al. Application of electrochemical impedance spectroscopy to commercial Li-ion cells: A review. *Journal of Power Sources*. 2020;480:228742. doi:10.1016/j.jpowsour.2020.228742

156. Randles JEB. Kinetics of rapid electrode reactions. *Discuss Faraday Soc*. 1947;1:11-19. doi:10.1039/DF9470100011

157. Harris FE. Complex Numbers and Functions. In: *Mathematics for Physical Science and Engineering*. Elsevier; 2014:87-110. doi:10.1016/B978-0-12-801000-6.00003-1

158. Lasia A. *Electrochemical Impedance Spectroscopy and Its Applications*. Springer New York; 2014. doi:10.1007/978-1-4614-8933-7

159. Schwarz M, Jendrusch M, Constantinou I. Spatially resolved electrical impedance methods for cell and particle characterization. *ELECTROPHORESIS*. 2020;41(1-2):65-80. doi:10.1002/elps.201900286

160. Dincer C, Bruch R, Costa-Rama E, et al. Disposable Sensors in Diagnostics, Food, and Environmental Monitoring. *Advanced Materials*. 2019;31(30):1806739. doi:10.1002/adma.201806739

161. Hassan Q, Ahmadi S, Kerman K. Recent Advances in Monitoring Cell Behavior Using Cell-Based Impedance Spectroscopy. *Micromachines*. 2020;11(6):590. doi:10.3390/mi11060590

162. Yoo EH, Lee SY. Glucose Biosensors: An Overview of Use in Clinical Practice. *Sensors (Basel)*. 2010;10(5):4558-4576. doi:10.3390/s100504558

163. Pullano SA, Greco M, Bianco MG, Foti D, Brunetti A, Fiorillo AS. Glucose biosensors in clinical practice: principles, limits and perspectives of currently used devices. *Theranostics*. 2022;12(2):493-511. doi:10.7150/thno.64035

164. Rao AN, Avula MN, Grainger DW. 3.34 Biomaterials Challenges in Continuous Glucose Monitors In Vivo. In: *Comprehensive Biomaterials II*. Vol 3. Elsevier; 2017:755-770. doi:10.1016/B978-0-12-803581-8.09314-0

165. Witkowska Nery E, Kundys M, Jeleń PS, Jönsson-Niedziółka M. Electrochemical Glucose Sensing: Is There Still Room for Improvement? *Anal Chem*. 2016;88(23):11271-11282. doi:10.1021/acs.analchem.6b03151

166. Lee I, Loew N, Tsugawa W, et al. The electrochemical behavior of a FAD dependent glucose dehydrogenase with direct electron transfer subunit by immobilization on self-assembled monolayers. *Bioelectrochemistry*. 2018;121:1-6. doi:10.1016/j.bioelechem.2017.12.008

167. Okuda-Shimazaki J, Yoshida H, Sode K. FAD dependent glucose dehydrogenases – Discovery and engineering of representative glucose sensing enzymes -. *Bioelectrochemistry*. 2020;132:107414. doi:10.1016/j.bioelechem.2019.107414

168. Boland S, Kavanagh P, Leech D. Mediated Enzyme Electrodes for Biological Fuel Cell and Biosensor Applications. *ECS Transactions*. 2008;13(21):77-87. doi:10.1149/1.3036213

169. Jayakumar K, Bennett R, Leech D. Electrochemical glucose biosensor based on an osmium redox polymer and glucose oxidase grafted to carbon nanotubes: A design-of-experiments optimisation of current density and stability. *Electrochimica Acta*. 2021;371:137845. doi:10.1016/j.electacta.2021.137845

170. Heller A. Integrated medical feedback systems for drug delivery. *AIChE Journal*. 2005;51(4):1054-1066. doi:10.1002/aic.10489

171. Mao F, Mano N, Heller A. Long Tethers Binding Redox Centers to Polymer Backbones Enhance Electron Transport in Enzyme "Wiring" Hydrogels. *J Am Chem Soc*. 2003;125(16):4951-4957. doi:10.1021/ja029510e

172. Fagadar-Cosma E, Plesu N, Lascu A, et al. Novel Platinum-Porphyrin as Sensing Compound for Efficient Fluorescent and Electrochemical Detection of H2O2. *Chemosensors*. 2020;8(2):29. doi:10.3390/chemosensors8020029

173. Wang Y, Jonkute R, Lindmark H, Keighron JD, Cans AS. Molecular Crowding and a Minimal Footprint at a Gold Nanoparticle Support Stabilize Glucose Oxidase and Boost Its Activity. *Langmuir*. 2020;36(1):37-46. doi:10.1021/acs.langmuir.9b02863

174. Gerlache M, Senturk Züh, Quarin G, Kauffmann J. Electrochemical behavior of H2O2 on gold. *Electroanalysis*. 1997;9(14):1088-1092. doi:10.1002/elan.1140091411

175. Sitnikova NA, Komkova MA, Khomyakova IV, Karyakina EE, Karyakin AA. Transition Metal Hexacyanoferrates in Electrocatalysis of H2O2 Reduction: An Exclusive Property of Prussian Blue. *Analytical Chemistry*. 2014;86(9):4131-4134. doi:10.1021/ac500595v

176. Buser HJ, Schwarzenbach D, Petter W, Ludi A. The crystal structure of Prussian Blue: Fe4[Fe(CN)6]3.xH2O. *Inorg Chem*. 1977;16(11):2704-2710. doi:10.1021/ic50177a008

177. Karyakin AA. Advances of Prussian blue and its analogues in (bio) sensors. *Current Opinion in Electrochemistry*. 2017;5(1):92-98. doi:10.1016/j.coelec.2017.07.006

178. Mayer AJ, Beynon OT, Logsdail AJ, et al. Direct monitoring of the potassium charge carrier in Prussian blue cathodes using potassium K-edge X-ray absorption spectroscopy. *J Mater Chem A*. 2023;11(37):19900-19913. doi:10.1039/D3TA02631K

179. Silva WO, Costa Bassetto V, Baster D, Mensi M, Oveisi E, Girault HH. Oxidative Print Light Synthesis Thin Film Deposition of Prussian Blue. *ACS Applied Electronic Materials*. 2020;2(4):927-935. doi:10.1021/acsaelm.9b00854

180. Sitnikova NA, Borisova AV, Komkova MA, Karyakin AA. Superstable Advanced Hydrogen Peroxide Transducer Based on Transition Metal Hexacyanoferrates. *Anal Chem*. 2011;83(6):2359-2363. doi:10.1021/ac1033352

181. Zamponi S, Berrettoni M, Kulesza PJ, et al. Influence of experimental conditions on electrochemical behavior of Prussian blue type nickel hexacyanoferrate film. *Electrochimica Acta*. 2003;48(28):4261-4269. doi:10.1016/j.electacta.2003.08.001

182. Calixto-Lozada O, Vazquez-Samperio J, Córdoba-Tuta E, Reguera E, Acevedo-Peña P. Growth of cobalt hexacyanoferrate particles through electrodeposition and chemical etching of cobalt precursors on reticulated vitreous carbon foams for Na-ion electrochemical storage. *Solid State Sciences*. 2021;116. doi:10.1016/j.solidstatesciences.2021.106603

183. Son Y, Shin D, Kang M, Lee CS. Coating 1-Octanethiol-Coated Copper Nano-Ink on a Paper Substrate via Multi-Pulse Flash Light Sintering for Application in Disposable Devices. *Electronic Materials*. 2020;1(1):28-39. doi:10.3390/electronicmat1010004

184. Son YH, Jang JY, Kang MK, Ahn S, Lee CS. Application of flash-light sintering method to flexible inkjet printing using anti-oxidant copper nanoparticles. *Thin Solid Films*. 2018;656:61-67. doi:10.1016/j.tsf.2018.04.034

185. Jang YR, Joo SJ, Chu JH, et al. A Review on Intense Pulsed Light Sintering Technologies for Conductive Electrodes in Printed Electronics. *Int J of Precis Eng and Manuf-Green Tech*. 2020;8(1):327-363. doi:10.1007/s40684-020-00193-8

186. Kim HS, Dhage SR, Shim DE, Hahn HT. Intense pulsed light sintering of copper nanoink for printed electronics. *Appl Phys A*. 2009;97(4):791-798. doi:10.1007/s00339-009-5360-6

187. Druffel T, Dharmadasa R, Lavery BW, Ankireddy K. Intense pulsed light processing for photovoltaic manufacturing. *Solar Energy Materials and Solar Cells*. 2018;174:359-369. doi:10.1016/j.solmat.2017.09.010

188. Costa Bassetto V, Oliveira Silva W, Pereira CM, Girault HH. Flash light synthesis of noble metal nanoparticles for electrochemical applications: silver, gold, and their alloys. *J Solid State Electrochem*. 2020;24(8):1781-1788. doi:10.1007/s10008-020-04521-5

189. Rekertaitė AI, Valiūnienė A, Virbickas P, Ramanavicius A. Physicochemical Characteristics of Polypyrrole/(Glucose oxidase)/(Prussian Blue)-Based Biosensor Modified with Ni- and Co-Hexacyanoferrates. *Electroanalysis*. 2019;31:50-57. doi:10.1002/elan.201800526

190. E. Banks C, Killard T, Jill Venton B. Introduction to electrochemistry for health applications. *Analytical Methods*. 2019;11(21):2736-2737. doi:10.1039/C9AY90069A

191. Lino C, Barrias S, Chaves R, Adega F, Martins-Lopes P, Fernandes JR. Biosensors as diagnostic tools in clinical applications. *Biochimica et Biophysica Acta (BBA) - Reviews on Cancer*. 2022;1877(3):188726. doi:10.1016/j.bbcan.2022.188726

192. McKeating KS, Aubé A, Masson JF. Biosensors and nanobiosensors for therapeutic drug and response monitoring. *Analyst*. 2016;141(2):429-449. doi:10.1039/C5AN01861G

193. Lee I, Probst D, Klonoff D, Sode K. Continuous glucose monitoring systems - Current status and future perspectives of the flagship technologies in biosensor research. *Biosensors and Bioelectronics*. 2021;181. doi:10.1016/j.bios.2021.113054

194. Teymourian H, Parrilla M, Sempionatto JR, et al. Wearable Electrochemical Sensors for the Monitoring and Screening of Drugs. *ACS Sens*. 2020;5(9):2679-2700. doi:10.1021/acssensors.0c01318

195. Teymourian H, Barfidokht A, Wang J. Electrochemical glucose sensors in diabetes management: an updated review (2010–2020). *Chem Soc Rev*. 2020;49(21):7671-7709. doi:10.1039/D0CS00304B

196. Kappalakandy Valapil K, Filipiak MS, Rekiel W, et al. Fabrication of ITO microelectrodes and electrode arrays using a low-cost CO_2 laser plotter. *Lab Chip*. Published online 2023:10.1039.D3LC00266G. doi:10.1039/D3LC00266G

197. Michalak M, Kurel M, Jedraszko J, et al. Voltammetric pH Nanosensor. *Anal Chem*. 2015;87(23):11641-11645. doi:10.1021/acs.analchem.5b03482

198. Nunes Kirchner C, Hallmeier KH, Szargan R, Raschke T, Radehaus C, Wittstock G. Evaluation of Thin Film Titanium Nitride Electrodes for Electroanalytical Applications. *Electroanalysis*. 2007;19(10):1023-1031. doi:10.1002/elan.200703832

199. Jedraszko J, Michalak M, Jönsson-Niedziolka M, Nogala W. Hopping mode SECM imaging of redox activity in ionic liquid with glass-coated inlaid platinum nanoelectrodes prepared using a heating coil puller. *Journal of Electroanalytical Chemistry*. 2018;815:231-237. doi:10.1016/j.jelechem.2018.03.032

200. Pinheiro T, Silvestre S, Coelho J, et al. Laser-Induced Graphene on Paper toward Efficient Fabrication of Flexible, Planar Electrodes for Electrochemical Sensing. *Advanced Materials Interfaces*. 2021;8(22):2101502. doi:10.1002/admi.202101502

201. Horiuchi T, Niwa O, Morita M, Tabei H. Limiting Current Enhancement by Self-Induced Redox Cycling on a Micro-Macro Twin Electrode. *J Electrochem Soc*. 1991;138(12):3549. doi:10.1149/1.2085457

202. Burcu Aydın E. A label-free and sensitive impedimetric immunosensor for TNF α biomarker detection based on epoxysilane-modified disposable ITO-PET electrode. *International Journal of Environmental Analytical Chemistry*. 2020;100(4):363-377. doi:10.1080/03067319.2019.1679807

203. Kim S, Ramasamy S, Bennet D. Drug and bioactive molecule screening based on a bioelectrical impedance cell culture platform. *IJN*. Published online December 2014:5789. doi:10.2147/IJN.S71128

204. Rahman ARA, Register J, Vuppala G, Bhansali S. Cell culture monitoring by impedance mapping using a multielectrode scanning impedance spectroscopy system (CellMap). *Physiol Meas*. 2008;29(6):S227-S239. doi:10.1088/0967-3334/29/6/S20

205. Padilha Leitzke J, Zangl H. A Review on Electrical Impedance Tomography Spectroscopy. *Sensors*. 2020;20(18):5160. doi:10.3390/s20185160

206. Witzel F, Fritsche-Guenther R, Lehmann N, Sieber A, Blüthgen N. Analysis of impedance-based cellular growth assays. *Bioinformatics*. 2015;31(16):2705-2712. doi:10.1093/bioinformatics/btv216

207. Kober EM, Caspar JV, Patrick Sullivan B, Meyer TJ. Synthetic Routes to New Polypyridyl Complexes of Osmium(II). *Inorganic Chemistry*. 1988;27(25):4587-4598. doi:10.1021/ic00298a017

208. Forster RJ, Vos JG. Synthesis, Characterization, and Properties of a Series of Osmium- and Ruthenium-Containing Metallopolymers. *Macromolecules*. 1990;23(20):4372-4377. doi:10.1021/ma00222a008

209. Gallaway JW, Barton SAC. Kinetics of redox polymer-mediated enzyme electrodes. *Journal of the American Chemical Society*. 2008;130(26):8527-8536. doi:10.1021/ja0781543

210. Ohara TJ, Rajagopalan R, Heller A. Glucose Electrodes Based on Cross-Linked [Os(bpy)2CI] Complexed Poly(1 -vinylimidazole) Films. 1993;65(23):3512-3517. doi:10.1021/ac00071a031

211. Melow SL, Miller DR, Gizzie EA, Cliffel DE. A low-interference, high-resolution multianalyte electrochemical biosensor. *Analytical Methods*. 2020;12(31):3873-3882. doi:10.1039/d0ay00528b

212. Jeon WY, Choi YB, Lee BH, et al. Glucose detection via Ru-mediated catalytic reaction of glucose dehydrogenase. *Advanced Materials Letters*. 2018;9(3):220-224. doi:10.5185/amlett.2018.1947

213. Calhoun MC, Stachurski CD, Winn SL, et al. Trace Oxygen Affects Osmium Redox Polymer Synthesis for Wired Enzymatic Biosensors. *J Electrochem Soc*. 2022;169(1):016506. doi:10.1149/1945-7111/ac42a0

214. Unal HI, Erol O, Gumus OY. Quaternized-poly(N-vinylimidazole)/montmorillonite nanocomposite: Synthesis, characterization and electrokinetic properties. *Colloids and Surfaces A: Physicochemical and Engineering Aspects*. 2014;442:132-138. doi:10.1016/j.colsurfa.2013.04.054

215. Singhal S. Characterisation of pH and Glucose Sensors for use in Cell Culture. 2009;(January).

216. Asayama S, Hakamatani T, Kawakami H. Synthesis and characterization of alkylated poly(1-vinylimidazole) to control the stability of its DNA polyion complexes for gene delivery. *Bioconjugate Chemistry*. 2010;21(4):646-652. doi:10.1021/bc900411m

217. Zaoui A, Cherifi Z, Belbachir M. Ultrasound-induced synthesis of an imidazolium based poly(ionic liquid) in an aqueous media: A structural, thermal and morphological study. *Ultrasonics Sonochemistry*. 2019;55(January):149-156. doi:10.1016/j.ultsonch.2019.02.027

218. Thangaraj V, Bhaskarapillai A, Velmurugan S. Synthesis of a crosslinked poly(ionic liquid) and evaluation of its antimony binding properties. *Journal of Hazardous Materials*. 2020;384:121481. doi:10.1016/j.jhazmat.2019.121481

219. Fan B, Wan J, McKay A, Qu Z, Thang SH. Facile synthesis of well-controlled poly(1-vinyl imidazole) by the RAFT process. *Polymer Chemistry*. 2020;11(35):5649-5658. doi:10.1039/d0py00985g

220. Karyakin A, Karyakina E, Gorton L. Prussian-Blue-based amperometric biosensors in flow-injection analysis. *Talanta*. 1996;43(9):1597-1606. doi:10.1016/0039-9140(96)01909-1

221. Karyakin AA, Karyakina EE, Gorton L. The electrocatalytic activity of Prussian blue in hydrogen peroxide reduction studied using a wall-jet electrode with continuous flow. *Journal of Electroanalytical Chemistry*. 1998;456(1-2):97-104. doi:10.1016/S0022-0728(98)00202-2

222. Katic V, Dos Santos PL, Dos Santos MF, et al. 3D Printed Graphene Electrodes Modified with Prussian Blue: Emerging Electrochemical Sensing Platform for Peroxide Detection. *ACS Appl Mater Interfaces*. 2019;11(38):35068-35078. doi:10.1021/acsami.9b09305

223. De Mattos IL, Gorton L, Ruzgas T, Karyakin AA. Sensor for hydrogen peroxide based on Prussian Blue modified electrode: Improvement of the operational stability. *Analytical Sciences*. 2000;16(8):795-798. doi:10.2116/analsci.16.795

224. Jirakunakorn R, Khumngern S, Choosang J, Thavarungkul P, Kanatharana P, Numnuam A. Uric acid enzyme biosensor based on a screen-printed electrode coated with Prussian blue and modified with chitosan-graphene composite cryogel. *Microchemical Journal*. 2020;154:104624. doi:10.1016/j.microc.2020.104624

225. Borisova AV, Karyakina EE, Cosnier S, Karyakin A. Current-Free Deposition of Prussian Blue with Organic Polymers : Towards Improved Stability and Mass Production of the Advanced Hydrogen Peroxide Transducer. 2009;(3):409-414. doi:10.1002/elan.200804408

226. Busquets MA, Estelrich J. Prussian blue nanoparticles: synthesis, surface modification, and biomedical applications. *Drug Discovery Today.* 2020;25(8):1431-1443. doi:10.1016/j.drudis.2020.05.014

227. Lin J. Nickel hexacyanoferrate modified screen-printed carbon electrode for sensitive detection of ascorbic acid and hydrogen peroxide. *Front Biosci.* 2005;10(1-3):483. doi:10.2741/1544

228. Wang Z, Hao X, Zhang Z, Liu S, Liang Z, Guan G. One-step unipolar pulse electrodeposition of nickel hexacyanoferrate/chitosan/carbon nanotubes film and its application in hydrogen peroxide sensor. *Sensors and Actuators B: Chemical.* 2012;162(1):353-360. doi:10.1016/j.snb.2011.12.099

229. Heffner H, Soldera M, Lasagni AF. Optoelectronic performance of indium tin oxide thin films structured by sub-picosecond direct laser interference patterning. *Sci Rep.* 2023;13(1):9798. doi:10.1038/s41598-023-37042-y

230. Particle Re-Deposition During Ultrashort Pulse Laser Ablation of ITO Thin Films Using Single- and Multi-Beam Processing. *JLMN.* Published online December 2022. doi:10.2961/jlmn.2022.03.2007

231. Hallum GE, Kürschner D, Redka D, Niethammer D, Schulz W, Huber HP. Time-resolved ultrafast laser ablation dynamics of thin film indium tin oxide. *Opt Express, OE.* 2021;29(19):30062-30076. doi:10.1364/OE.434515

232. Singh G, Sheokand H, Ghosh S, Srivastava KV, Ramkumar J, Ramakrishna SA. Excimer laser micromachining of indium tin oxide for fabrication of optically transparent metamaterial absorbers. *Appl Phys A.* 2018;125(1):23. doi:10.1007/s00339-018-2013-7

Institute of Physical Chemistry
Polish Academy of Sciences

Kasprzaka 44/52
01-224 Warsaw, Poland

www.ichf.edu.pl